Characterization of seismic rupture processes along the Colombian subduction zones

コロンビアの沈み込み帯における地震破壊過程に関する研究

BERMUDEZ BARRIOS Juan Carlos

A dissertation for the degree of Doctor of Science
Department of Earth and Environmental Sciences,
Graduate School of Environmental Studies, Nagoya University

2020

ABSTRACT

Colombia, located northwest of the South American plate (SAP), is affected by northern and western subductions of the Caribbean and Nazca plates, respectively, and NE-SE convergence of the Choco-Panama block. These interactions have resulted in intracontinental deformation, characterized by the uplifting of the mountain chains along Colombia (Northern Andes), and the fault systems observed in the cordilleras and valleys of this Andean chain. Colombia is tectonically active. Several large earthquakes have ruptured in the Colombia-Ecuador subduction zone (CESZ) during the last century. Among them, the Colombia-Ecuador earthquake in 1906 (M_w 8.4) and the Tumaco earthquake in 1979 (M_w 8.3) generated destructive tsunamis. By contrast, in the Caribbean region, no large historical earthquakes have been reported to date.

It is important to characterize the seismic rupture processes and their relation with interplate coupling along the Colombian subduction zones. In the Colombia-Ecuador subduction zone, I searched for very-low-frequency (VLF) earthquakes and repeating earthquakes. In searching for these special types of earthquakes, visual searching across the continuous waveforms from broadband seismic sensors managed by the Colombian Geological Survey (SGC) was performed for VLF earthquakes, and waveform similarity analysis by estimating cross-correlation coefficients between earthquakes pairs recorded by broadband and short-period seismic sensors from the SGC seismic network was performed for repeating earthquakes.

I searched for VLF earthquakes within the continuous data in the time period from Jan 2016 to Sep 2017. However, I did not find VLF earthquakes in the region within this period. I provide three possible reasons to explain this fact: (1) the low detection capacity of the network because the stations used are sparse, (2) the possible presence of materials in the accretionary prism characterized by low or no dehydration; the fluid cannot weaken faults and earthquakes with low drop stress are not generated, (3) the scarce occurrence of large earthquakes, which increase the VLF activity in neighboring regions to their hypocenters. Further searching for VLF activity through synthetic waveforms obtained by seismic waves propagation modeling with use of the matched filter is required in this region.

I searched for repeating earthquakes in the time period between 1993 and 2018. A threshold for the cross-correlation value of 0.9 was used to identify the waveform similarity and to select repeating earthquakes, in which sequences of events occurred in very short-time intervals were excluded because they may represent triggered events. Repeating earthquakes were found near the trench and beneath the coastal region. This distribution indicates that

repeating earthquakes did not occur within the large slip of the 1979 Tumaco earthquake, where relatively large interplate coupling was estimated by Sagiya & Mora-Páez (2019). Those repeating earthquakes located offshore near the trench suggest that the interplate coupling in this region is low, which is in clear contrast to the large slip in the 1906 Colombia-Ecuador earthquake trench in the southern part of CESZ, since repeating earthquakes are not expected in large slip areas where strong interplate coupling exits. This suggests that rupture modes are different between the northern and southern parts of the CESZ near the trench.

In the southern Caribbean subduction zone, northwestern Colombia, repeating earthquakes were also searched within 1993 and 2018. I used a similar methodology used in CESZ for this region. Repeating earthquakes were found in the region corresponding to a low interplate coupling region or a slip excess region, estimated by Lizarazo (2020).

In Colombia-Ecuador subduction zone, I found repeating earthquakes but I did not find VLF earthquakes. The repeating earthquake distribution is consistent with the coupling model, and the intercoupling region represented by a heterogeneous pattern with a clear region of strong coupling surrounding by a wide homogeneous region representing weak coupling. This characterization of this subduction zone is comparable to the northeastern Japan subduction zone, since few VLF earthquakes have been found there, and the repeating earthquakes distribution are consistent with the bimodal coupling model estimated for that region.

In southern Caribbean subduction zone, I found repeating earthquakes; and searching for VLF earthquakes in this region is yet to be done. Similar to the Colombia subduction zone, the intercoupling region shows a heterogeneous pattern with a clear region of strong coupling surrounding by a homogeneous region which represents weak coupling. The repeating earthquake distribution is also consistent with this coupling model.

I found repeating earthquakes in the Colombia subduction zone and the southern Caribbean subduction zone, and they are the first repeating earthquakes reported in these subduction zones. These repeating earthquakes were located in regions surrounding the possible large asperities estimated by the coupling models or the rupture model. The distributions of these repeating earthquakes contribute to constrain the geometry of the asperity, which is important for seismic hazard estimation to determine the size of a possible forthcoming large earthquake.

ACKNOWLEDGMENTS

I thank the Japanese Government for the support throughout the MEXT scholarship and the SATREPS project in collaboration with the Colombian Geological Survey. I also thank my advisor, professor Hiroyuki Kumagai, for taking me as his student, for his suggestions and comments. Thanks to professor Takeshi Sagiya, Masahiro Yoshimoto, and Sindy Lizarazo for sharing and letting me use their scientific research results. Thanks to professor Naoki Uchida for his helpful recommendations, and to the Colombian Geological Survey staff for providing me the dataset used in this study.

My deepest thanks and gratitude to my family for their unconditional support and the thrust deposited on me, to my girlfriend, who has been accompanying me despite the distance, advising and giving me support words to stand up in the difficult times lived here. To my friends of Nagoya Futsal, who made for me less complicated my life in Japan.

TABLE OF CONTENTS

Page

ABSTRACT v

ACKNOWLEDGMENTS vii

LIST OF TABLES xi

LIST OF FIGURES xii

1. INTRODUCTION 17

1.1Introduction 17
2. TECTONIC SETTING 22

2.1 Nazca, Caribbean and South American plates 22
2.2 Historical earthquakes 30
3. SLOW EARTHQUAKES 33

3.1 Slow-slip earthquakes 36
3.2 Non-volcanic tremor 36
3.3 Low-frequency earthquakes 38
3.4 Very-low-frequency earthquakes 38
4. REPEATING EARTHQUAKES 41

4.1 Definition of repeating earthquakes 41
4.2 Detection of repeating earthquakes 41
4.3 Previous studies of repeating earthquakes 43
5. METODOLOGY 46

5.1 Cross correlation 46
5.2 Matched-filter technique 47
5.3 Seismological network of Colombia 50
5.4 VLF earthquake search 52
5.4.1 Data 52
5.4.2 Visual search 53
5.4.3 Software 53
5.5 Repeating earthquake search 55
5.5.1 Nazca and South American plates boundary 55
5.5.1.1 Data 55
5.5.1.2 Searching of repeating earthquakes 58
5.5.2 Caribbean and South American plates boundary 62
5.5.2.1 Data 62
6. RESULTS 66

6.1 Very-low-frequency earthquakes 66
6.2 Repeating earthquakes in the Colombia-Ecuador subduction zone 70
6.2.1 Slip rate estimation 82
6.3 Repeating earthquakes along Caribbean and South America plate boundary 85
6.3.1 Slip rate estimation 88

7. Discussion 96

7.1 Very-low-frequency earthquakes 96
7.2 Repeating earthquakes in Colombia subduction zone 97
7.3 Repeating earthquakes in southern Caribbean subduction zone 104
8. Conclusions 108

Bibliography 110

LIST OF TABLES

Table Page

Table 1: Sequences, the number of earthquakes in each sequence, and slip rates estimated by using time-predictable (TP) and size-predictable (SP) models (Bermúdez-Barrios & Kumagai, 2020).....81

Table 2: Sequences, the number of earthquakes in each sequence, and slip rates estimated by using time-predictable (TP) and size-predictable (SP) models.....95

LIST OF FIGURES

Figure Page

Figure 1: Main tectonic structures involved in the tectonic setting of Colombia. WC: Western Cordillera, CC: Central cordillera, EC: Eastern Cordillera.....25

Figure 2: Different models related to the tectonic setting in Colombia. (a) the model presented by Vargas & Mann (2013), (b) the model presented by Syracuse et al. (2016), (c) the model presented by Wagner et al. (2017). 29

Figure 3: Historical earthquakes larger than magnitude (M) of 7 that occurred along the Colombia-Ecuador subduction zone between 1900 and 2020. 32

Figure 4: Different examples of slow earthquakes. (a) Tremor and (b) very-low-frequency (VLF) earthquakes from Japan, filtered between 2–8 and 0.005–0.05 Hz, respectively. (c) Low-frequency earthquakes (LFE) from Japan. (d) Top: daily GPS EW displacement measured on Vancouver Island; Bottom: averaged and detrended GPS data (pink lines show the fit trend) indicating a slow-slip event (shaded). (e) Slow slip in differential shear strain measured in western Washington. Strain transient onset coincides with increased tremor activity. Modified from Peng & Gomberg (2010).....35

Figure 5: Schematic illustration showing the asperity distributions surrounded by the aseismic area in the boundary plate region. Various sizes of asperities are distributed on the plate boundary. (a) Areas other than asperities slip aseismically, and (b) small asperities eventually rupture as earthquakes, and they can rupture recurrently, generating the repeating earthquakes. Modified from Matsuzawa et al. (2004).....44

Figure 6: Examples of correlation obtained in this study. The signals blue (2010), purple (2012), and wine (2015) color represent 3 different earthquakes. They were correlated each other, and the signals colored by green, pink and orange represent the correlation functions for the individual pairs. 48

Figure 7: Matched-filter technique: Template signal (blue) run over the continuous data (orange) measuring similarity between the template and the continuous data throughout estimation of the cross-correlation coefficients by using cross correlation technique. 49

Figure 8: Matched filter after cross correlation signals. Blue signals are the cross-correlation signals after measuring similarity between a template and the continuous data at each station. Slightly earlier from 20000 s there is a signal detected by high cross correlation value. The stacked cross-correlation function enhances (orange) the detection of the signal.....51

Figure 9: Broadband stations used in searching for VLF earthquakes. Colombia Geological Survey (red), Geophysics Institute - National Polytechnic School (blue), and Incorporated Research Institutions for Seismology (yellow).....54

Figure 10: Example waveform plots searching for VLF earthquakes, using the software SEISAN. This figure shows three panels, the first, second and third panels display the raw data, the filtered signal with the bandpass filter between 0.02 and 0.05 Hz and the signal filtered by the bandpass filter between 2.0 and 8.0 Hz, respectively. 56

Figure 11: (a) Locations of broadband (red triangles) and short period (green triangles) seismic stations used in the present study. The stations with black stars represent those installed after 2009. (b) The number of stations operated per year from 2003 to 2018..... 57

Figure 12: Source distributions of earthquakes used in this study. The hypocenter locations of earthquakes were obtained from the SGC catalog for the selected event within the area (1: 1.34°N, 80.51°W, 2: 4.5°N, 78.28°W, 3: 3.76°N, 70.00°W, 4: 0.60°N, 79.22°W). Right panels represent the cross sections along A–A′ and B–B′ (Bermúdez-Barrios & Kumagai, 2020). 59

Figure 13: Uncertainty in hypocentral parameters estimated by routine hypocenter determinations by SGC for earthquakes located in the Colombia-Ecuador subduction zone between 1993 and 2018..... 60

Figure 14: Sketch to explain the spatial separation between earthquakes and the selection of neighbor events. The first stage, $n = 0$, represents all events without selecting any events. The stage, $n = 1$, one reference event (RE) (red star) is selected and all events far from RE less than 50 km is selected as neighbor event (NE) (blue star). The same procedure is done for stage $n = 2$ and $n = 3$ and so on until run all events in the catalog..... 61

Figure 15: Locations of broadband (red triangles) and short period (green triangles) seismic stations used in the search for repeating earthquakes in the southern Caribbean subduction zone. The stations with black stars represent those installed after 2009..... 63

Figure 16: Source distribution of earthquakes used in this study. The hypocenter locations of earthquakes were obtained from the SGC catalog for the selected event within the area: (10.00°N, 79.51°W), (15.00°N, 73.50°W), (11.46°N, 70.54°W), (6.45°N, 76.54°W). Right panels represent the cross sections along A–A′ and B–B′..... 64

Figure 17: Uncertainty in hypocentral parameters estimated by routine hypocenter determinations by SGC for earthquakes located in the southern Caribbean subduction zone between 1993 and 2018..... 65

Figure 18: Example of an event originated in the west coast of Mexico, showing similar features to a VLF earthquake. Top left and right panels are the signals filtered in 2–8 Hz and 0.02–0.05 Hz, respectively. The bottom panel shows the low-pass filtered waveforms plotted again distance. 67

Figure 19: As in Figure 17, but an event occurred in the Tonga region..... 68

Figure 20: As in Figure 17, but an event occurred in the Nazca-Cocos plate boundary. 69

Figure 21: Frequency distribution of the cross-correlation coefficients between earthquakes pairs with hypocenter differences of < 50 km, located within the Colombia-Ecuador subduction zone (Bermúdez-Barrios & Kumagai, 2020).....71

Figure 22: Plots of epicentral locations of earthquakes found by the cross-correlation (CC) waveform analysis with CC threshold values of 0.80. 0.85, 0.90, and 0.95; the color scale represents the individual sequences (Bermúdez-Barrios & Kumagai, 2020).....73

Figure 23: The number of earthquakes against the time intervals of successive earthquakes found by using cross correlation (CC) threshold values of 0.80 (gray) and 0.90 (black). (a) 0 to 12 years with 4-month interval bins. (b) 0 to 30 days with 1-day interval bins (Bermúdez-Barrios & Kumagai, 2020).....75

Figure 24: Spatial distributions of the groups of possible repeating earthquakes found by using cross correlation (CC) threshold values of 0.80, 0.85, and 0.90 and minimum time intervals of 0 days, 5 days, and 4 months. The color scale represents the individual sequences (Bermúdez-Barrios & Kumagai, 2020).....76

Figure 25: Examples of seismograms from repeating earthquake sequences recorded at different stations. (a) Record of the earthquakes that occurred at 18:56 on February 18, 2012 with M_L 2.3 (black) and at 15:07 on February 29, 2016 with M_L 2.3 (gray), recorded at SOTO and GCUF stations. (b) Record of the earthquakes that occurred at 06:06 on November 02, 2007 with M_L 2.7 (black) and at 23:39 on August 11, 2016 with M_L 2.9 (gray), recorded at CUM and CRU stations (Bermúdez-Barrios & Kumagai, 2020). 77

Figure 26: Distributions of the estimated repeating earthquakes using a cross-correlation (CC) threshold value of 0.90 and a minimum time interval of 4 months. (a) Epicenter locations of the repeating earthquakes, with the size of stars representing the magnitude of earthquake and the color scale representing the sequences. (b) Averaged epicenter locations of the repeating earthquakes in the individual sequences, with the size of the stars representing the number of earthquakes (No. of Eqs.) in each sequence. Regions Z1–Z4 are used to separate the sequences (Bermúdez-Barrios & Kumagai, 2020).....79

Figure 27: Magnitude-time plots of the repeating earthquakes in the individual sequences in regions Z1–Z4. The color scale represents the sequences and is the same as that used in Figure 25 (Bermúdez-Barrios & Kumagai, 2020).....80

Figure 28: Plots of cumulative slip of the repeating earthquakes in the individual sequences in regions Z1–Z4 during 1993–2018. Slip rates are shown at the bottom of each panel as references (Bermúdez-Barrios & Kumagai, 2020).....83

Figure 29: Plot of M_L against M_w for 102 events, for which both M_L and M_w were measured among 1,442 events analyzed in this study. Gray circles represent whole 102 events, and overlapped with black circles events with 2.0 < M_w <4.0, selected for fitting to a first-degree polynomial. The slope for the fit was 0.92, and the intersection point with vertical axes was −0.14. The fitting is represented by the red line. The equation represents the relationship between M_L and M_w (Bermúdez-Barrios & Kumagai, 2020).....84

Figure 30: Frequency distribution of the cross-correlation coefficients between earthquakes pairs with hypocenter differences of < 50 km located in the Southern Caribbean subduction zone. 86

Figure 31: Distribution of earthquakes with CC < 0.9, in which the size of stars represents the magnitude and the color scale indicates the individual sequences. No restrictions by recurrence time intervals between successive earthquakes were applied.....87

Figure 32: Frequency distributions of time intervals of successive earthquakes found by using cross correlation (CC) threshold values of 0.80 (gray) and 0.90 (black). (a) 0 to 18 years with 4-month interval bins. (b) 0 to 30 days with 1-day interval bins. 89

Figure 33: Distributions of the estimated repeating earthquakes using a cross-correlation (CC) threshold value of 0.90 and a minimum time interval of 11 months. (a) Epicenter locations of the repeating earthquakes, with the size of stars representing the magnitude of earthquake and the color scale representing the sequences. Regions Z1–Z6 are used to separate the sequences. (b) Averaged epicenter locations of the repeating earthquakes in the individual sequences, with the size of the starts representing the number of earthquakes (No. of Eqs.) in each sequence. 90

Figure 34: Magnitude-time plots of the selected repeating earthquakes in the individual sequences in regions Z1–Z6. These regions are shown in the Figure 32a. 91

Figure 35: Plots of M_L against M_w for 363 events, for which both M_L and M_w were measured among 5,805 events analyzed in this study. Purple circles represent whole the 363 events, and overlapped with green circles events with 2.0 < M_w < 4.0, selected for fitting to a first-degree polynomial. The slope for the fit was 0.96, and the intersection point with vertical axes was −0.24. The fitting is represented by the red line. The equation represents the relationship between M_L and M_w.....93

Figure 36: Plots of cumulative slip of the repeating earthquakes in the individual sequences in regions Z1, Z3, Z4 and Z6, in the southern Caribbean subduction zone, during 1993–2018. Slip rates are shown at the bottom of each panel as references.....94

Figure 37: Plots of completeness magnitude (M_c) as a function of time, for the catalog of earthquakes located in the Colombia subduction zone. 99

Figure 38: Locations of the repeating earthquakes (colored stars) with the background seismicity (gray circles) in our study area. The color scale representing depth in this figure. The arrow indicates the location of the earthquake with magnitude M_w 6.7, with normal focal mechanism, occurred in 2007-09-10 (Bermúdez-Barrios & Kumagai, 2020). 101

Figure 39: Spatial distributions of the sequences of the repeating earthquakes (colored stars), the interplate coupling (purple area) estimated by Sagiya & Mora-Páez, (2019) and slip distributions (colored squares) estimated by Yoshimoto et al. (2017) for the 1906 Colombia-Ecuador earthquake (Bermúdez-Barrios & Kumagai, 2020)..... 103

Figure 40: (Top) Spatial distributions of the sequences of the repeating earthquakes (colored stars). (Bottom) Spatial distributions of the sequences of the repeating earthquakes (colored stars), over the background seismicity. The whole seismicity reported in the catalog used for the current study..... 106

Figure 41: Spatial distributions of the sequences of the repeating earthquakes (colored stars), the interplate coupling (inset figure) estimated by Lizarazo (2020), red color indicating strong coupling and blue color indicanding weak coupling..... 107

CHAPTER 1

1. INTRODUCTION

1.1 Introduction

Understanding processes occurring in the interplate seismogenic zone, where destructive, tsunamigenic, great subduction earthquakes may occur, is important to seismic and tsunami hazard assessment around the subduction zone. Colombia-Ecuador and southern Caribbean regions are two subduction zones in western and northwestern Colombia, respectively. The proven earthquake and tsunami potentials of the Colombia-Ecuador subduction highlight the importance of studying this region. The potential for generating tsunamigenic earthquakes in the southern Caribbean subduction zone is puzzling due to seismicity distribution and the lack of historical data; however, the study of this subduction zone is important because of the large coastal population and the high economic activity in the region may be severely affected.

The tectonic environment in Colombia is complex. Colombia is located in the northwestern South American corner where three lithospheric plates interact: the Nazca and Caribbean plates of oceanic origin, and the older continental South American plate. Currently, the Nazca plate is subducting to the east beneath the South American plate along the Colombia-Ecuador trench, producing intense crustal deformation with a velocity of approximately 5.4 cm/yr and the Caribbean plate is subducting to the southeast with a velocity of 2 cm/yr (Mora-Páez et al., 2019; Trenkamp et al., 2002). Different subduction styles and angles along the Pacific and Caribbean margins in northwestern South America seem to be promoted by contrasting conditions of the seafloor relief, age, thickness, thermal structure, and converging velocity of the subducting slabs. Although there is a general consensus regarding the active nature of the continental margin along the Pacific and Caribbean coasts of Colombia, there is still a number of fundamental unknowns about the tectonic nature of this region. There is still debate about the limits between the oceanic Nazca and Caribbean plates, and their subduction geometries beneath South America, which suggest complex interactions among these plates.

Based on geophysical modeling, earthquake distribution, geodetic data and geologic observations, different models of the tectonic configuration in northwestern South America have been proposed by several studies in recent years, providing different interpretations of the possible interactions among the plates.

Due to the this intense interaction between the Nazca and South American plates, along the Colombia-Ecuador subduction zone (CESZ), several large subduction earthquakes have ruptured in the zone between Guayaquil-Ecuador and Tumaco-Colombia, and some of them generated destructive tsunamis (Kanamori & McNally, 1982): The 1942 earthquake (M_w 7.8) (Swenson & Beck, 1996), which occurred again in 2016 (M_w 7.7) (Yoshimoto et al., 2017a), the 1958 (M_w 7.7), and 1979 (M_w 8.1) earthquakes and the largest in 1906 (M_w 8.4) which ruptured the offshore region without overlaps of the above-mentioned ruptures. Therefore, it is inferred that along CESZ there must be two rupture domains: one near the trench and the other near the coast, pointing to the existence of a depth-dependent complex rupture mode along the subduction megathrust region (Yoshimoto et al., 2017a).

In the Caribbean region, significant amount of large to great earthquakes with tsunamigenic potential have occurred around the Caribbean plate with intense activity in eastern boundary of the Caribbean plate and few events in the western side (Hillebrandt-Andrade, 2013). However, in the southern Caribbean plate, the absence of historical records of large or great earthquakes is consistent with the observed low rate of modern seismicity along this slowly subducting margin, and the fact that no tsunami events have been recorded along the Colombian-Caribbean coastline over the last 500 years. The lack of data in this region makes difficult to estimate the seismic hazard.

An appropriate seismic hazard estimation is important since the destructive potential of potential events is the highest when largely populated areas may be affected, especially a population that is not well informed or prepared for tsunami hazards, such as several coastal regions near the Colombia-Caribbean Sea. Hundreds of thousands of residents, tourists, and tourist-industry workers are potentially at risk from tsunamis and earthquakes around the densely populated urban and tourist areas of the Caribbean coasts.

In view of the intense historical earthquake activity and the microearthquake activity in the Nazca-South America margin and the unknown probability of an impending earthquake with tsunamigenic potential in the Colombia Caribbean coast, the study of the subduction-related processes that occurred in the interplate regions is important. The characterization of the seismic rupture processes, and how these processes are related with the interplate coupling as well as the distribution of aseismic slip can provide a better understanding of stress accumulation on and around coseismic slip areas associated with severe earthquakes.

To interpret the seismic activity in relation to the subduction interplate processes, we need information about the spatiotemporal change of interplate coupling. Chlieh et al. (2014) by using Global Positioning System (GPS) data from a dense GPS network deployed in Ecuador presented a highly heterogeneous pattern of interplate coupling between the subducting oceanic Nazca plate and the South American plate in the interplate region ranging from 2.5°S to 2.5°N. Sagiya & Mora-Páez (2019) based on the analyses of geodetically surveying data and GPS data from the Colombian Geological Survey (SGC) revealed a broad pattern of the interplate coupling in the northern part of CESZ. Subsequently, Lizarazo (2020) analyzed data from continuous GPS data deployed along Colombia and Caribbean, and by geodetic inversion analysis estimated an interplate coupling model for the Colombia-Ecuador and the southern Caribbean subduction zones. This interplate coupling model for the southern Caribbean subduction zone was the first model in this region.

Slow earthquakes and repeating earthquakes have been found in some subduction zones along Pacific plate boundaries and they have been used to characterize slow slip processes and slip rate distributions, which are thought to be related with the process of building up and releasing stresses in and around megathrust earthquake rupture zones. Very-low-frequency (VLF) earthquakes as one category of slow earthquakes have been found in different subduction zones around the world such as Nankai (Obara & Ito, 2005), Cascadia (Beroza & Ide, 2011), Mexico (Dominguez et al., 2016) among others, and previous studies have reported repeating earthquakes identified in different tectonic environments (Nadeau & Johnson, 1998; Matsuzawa et al., 2004; Bohnhoff et al., 2017), and others have estimated slip rate distributions in northeastern Japan (Igarashi et al., 2003; Uchida et al., 2004; Uchida & Matsuzawa, 2011; Uchida, 2019), Mexico trench (Dominguez et al., 2016), Tonga-Kermadet trench (Wen-che, 2013). However, studies for VLF earthquakes and repeating earthquakes along Colombia-Ecuador and southern Caribbean subduction zones have not been carried out yet.

In this study, I systematically investigated VLF earthquakes and repeating earthquakes along the Colombia-Ecuador and southern Caribbean subduction zones. VLF earthquakes were first searched visually by using the continuous waveform from the broadband seismometer Colombia and Ecuador networks. Then, template candidates were used to detect possible VLF events by cross correlation matched-filter algorithm between January 2016 and September 2018. Similarly, repeating earthquakes were also investigated along the northern part of Colombia-Ecuador subduction zone (1° – 4°N) and southern Caribbean subduction zone (7°–13°N) using

broadband and short-period seismic waveform data from the SGC seismic network between 1993 and 2018. By using cross correlation technique, waveform similarity was evaluated. I performed waveform similarity analysis using cross correlation values of earthquake pairs based on the hypocentral differences among events reported in the SGC earthquake catalog.

In the search for VLF earthquakes in the Colombia-Ecuador region within the time range mentioned above, no evidence was found about VLF activity. I addressed three possible reasons explaining why VLF earthquakes were not found in the Colombia-Ecuador subduction zone: 1) the low detectability by the network used in this study, 2) the absence of fluid that cannot weaken the fault, avoiding low drop stress, and 3) the absent of large earthquakes with magnitudes larger than 6.

Repeating earthquakes were found near the trench and beneath the coastal region in the northern part of the Colombia-Ecuador subduction zone. This distribution indicates that repeating earthquakes did not occur within the large slip area of the 1979 Tumaco earthquake and around the relatively large interplate coupling area estimated by Sagiya & Mora-Páez (2019). The estimated repeating earthquakes located offshore near the trench suggest that interplate coupling in this region is low. Large slip of the 1906 Colombia-Ecuador earthquake along the trench in southern part of the Colombia-Ecuador subduction zone was estimated by Yoshimoto et al. (2017a), and therefore, the northern and southern parts of the Colombia-Ecuador subduction zone along the trench may be affected by different rupture modes.

I found repeating earthquakes in the Caribbean region in the intraplate area and near the coast. This distribution agrees with the description of the repeating earthquake given by Igarashi et al. (2003) since most of repeating earthquakes did not occur in strongly coupled areas inferred from GPS data analyses. The distribution of the repeating earthquakes found here is consistent with the coupling model presented by Lizarazo (2020) due to the repeating earthquakes are distributed within the low coupling region and around the large asperity which is represented by the strong coupling region pattern according to Lizarazo (2020). These results here are also consistent since earthquakes within the strong coupling region did not show high waveform similarity with their neighbors, which means they are not repeating earthquakes. I found two other groups of repeating earthquakes; however, the mechanisms generating these earthquakes did not correspond plate subduction. One group occurs near the Murindo seismic zone featured by the existence of a strike-slip fault system (Nadeau & Johnson, 1998). The other group was located in a region where mining activities are carried out; therefore, the repeating earthquakes

found here may be triggered by these mining activities.

This thesis consists of eight chapters. In Chapter 1 (current chapter), I presented the motivation of this research and outline the main results of my investigations. In Chapter 2 the main tectonic settings and a brief review of historic earthquakes in the Colombia Ecuador subduction zone are described. Chapters 3 and 4 are dedicated to present a review of slow earthquakes and repeating earthquakes respectively. Chapter 5 presents a description of the techniques and methods used in this research. Chapters 6 and 7 present results obtained in the different stages of my research and how the results can be interpreted, and finally in Chapter 8 concluding remarks are presented.

CHAPTER 2

2. TECTONIC SETTING

2.1 Nazca, Caribbean and South American plates

Colombia is located in the northwestern corner of South American where three lithospheric plates interact: the Nazca and Caribbean plates of oceanic origin, and the older continental South American plate. Currently, the Nazca plate is converging east-northeastward relative to the stable South America plate along the Colombia-Ecuador trench at a rate of 54.8 mm/yr and the Caribbean plate converges east-southeastward at 18.2 mm/yr (Mora-Páez et al., 2019). Different subduction styles and angles along the Pacific and Caribbean margins in northwestern South America seem to be promoted by contrasting conditions of the seafloor relief, age, thickness, thermal structure, and converging velocity of the subducting slabs (Figure 1).

The Andean Volcanic Arc between 5°N and 40°S is the result of the subduction of the Nazca plate beneath the western margin of the South American plate. Subduction geometry is characterized by along-strike variations of the subducted Nazca plate from normal to steep segments (> 25°), where active volcanism occurs, to subhorizontal flat-slab segments (< 10°), where the continental-margin volcanic arc is interrupted by volcanically inactive gaps. In this sense, the Peruvian and the Pampean flat-slab segments in South America have recorded the shifting, expansion, and cessation of the volcanic arc through time (Ramos, 1999), and they are associated with the subduction of the Nazca and Juan Fernandez aseismic ridges, respectively. In Colombia, Nazca-related volcanism ceased north of ~5°N and there is not known volcanism linked to the subduction of the Caribbean plate.

Although there is a consensus regarding the active nature of the continental margin along the Pacific and Caribbean coasts of Colombia, there is still debate about the limits of the oceanic Nazca and Caribbean plates and their subduction geometries beneath South America, which suggest complex interactions along these plates. Based on geophysical modeling, earthquake distribution, geodetic data and geologic observations, different models of the tectonic

configuration in northwestern South America have been proposed by several recent studies providing interpretations of the possible interactions among the plates.

Most of the competing hypotheses regarding the structure and interaction between the plates consider two key aspects: the distribution of the Wadati-Benioff seismicity beneath Colombia which is located in two bands with a right-lateral offset of ~250 km at approximately 5.5°N and the northern termination at this latitude of the north-south active volcanic arc. Some authors attribute the southern segment to the subduction of the Nazca plate and the northern segment to the Caribbean plate (Penington, 1981; Taboada et al., 2000; Vargas & Mann, 2013; Vargas, 2020), whereas another group of models attributes the southern and northern segments to a Nazca origin (Chiarabba et al., 2015; Syracuse et al., 2016; Wagner et al., 2017). Although different interpretations have been proposed, seismicity patterns and tomographic studies have not been conclusive to definitively link the northern segment to the Caribbean slab, the Nazca slab, or both (Wagner et al., 2017).

Pennington (1981) from the analysis of earthquake hypocenter locations and focal mechanisms identified two zones where the intermediate-depth seismicity is clustered beneath Colombia, and interpreted them as segments of the subducted lithosphere. The northern zone known as the Bucaramanga segment extends from about 5.2° to 11°N and comprises the Bucaramanga nest, a small region of the most intense intermediate-depth seismicity globally. The alignment of hypocenters suggests a single Wadati-Benioff zone which seems to be continuous with the Caribbean seafloor northwest of Colombia and it most likely dips at 20–25° toward N109°E. There is no subduction-related volcanism associated with this shallow-dipping Bucaramanga segment. The zone south of 5.2°N is called as the Cauca segment where the slab is continuous with the Nazca oceanic crust subducting beneath South America along the Colombia-Ecuador trench. This segment is dipping at 35° toward N120°E. According to Pennington (1981), the more steeply dipping Cauca segment is separated from the shallow-dipping Bucaramanga segment by a tear or what he called the Bucaramanga-Cauca hinge fault, and this tear is nearly parallel to the dip directions of the segments. He also suggests that the Bucaramanga and Cauca segments appear to represent fragments of one continuous plate which was divided into two during subduction.

Hilst & Mann (1994) used seismic tomography and earthquake hypocenters to investigate the complex structure below northwestern South America and obtained additional information mainly about the Bucaramanga slab defined by Pennington (1981). Their tomographic images

revealed two slab structures north of the Panama arc in the Caribbean region: the one, a shallow-dipping slab called the Maracaibo slab with an estimated dip angle and dip direction of 17° and 150°, respectively. The other, a steeper structure that coincides with the southern part of the Bucaramanga segment (Pennington, 1981), referred to as the "redefined Bucaramanga slab" with an average dip of 50° in the direction of 125°. The "redefined Bucaramanga slab" extends as far as 10°N and correlates to the oceanic Nazca plate, whereas the northern Maracaibo slab correlates to the subducted oceanic plateau of the Caribbean plate. Results suggest an overlap between these two slabs occurring over a lateral distance of ~250 km. Further south of the study region, the Cauca segment is found, closely related to the subduction of the Nazca plate.

Vargas & Mann (2013) from earthquake distribution combined with coda-wave attenuation images exposed the presence of the ~240 km long east-west-oriented slab tear at ~5.6°N latitude which is called the Caldas tear. This separates the southeastward shallow subduction (20°–30° dip) related to the down-dip extension of the Panama arc to the north from eastward steeper subduction (30–40° dip) of the Nazca oceanic plate with ~15–22 km depth crustal thickness to the south. Vargas & Mann (2013) proposed that the Panama arc coupled with the Caribbean plate has acted as a tectonic indenter in northwestern South America since 9–12 Ma, promoting the segmentation of the Wadati-Benioff zone seismicity which is collinear with the Sandra oceanic spreading rift. In northern Panama

Figure 1: Main tectonic structures involved in the tectonic setting of Colombia. WC: Western Cordillera, CC: Central cordillera, EC: Eastern Cordillera.

Arc, the Caribbean oceanic plateau whose thickness is greater than 20 km subducts with an angle of < 15° dip. The Caldas tear lithospheric weakness zone is considered to be the current border between the Nazca and Caribbean plates (Figure 2a).

Chiarabba et al. (2015) from earthquake relocation and body wave tomographic images highlighted the offset of the Wadati-Benioff zone at 5°N and interpreted this as an EW slab tear along which the Nazca plate is segmented. This interpretation is different from that given by Vargas & Mann (2013) who attributed this tear to the limit between the Nazca and Caribbean plates. The tear separates a steeper Nazca segment to the south from a shallowly dipping subduction to the north which extends from the Colombia-Ecuador trench to the Eastern Cordillera so that the Nazca plate is subducting as far north as the limit between the Panama Arc and the Caribbean plate, and the Bucaramanga nest is part of this subduction. Flat subduction geometry was associated with the high plate interface coupling caused by the entry of a young thick-buoyant oceanic crust into the trench. The slab tear is aligned with the Coiba transform fault, separating the Coiba and Malpelo microplates (Sallarès et al., 2003), which seems to have served as a preexisting plane of weakness to cause tearing. The absence of volcanism at latitudes > 5°N is in accordance with the change from steeper to shallow subduction. Chiarabba et al. (2015) proposed that the lack of a volcanic arc is the result of the strong coupling between plates which creates a barrier for upward fluid migration avoiding the mantle wedge hydration and melting from observations of V_p/V_s ratios below the Eastern Cordillera. Although they were unable to image the southern part of the Caribbean plate, they suggested that the subduction of the Caribbean plate should be located north of the Bucaramanga nest.

Syracuse et al. (2016) from hypocentral relocations and V_p and V_s models resulting from the joint inversion of local body wave arrivals, surface wave dispersion measurements, and gravity data pointed out the existence of a tear in the Nazca slab at 5°N agreeing with the model proposed by Chiarabba et al. (2015). This tear could have been formed upon subduction of a zone of weakness in the plate such as the Sandra Ridge (Vargas & Mann, 2013) (or Coiba transform fault, Sallarès et al., 2003). North of the tear, the slab is flat based on the low dip angle of seismicity in the Bucaramanga segment down to 100 km depth but further east it gradually steepens reaching a maximum of 160–190 km depth. Syracuse et al. (2016) found differences in seismicity patterns between two portions of this segment north and south of 7.5°N, suggesting that the northern slab from this point may have a Caribbean origin and that the boundary between Nazca and Caribbean plates could be related to the Bucaramanga nest (Figure 2b).

Regarding the Caribbean subduction, the slab seismicity is not continuous between the Caribbean trench and the intermediate-depth earthquakes in the southern Caribbean segment suggesting flat-slab subduction. An explanation for the lack of continuity in shallow seismicity may include poor station coverage in northern Colombia by the National Seismological Network of Colombia (RSNC) of the SGC, relatively slow convergence between the Caribbean and South American plates resulting in a lower seismicity rate and abnormal stress patterns within this segment due to subduction of the Caribbean large igneous province. It is also possible that tectonic tremor is present here, although it has not yet been observed.

The Bucaramanga-Cauca boundary also marks a north-south transition from non-volcanogenic to volcanogenic portions of the subduction zone. Two factors may contribute to the lack of volcanism in flat-slab systems: the lesser hydration of the incoming plate limiting the melting of the mantle wedge and arc formation, and the thermal structure of the slab and mantle wedge. Flat slabs are often associated with locations of aseismic ridges and thickened incoming plate and may be linked to the subduction of a buoyant slab.

Wagner et al. (2017) through compilation of ages of igneous rocks and locations over the past 14 Ma concluded that the Nazca plate extends north of the Caldas tear comprising part of the flat slab, but they were unable to set how far to north the Nazca plate extends or where the boundary between the Nazca and Caribbean plates is located (Figure 2c). They found no evidence for different volcanic activity before 3.5 Ma over the current location of the Caldas tear, which suggests that the segment subducting north of the tear today belongs to the same plate that is subducting south of this tear, in contradiction to earlier studies proposing that the offset represents the boundary between two different plates (Vargas & Mann, 2013). Wagner et al. (2017) proposed that young age of the oceanic crust along both sides of the Sandra Ridge provided the plate buoyancy which facilitated the gradual formation of an initial broader flat slab geometry from ~3°N to 7°N (between 9 and 5.9 Ma), but as the age increases on both sides of the ridge far from the axis, the buoyancy is reduced. The preservation of the flat slab north of the ridge may be due to the subducted buoyant feature previously proposed by Chiarabba et al. (2015) but the flat slab to the south has no such buoyant feature. The Sandra Ridge may have provided a zone of weakness along which the southern flat slab, once gravitationally unstable, began to sink and could fail after 4 Ma.

The most recent tectonic model, which was elaborated by Vargas (2020) based on earthquake distributions, gravity forward modeling and b-values, highlighted three subduction

scenarios in northwestern South America showing variations in the subduction geometries along the Pacific and Caribbean margins. The northernmost scenario corresponds to a slab with low subduction angle (12 to 24°) related with the Caribbean plate. The central scenario, between 5.5° and 7°N approximately, proposed a possible transition zone between the Nazca and Caribbean plates north of the Caldas tear. And, the southern scenario proposed a steeper subduction slab (~30–34°) associated with the Nazca plate. Vargas (2020) also found other minor tears in the lithospheric system, in addition to the Caldas lithospheric tear (Vargas & Mann, 2013). These minor tears could play relevant roles in mechanically accommodating changes in the dips and strikes of the Caribbean and Nazca Plates under northwestern South America.

Scarce seismicity in northwestern Colombia including the continental areas of Sinú-San Jacinto, Lower Magdalena Basin, Panamá and Santa Marta Massif suggests low activity that increases eastward and deeper. An interpretation of this pattern is related to the change in the subduction angle of the Caribbean plate under the South American plate from ~12° to > 24° under Middle Magdalena Basin Valley. Although a flat subduction of the Caribbean plate is proposed (Chiarabba et al., 2015; Syracuse et al., 2016), observations suggested a steepest subduction angle near the Santa Massif, north Colombia and

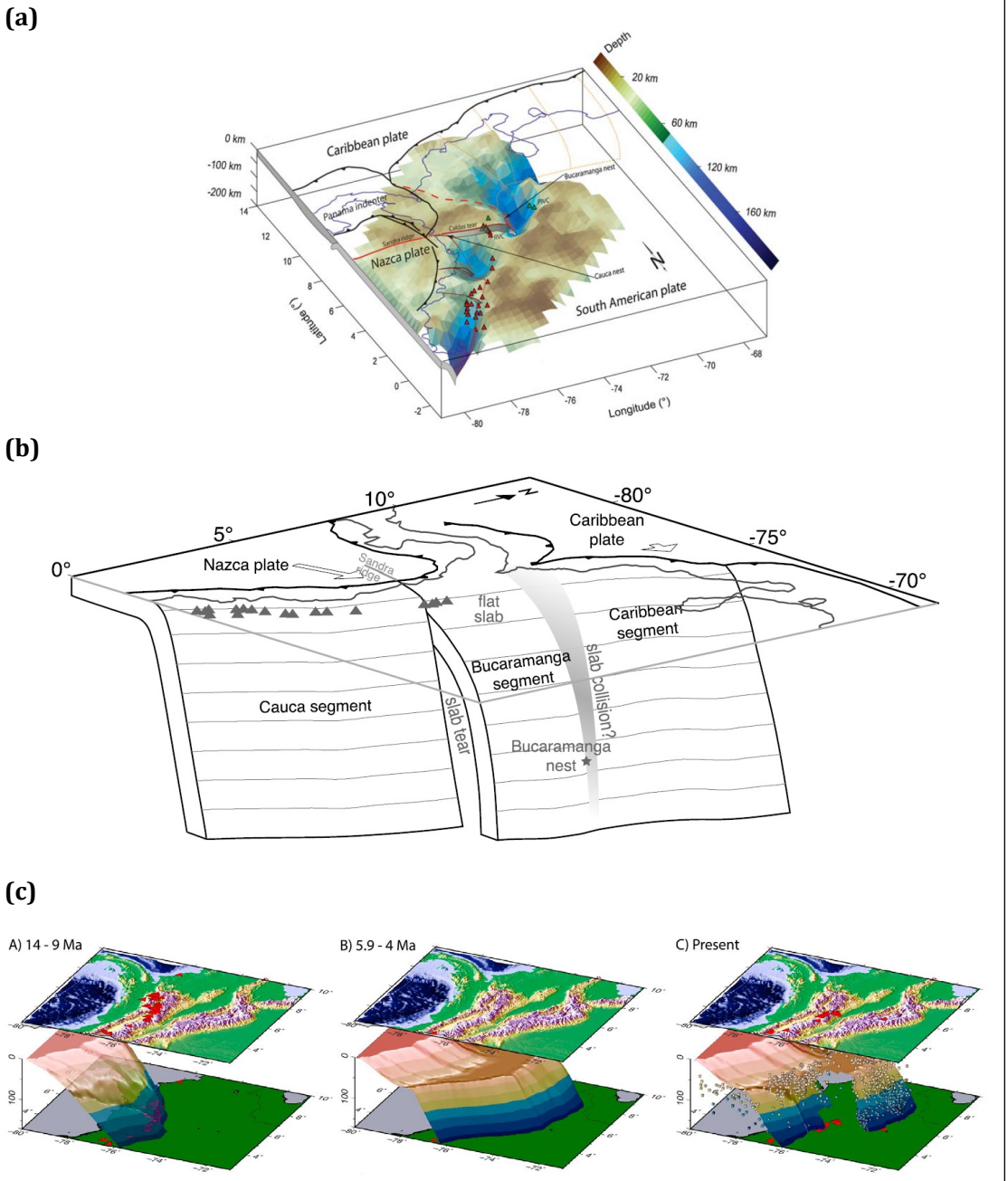

Figure 2: Different models related to the tectonic setting in Colombia. (a) the model presented by Vargas & Mann (2013), (b) the model presented by Syracuse et al. (2016), (c) the model presented by Wagner et al. (2017).

Venezuela, which could mean an alternative change from flat subduction in the south (near the Caldas tear) to steeper subduction in the north, changing the strike of the subduction surface in the north as well.

2.2 Historical earthquakes

Because the earthquake cycle is a long-term process, studies of different earthquakes over a long-time interval are essential for thorough understanding of earthquake phenomena. Due to the rapid convergence of Nazca plate beneath the North Andean block, with a rate of 54 mm/yr (Mora-Páez et al., 2018), an intense crustal deformation has been caused, and consequently several large to great earthquakes occurred along the Colombia-Ecuador subduction zone. Some of the earthquakes were highly destructive, caused tsunami and generated significant human and economic loss as well as secondary environment effects.

The large subduction earthquakes have ruptured along this subduction zone between Guayaquil in Ecuador and Tumaco in Colombia, and some of them generated destructive tsunamis: The 1942 earthquake (M_w 7.8) (Swenson & Beck, 1996), which ruptured again in 2016 (M_w 7.7) (Yoshimoto et al., 2017a; Nocquet, et al., 2017; Ye, et al., 2016), the 1958 (M_w 7.7) and 1979 (M_w 8.1) earthquakes, and the largest in 1906 (M_w 8.4–8.8) (Figure 3).

Kanamori & McNally (1982) estimated the size of the 1906 earthquake to be M_w 8.8, and considered that the earthquakes in 1942, 1958 and 1979 ruptured separate portions of the plate boundary segment that was previously ruptured during the 1906 earthquake. They concluded that the sum of the seismic moment of the 1942, 1958 and 1979 events is five times smaller than that of the 1906 event, and explained the difference based on the asperity model. They suggested that the fault zone is held by asperities distributed between zones considered as week zones.

Mendoza & Dewey (1984) relocated the seismic activity associated with the 1942, 1958 and 1979 earthquakes and showed that aftershock distributions of these earthquakes were consistent with the hypothesis that each shock involved interplate thrust faulting along the independent portions of the plate boundary.

Yoshimoto et al. (2017a), by analyzing tsunami waveforms associated with the 1906 earthquake, estimated M_w 8.4 for this earthquake, and showed that the slip occurred near the trench off the source of the three large events in 1942, 1958 and 1979; therefore, the 1906

earthquake ruptured the offshore region without overlaps of the source of regions of the three large events. Thus, along CESZ there must be two rupture domains: one near the trench and the other near the coast, and this feature points to the existence of a depth-dependent complex rupture mode along the subduction region. Thus, the Colombia-Ecuador subduction zone is probably one of the best examples of different modes of earthquake ruptures.

Regarding the Caribbean region, several large to great earthquakes have occurred in the eastern and northeastern parts of the Caribbean Plate, and in the past 500 years more than 75 tsunamis have been documented in the Caribbean and adjacent regions (Hillebrandt-Andrade, 2013). However, large earthquakes in the northwestern part of Colombia or southern part of the Caribbean plate have not been reported in either historical or instrumental records.

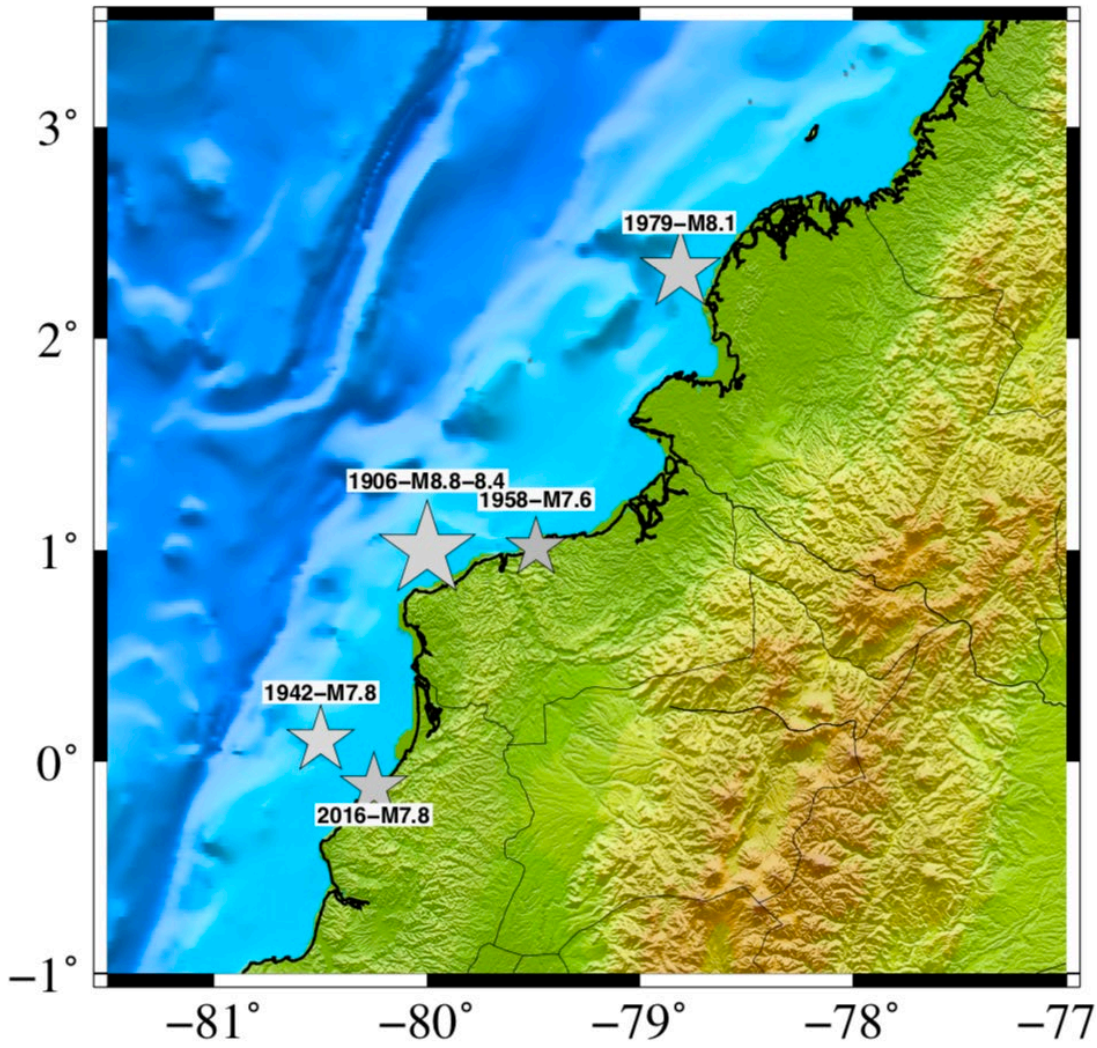

Figure 3: Historical earthquakes larger than magnitude (*M*) of 7 that occurred along the Colombia-Ecuador subduction zone between 1900 and 2020.

CHAPTER 3

3. SLOW EARTHQUAKES

VLF earthquakes are the principal focus of this chapter. They are one member of a special class of earthquakes called slow earthquakes, a new and exciting branch of seismology. VLF earthquakes are linked intimately to processes involving other members of the slow earthquake family and I introduce a general context of slow earthquakes.

Slow earthquakes provide phenomenological evidence for the existence of a transition zone between locked and creeping zones proposed by thermal modeling studies and the partial release of slip deficit (Obara & Kato, 2016). The recurrence time associated with the megathrust earthquake occurrence such as the Sumatra earthquake in 2004 (M_w 9.1) or the Tohoku-oki earthquake in 2011 (M_w 9.0), is highly related to the plate convergence rate. However, whether slip occurs downdip or updip of the locked interplate region in the transition zone, the recurrence time of the megathrust earthquake could be notably affected. Therefore, it is important to further understand slow earthquakes and to uncover how the slow earthquakes could affect the seismic hazard estimation along the subduction zone.

This interesting branch of seismology has been studied intermittently over the past 50 years (Beroza & Ide, 2011) throughout the improvement of the long-period seismographs (e.g. Benioff & Press, 1958) and the development for mathematical models for aseismic slip faulting (e.g. Yamashita, 1980). Slow earthquakes are a distinct group of earthquakes whose main characteristic is the long time needed to release their energy during their slip. This time can be relatively longer than the time taken by classical earthquakes to release their energy. Slow earthquakes release the energy slower than regular earthquakes; thus, these earthquakes are called slow earthquakes.

Slow earthquakes are most often observed outside of seismogenic zones in subduction zones. Due to the interaction between continental and oceanic plates, there is a contact area where the two blocks are locked. When the oceanic plate slides under the continental plate, the latter one is dragged and accumulates shear stress. When the stress is accumulated and has reached a limit, a sudden slide occurs on the fault plane. This is what is known as a regular earthquake, capable of generating strong shaking and tsunamis. However, just at the moment when the stress is built up to the limit, an unusual slow slide occurs on the fault plane, this is what is known as a slow earthquake. The slow earthquakes can be represented through different seismic signals. The

signals vary according to how fast or slow is the sliding on the fault plane. Therefore, different phenomena can occur during the slow slide process, and they are described in detail in Figure 4.

Slow earthquakes show an intermediate type of fault slip that changes between the fast rupture of regular earthquakes and stable sliding along a megathrust fault interface, and they have most often been reported in subduction zones along the interface between the subducting slab and the overlying crust where the frictional regime changes from brittle to ductile known as the frictional transition zone (Obara & Kato, 2016). Slow earthquakes and classical earthquakes differ in several important respects even though slow earthquakes are located on the same faults that host ordinary, fast earthquakes. They grow steadily, rather than explosively, with time, and their stress drops are low (Brodsky & Mori, 2007; Ide et al., 2007; Beroza & Ide, 2009). There is a wide range of characteristics in the source time properties of slow earthquakes that allow to discover several mechanisms of the relaxation of accumulated stress in the transition zone. They can be grouped in two distinct categories, geodetic and seismic events: The geodetic slow earthquakes are known as slow slip events (SSE), and are characterized by either long-term duration from months to years or short-term duration from days to few weeks. The other category is the family of slow earthquakes that includes VLF earthquakes with dominant periods ranging between 20 to 50 seconds, low-frequency earthquakes with dominant frequencies of several Hz, and non-volcanic tremors, in the 1–10 Hz frequency band (Obara, 2002; Beroza & Ide, 2011; Obara & Kato, 2016; Ito et al., 2007).

Some examples of slow earthquakes are shown in Figure 4. It is important to highlight that the different kinds of slow earthquakes do not occur as independent

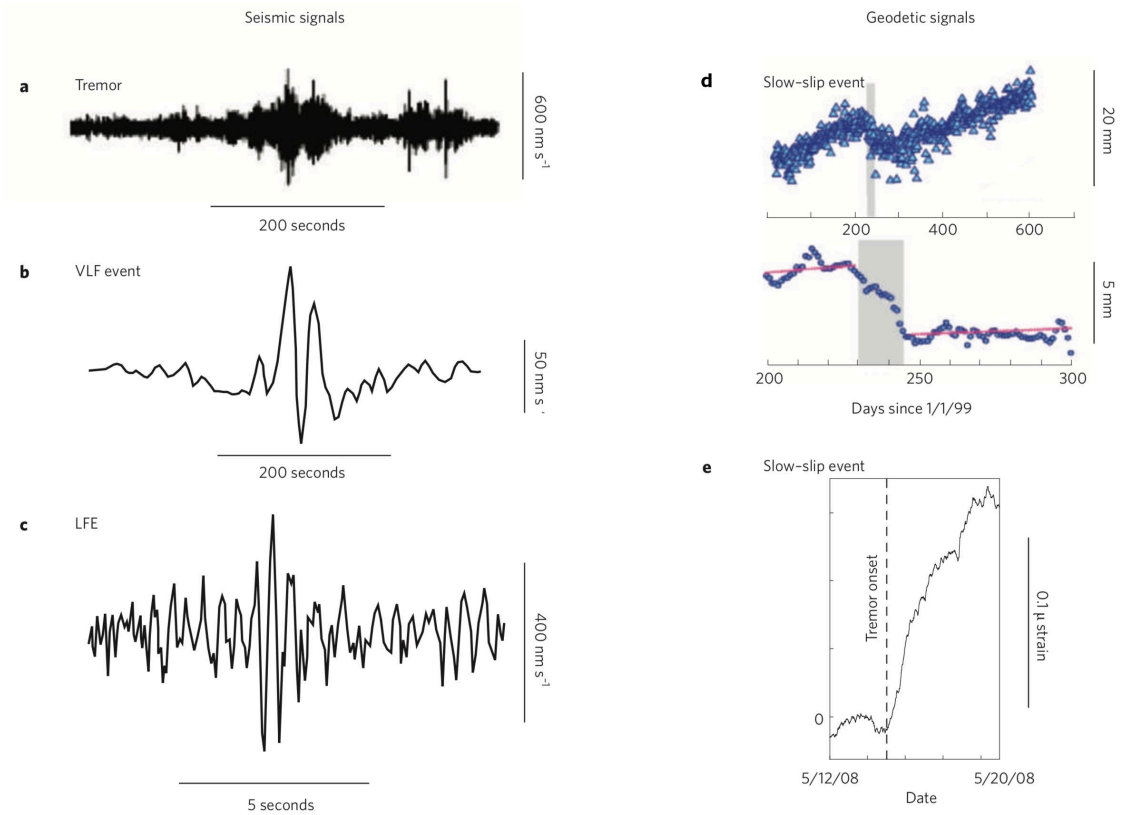

Figure 4: Different examples of slow earthquakes. (a) Tremor and (b) very-low-frequency (VLF) earthquakes from Japan, filtered between 2–8 and 0.005–0.05 Hz, respectively. (c) Low-frequency earthquakes (LFE) from Japan. (d) Top: daily GPS EW displacement measured on Vancouver Island; Bottom: averaged and detrended GPS data (pink lines show the fit trend) indicating a slow-slip event (shaded). (e) Slow slip in differential shear strain measured in western Washington. Strain transient onset coincides with increased tremor activity. Modified from Peng & Gomberg (2010).

phenomena. They have been found in several studies, occurring simultaneously in the transition zone.

Many of the discoveries concerning slow earthquakes have been successful because of implementing a new generation of relatively densely spaced and highly sensitive earthquake-monitoring networks that have enhanced such phenomena detectability. Slow earthquakes have been observed in subduction zones along the Pacific Rim in Japan, Cascadia, Alaska, Mexico, New Zealand, and Costa Rica.

3.1 Slow-slip earthquakes

Slow slip events, categorized as geodetic slow earthquakes, are a group of events whose main characteristic is their long duration process, which can vary from days to years. According to duration process, slow-slip events (SSE) can be classified as short-term SSE for event duration of days and long-term SSE for event duration of days or months. In several subduction zones, SSE have been observed to occur in the downdip part of the seismogenic zone. The short-term SSE occurred closed to the deeper stable sliding zone, while long-term SSE occurred near the shallower seismogenic zone. This behavior can be attributed to the thermal properties of the plate interface (Obara & Kato, 2016; Schwartz & Rokosky, 2007). SSE can initiate in or near the seismogenic zone, and the slow slip on fault does not radiate significant seismic energy; therefore, SSE can hardly generate energetic seismic waves, and if they generate some detectable waves, they are usually weak compared to an ordinary earthquake of the same size (Beroza & Ide, 2011).

Schwartz & Rokosky (2007) showed that seismic moment grows with the cube of the duration time for ordinary earthquakes, and seismic moment of SSE grows linearly with the duration. Since SSEs take longer time scales to drive their processes, they are not detected with standard seismic techniques. However, thanks to the improvement of monitoring networks, several reported SSE observations have been possible through continuous GPS networks that have helped to increased geodetic observations for the recording of this important class of geophysical phenomena (Schwartz & Rokosky, 2007). In general, geodetic slow earthquakes can be observed by using tiltmeters, strainmeters, or GPS networks (Figures 4d and 4e).

3.2 Non-volcanic tremor

Obara (2002) identified first in the Nankai Trough subduction zone of Japan a new source of seismic waves, nonvolcanic deep tremor, that is a weak but long duration train of shaking of the Earth. These new seismic waves were identified by using the high-sensitivity seismograph network (Hi-net) from the National Research Institute for Earth Science and Disaster Prevention (NIED), consisting of about 600 stations deployed throughout Japan to detect microseismicity. Before the deployment of Hi-net was difficult to identify nonvolcanic tremor using a single station or a few sparse stations due to small amplitudes of these seismic waves.

The small amplitude of the waves generated by non-volcanic tremors makes difficult to distinguish impulsive waves as in regular earthquakes; therefore, determining the hypocenter location of non-volcanic tremors is difficult using the conventional hypocenter determination methods (Figure 4a). Hypocenters of nonvolcanic tremor were estimated by the waveform envelope propagation, and Obara (2002) determined that the tremor was originated at depths of about 30 km near the Mohorovic discontinuity.

Active periods of nonvolcanic tremor lasted for a week or more and migrated laterally along the subduction zone near the seismic-aseismic transition on the plate interface. Individual tremor episodes typically lasted for tens of minutes with dominant seismic frequencies of 1 to 10 Hz (Rubinstein et al., 2010). This tremor is called nonvolcanic tremor because there is a different kind of tremor, volcanic tremor, often observed at active volcanoes.

Important properties are recognized in nonvolcanic tremors. Obara (2002) observed that tremor is episodic; some periods of concentrated activity lasting from days to weeks can be interrupted by longer periods of months with low or none tremor activity. He also found that tremor does not always remain in one region in an episode but tremor slowly migrates along strike with velocities of about 13 km day $^{-1}$. This migration could be related with the role for fluids in the dehydration process and could exhibit some similarities between nonvolcanic and volcanic tremor. Obara (2002) also found that occasionally, tremor contains relatively energetic and isolated pulses with predominant frequency of about 1 to 2 Hz, and these signals were identified as low frequency earthquakes. Shelly et al. (2007) demonstrated that this episodic tremor can be understood as a swarm of small, low frequency earthquakes, each one occurring as a shear faulting on interface region in the subduction zone. This suggests that tremor and the low frequency earthquakes can be a different manifestation of a single process.

3.3 Low-frequency earthquakes

Low-frequency earthquakes (LFEs) were found first in Japan; however, they were ignored before discovering these earthquakes because these events did not show a clear *P*-wave arrival. Despite this, the hypocenter determination was obtained through their *S*-wave identification; thus, LFEs were first cataloged as small earthquakes with anonymously low dominant frequencies (1–5 Hz) by the Japanese Meteorological Agency (Figure 4c) (Katsumata & Kamaya, 2003). LFEs were linked to non-volcanic tremor by Obara (2002). Nonvolcanic tremor was often observed to contain catalogued LFEs, and consequently, nonvolcanic tremors were suggested to be made up of many LFEs (Shelly et al., 2007). More careful analysis of LFEs showed that during periods of activity, a single LFE source produced many events over time (Shelly et al., 2006). Given that the source and the recording network are the same, each LFE source could therefore be defined by a set of characteristic waveforms, or templates, that could be used to find the rest of the events originating from the same source. Using the catalogued LFEs as templates, Shelly et al. (2007) showed that the overwhelming majority of LFEs provoked by the same source occurred within nonvolcanic tremor, which was evidence for the previous statement that nonvolcanic tremor is nothing more than a swarm or burst of LFEs. LFEs have been used as a proxy to characterize nonvolcanic tremor, given that LFEs are much more impulsive than nonvolcanic tremor with detectable phases and their above-mentioned close relationship among them.

The locations and focal mechanisms of LFEs are more robustly determined than nonvolcanic tremors thanks to impulsive arrivals and distinct phases, and they have proven to be similar to those of nonvolcanic tremors. Shelly et al. (2006) performed relocations of LFEs, providing a precisely relocated LFEs catalog, and showed that all LFEs occurred along the subduction interface; similar results have been found in other subduction zones in Costa Rica (Brown et al., 2009), Cascadia (Royer & Bostock, 2014), and Mexico (Frank et al., 2013).

3.4 Very-low-frequency earthquakes

VLF earthquakes were first identified in Japan in 2003 by Ishihara along the Nankai trough. This new type of earthquakes was registered by the broadband seismographs of F-net. VLF earthquakes were seen as anomalous events with their long-period waveforms, around 10 to 20 s with few or none high-frequency components (Figure 4b).

Ito & Obara (2006) detected VLF along the Nankai trough, Japan. The locations of VLF sources fell within the accretionary prism over the plate boundary between the Philippine Sea and Eurasian plates. They were distributed at depths near 10 km and within 50 to 70 km landward from the trough axis. The estimated fault mechanisms reveled the occurrences of VLF events with reverse faulting, and Ito & Obara (2006) concluded that VLF earthquakes were excited by the dynamic deformation of the accretionary prism.

Subsequently, Ito et al. (2007) examined data from Hi-net and F-net, and tested different filters varying between 1 to 0.005 Hz to identify some other unidentified long period waveforms radiated from the transition zone. Finally, by using a bandpass filter between 0.02 and 0.05 Hz clear anomalous seismic signals with VLF energy radiated from the transition zone were identified. Ito et al. (2007) estimated the apparent velocity from arrival times to be a value of 6 km/s, which indicated that the observed VLF signals consist of body waves. They also found several VLF seismic events and characterized them as follows: The VLF events were coincident with nonvolcanic tremor and slow slip events. The hypocenter locations for these events were along the strike of the subducting Philippine Sea plate, similar to the belt-like distribution of the nonvolcanic tremor and the slow slip events, and their estimated magnitudes were ranged between 3.1 and 3.5. Their fault mechanisms estimated by moment tensor solutions were explained by thrust faulting. Ito et al. (2007) concluded that after comparing a VLF event with a regular earthquake, both with a similar magnitude around 3.4 and very similar epicentral distance and depth, both events have a low-frequency component with similar amplitudes in the range of 0.02 to 0.05 Hz. However, high-frequency components between 2 and 8 Hz are not clearly visible in the VLF event. The monitoring of both nonvolcanic tremors and VLF earthquakes may be useful to assess the stress on the rupture zone of a megathrust earthquake. This is because the shear stress on the asperity of the megathrust earthquake may increase as a result of slow earthquakes in the downdip portion of the subduction zone. VLF earthquakes are also useful indicators for estimating the stress condition of the rupture zone of an anticipated megathrust earthquake (Ito et al., 2007).

According to the above-mentioned findings, it is possible to establish two categories of VLF earthquakes, one called shallow VLF earthquakes occurring in the shallow part of the accretionary prism (Ito & Obara, 2006), and the second one called deep VLF earthquakes occurring in the downdip portion of the subduction zone (Ito et al., 2007). The shallow VLFs are consistent with deformation of the accretionary prism, and the deep VLFs are consistent with plate-boundary slip (Beroza & Ide, 2011).

Moreover, deep VLF earthquakes accompanying tremor have been found in some subduction zones, such as the Nankai trough (Ito et al., 2007), the Cascadia subduction zone (Ghosh et al., 2015), and the Meso-American subduction zone (Maury et al., 2016). Shallow VLF earthquakes have been found in off shore regions near trenches, along the Nankai trough (Ito & Obara, 2006a), off-Tokachi, the southern part of the Hokkaido Pacific coast along the Kuril Trench (Asano et al., 2008), the Ryukyu Trench (Ando et al., 2012), off the Tohoku Pacific coast along the Japan Trench (Matsuzawa et al., 2015), and offshore of the Nicoya Peninsula, Costa Rica, along the Middle America Trench (Walter et al., 2013).

According to the observations mentioned above, it is important to highlight that different types of slow earthquakes have been detected in Nankai and Tohoku regions both with similar monitoring conditions. Shallow and deep VLF earthquakes in Nankai and very few shallow VLF earthquakes in Tohoku suggest that different frictional properties exist in the different subduction environments. The differences may be attributed to different thermal structure and fluid processes associated with the pore pressure and the coupling level (Matsuzawa et al., 2015).

CHAPTER 4

4. REPEATING EARTHQUAKES

4.1 Definition of repeating earthquakes

Repeating earthquakes are two or more earthquakes with similar waveform and location, rupturing the same asperity in different times, and can be detected with sensors located in permanent locations. Slight variations among repeating earthquakes can be related to small changes in source properties and/or in material properties of the surrounding rock. Different studies have reported the occurrence of repeating earthquakes in transform and subduction plate boundary fault systems, and the focal mechanism is also similar among repeating earthquakes (Uchida, 2019; Lengliné & Marsan, 2009).

4.2 Detection of repeating earthquakes

Different techniques and criteria have been used to detect repeating earthquakes. Confined earthquakes or distributed in a relatively small volume is an essential consideration to detect repeating earthquakes; therefore, an accurate hypocenter determination to estimate colocation of earthquakes is a straightforward way to identify repeating earthquakes (Lengliné & Marsan, 2009). High resolution hypocenter location by using ordinary travel time measurements and cross correlation of differential time measurement of direct *P* and *S* waves provides location accuracy better than the source sizes of earthquakes (Waldhauser & Ellsworth, 2000). Other useful method to estimate relative locations is a master-event algorithm used by Yu (2013). The source sizes are usually estimated by assuming typical values of earthquake stress drop. Colocation between two earthquakes is obtained when source areas are completely overlapped, however, the minimum overlapping areas commonly used to identify repeaters range from 50 % to 70 % (Lengliné & Marsan, 2009). One limitation by using this method is related to performance of the network stations since accurate hypocenter locations are not always available due to limited station coverage and/or timing accuracy (Uchida & Bürgmann, 2019).

Another different way to identify repeating earthquakes is to establish waveform similarity, even when earthquake locations are not well accurate. If the Earth structure and the observation location did not change, a common travel path from the earthquake source to the

station ensures highly similar waveforms. Therefore, a way to assess the similarity between earthquakes is to use the cross-correlation technique. Many studies have detected repeating earthquakes by using waveform correlation (Igarashi et al., 2003; Li et al., 2011; Kimura et al., 2006; Yu, 2013). A wide range of a cross-correlation coefficient threshold from 0.8 to 0.98 has been used, and threshold selection is related to the network coverage and noise levels. However, most of repeating earthquake studies commonly used the thresholds ranging from 0.90 to 0.98. Waveform coherence has been also used for the detection of repeating earthquakes with thresholds from 0.95 to 0.98. This method has a detection ability similar to that of cross correlation (Lengliné & Marsan, 2009; Dominguez et al., 2016). After detection of repeating earthquakes, careful analysis must be done to discard triggered events by nearby large earthquakes or aftershocks due to a main event.

4.2 Mechanism of repeating earthquakes

Previous studies interpreted repeating earthquakes as repeating ruptures in isolated asperities distributed over the interplate boundary due to the accumulated stress in each small asperity caused by the aseismic slip of the surroundings area. According to this interpretation, the distribution of repeating earthquakes is capable to infer aseismic slip in the surrounding area of the repeating earthquakes (Figure 5).

Igarashi et al. (2003) proposed the existence of two types of repeating earthquakes: burst and continual types. The burst-type repeating earthquakes are generated by nearby large earthquake and the subsequent stress build up in neighboring areas. Small asperities are surrounded by creeping regions, and these small asperities are distributed around a large asperity on the interplate boundary capable to cause large earthquakes, thus burst-type repeating earthquakes are generated by ruptures of the small asperities after a large interplate earthquake which is originated as slip of the large asperity on the interplate boundary. The released stress by the large earthquake accelerates the aseismic slip on the stable sliding region, and this aseismic slip increases stress over the small asperities and generates the repeating ruptures over short time periods. Burst-type repeating earthquakes can also been generated after a large interplate earthquake, when a preexisting fault plane near the interplate boundary region and small asperities surrounded by creeping region is activated. Therefore, it is possible that the burst-type events occur on preexisting fault planes within the overriding plate or along the plate boundary.

Continual-type repeating earthquakes are generated by the stress accumulation in the same small asperities surrounded by creeping region with fairly similar slip. It is expected that such mechanism occurs in a tectonic environment involving an interplate fault boundary system. Even if there are small asperities embedded in a creeping region on a preexisting fault within the plate, the averaged slip rate of the stable sliding is thought to be much smaller than the slip rate at the plate boundary; therefore, the amount of times that the asperity ruptures on the plate boundary would be much smaller than the times that the asperity ruptures on the fault. That is why the possibility to detect the repeating earthquakes on the plate boundary is more expected than within the plate. Thus, Igarashi et al. (2003) concluded that repeating earthquakes of continual type are expected on the plate boundary.

4.3 Previous studies of repeating earthquakes

Repeating earthquakes were first reported in the transform plate boundary along the Parkfield segment of the San Andreas fault (SAF) in California (USA). Waveform data registered by the borehole network of broadband seismographic stations for ten years were analyzed. The data showed that the seismicity in this region was clustered in sequences of two or more quasi-periodic earthquakes having the same hypocenter location and identical

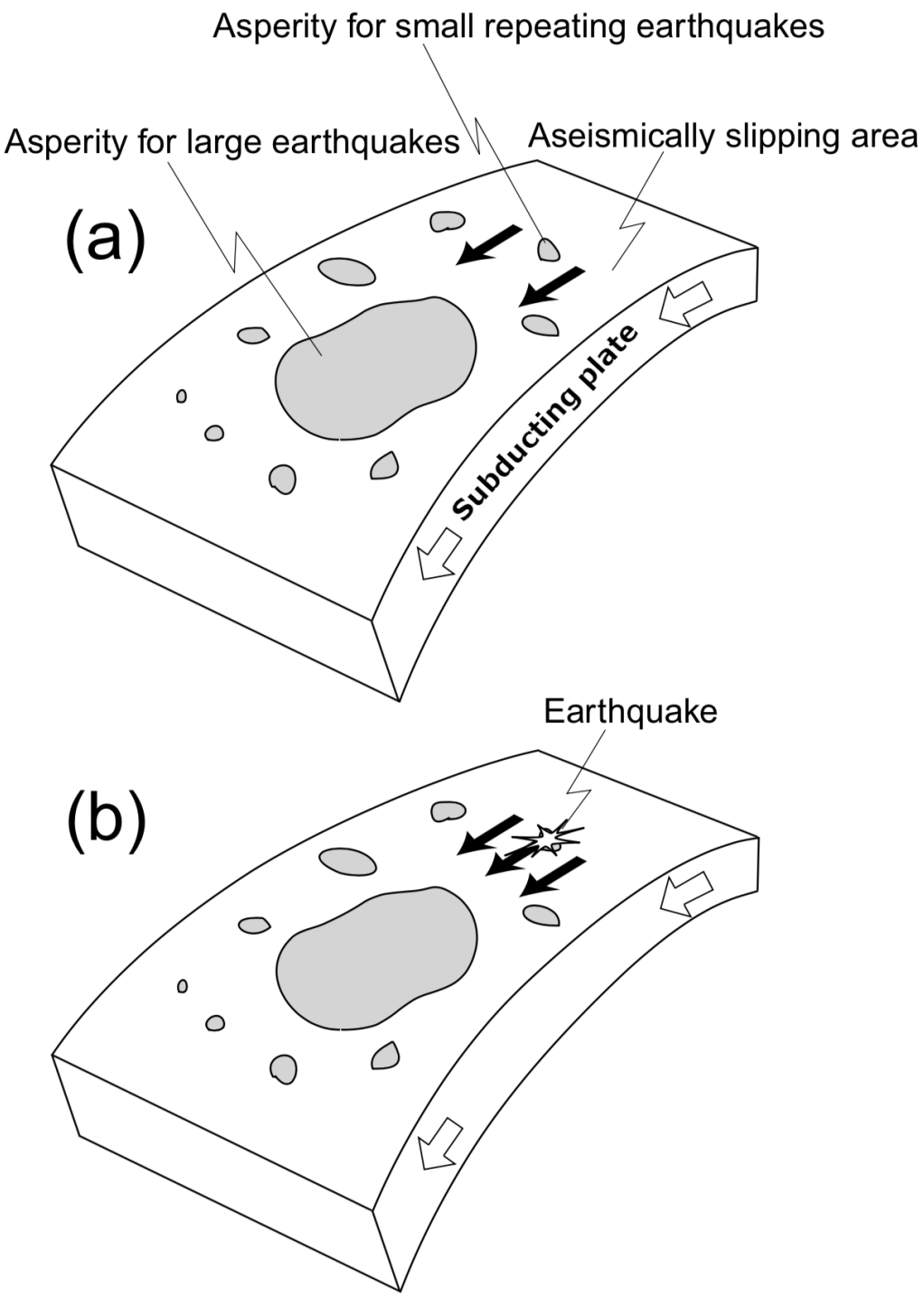

Figure 5: Schematic illustration showing the asperity distributions surrounded by the aseismic area in the boundary plate region. Various sizes of asperities are distributed on the plate boundary. (a) Areas other than asperities slip aseismically, and (b) small asperities eventually rupture as earthquakes, and they can rupture recurrently, generating the repeating earthquakes. Modified from Matsuzawa et al. (2004).

seismic waveform. Nadeau & Johnson, (1998) established an important scaling relationship between the amount of slip (d) and the scalar moment (M_0),

$$\log d = -2.36 + 0.17 \log M_0,$$

where the units of d, and M_0 are cm and dyne cm, respectively (Nadeau & Johnson, 1998).

There are other studies reporting the occurrence of repeating earthquakes in the strike-slip tectonic environment: Along the North Anatolian Fault (Turkey) (Bohnhoff et al., 2017) and Queen Charlotte Canada (Hayward & Bostock, 2107).

Along subduction plate boundaries, repeating earthquakes are frequently found in locations with fairly abundant microseismicity and variable interplate coupling in Japan, Vanuatu and Tonga-Kermadek, Costa Rica, and Mexico (Igarashi et al., 2003; Matsuzawa et al., 2004; Uchida et al., 2003; Yu, 2013; Yao et al., 2017; Dominguez et al., 2016).

Repeating earthquakes have been found along well recognized creeping faults and they are located away from locked zones. The area surrounding these large asperities is thought to be weakly coupled, and many small asperities might exist there, then, repeating earthquakes can occur in the surrounding area of large asperities (Igarashi et al., 2003). Repeating earthquakes can be used to determine if the interplate boundary fault is locked or creeping, to provide information about spatial-temporal variations in the quasi-static slip on the plate boundary, and to estimate the interplate coupling (Igarashi et al., 2003; Uchida 2019).

CHAPTER 5

5. METODOLOGY

5.1 Cross correlation

Throughout science, there exist situations to establish a measure of similarity between two quantities, in which the techniques of correlation are need. A review of the early development of the cross correlation techniques and their application in exploration geophysics is explained by Anstey & Lerwill (1966).

The process of cross correlation is useful in comparing two deterministic signals to provide a measure of similarity between two signals. A good method of measuring the similarity between two signals is to multiply them together, and to add the resulting products over a suitable interval. The resulting signal is called cross-correlation function and represents the similarity between the two signals as a function of the shift between them. Let us consider the signals $x(t)$ and $y(t)$ with $y(t) = x(t + \tau)$. Multiplying point by point and adding all the products, $x(t)x(t + \tau)$ for a maximum value is obtained when $\tau = 0$, as the product is the square of the function. Moreover, if $\tau \neq 0$, then the summing the products will result in a lower value, since a positive number times a negative number of results in a negative number and the sum will be less than or equal to the peak value.

For discrete function, of $x(k)$ and $y(k)$, the cross-correlation function is defined by:

$$R_{xy}(k) = \sum_{m=-\infty}^{\infty} x(m)y(m-k),$$

where k and m are integers. The similarity measure between two signals can be established through the correlation coefficient defined by:

$$CC = \frac{R_{xy}(k)}{\sqrt{R_{xx}(0)R_{yy}(0)}}.$$

The correlation coefficient CC always lies in the interval between –1 and 1. Two signals have correlation coefficient equal to 1 when only one of the signals is simply the other multiplied by a positive number. In this case, the signals are said to be perfectly correlated. Similarly, two signals have correlation coefficient equal to –1 when only one of the signals is simply the other

multiplied by a negative number, in which case they are said to be anticorrelated. With observational data, correlation coefficient reaching perfect correlation will almost never be achieved; therefore, values of CC near 1 indicates a high degree of waveform similarity and CC values far from 1 indicates low similarity (Gibbons & Ringdal, 2006). Sample signals are shown in Figure 6.

5.2 Matched-filter technique

The matched filter is a technique to detect a signal of interest with noise embedded in continuous data. A known form of the signal of interest is called the waveform template. The detection is done by computing the correlation coefficient between the waveform template and the continuous signal in a sliding window. As a result of this procedure, a correlation function is obtained. In most of seismology studies, continuous data have multichannels, and the correlation between the waveform template and continuous data results in multiple correlation functions (Figure 7).

To enhance the detection of the signal of interest, the correlation functions are stacked. Stacking plays an important role in improving signal-to-noise ratio (S/R) in seismic data processing. Before the stacking, a time correction is applied to the different correlation functions. Each correlation function is displaced by a shifting time value obtained by measuring the difference between the time at maximum amplitude and the start time of each signal in the waveform template. After applying time correction, the detections of the signal of interest on individual correlation function are aligned and the stacking is performed to improve the signal detection (Gibbons & Ringdal, 2006) (Figure 8).

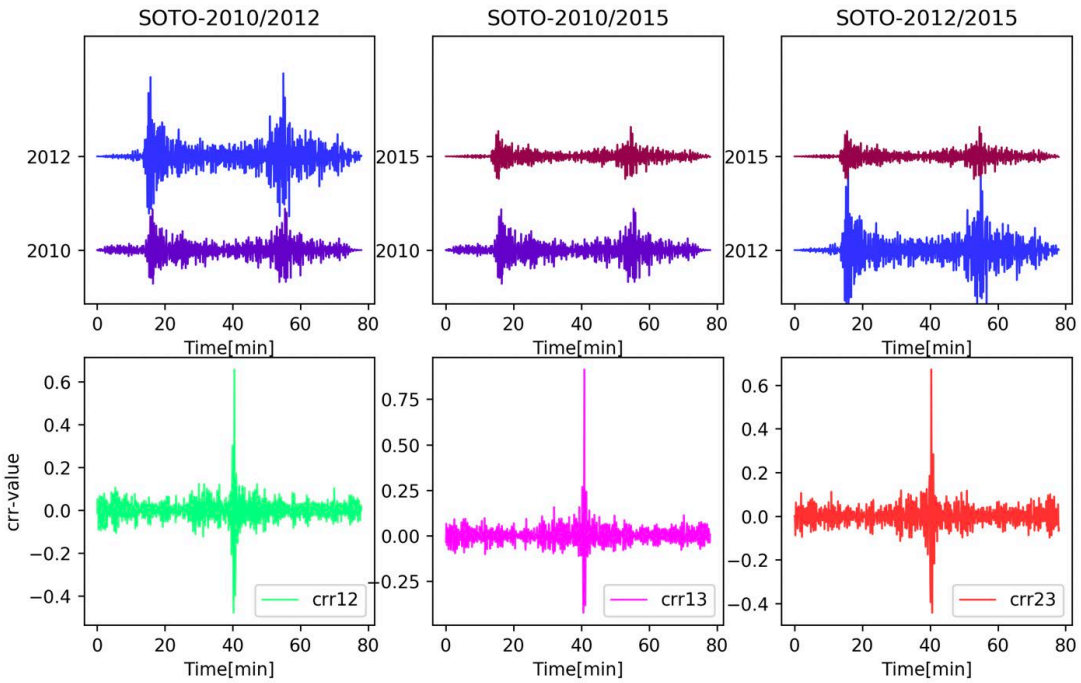

Figure 6: Examples of correlation obtained in this study. The signals blue (2010), purple (2012), and wine (2015) color represent 3 different earthquakes. They were correlated each other, and the signals colored by green, pink and orange represent the correlation functions for the individual pairs.

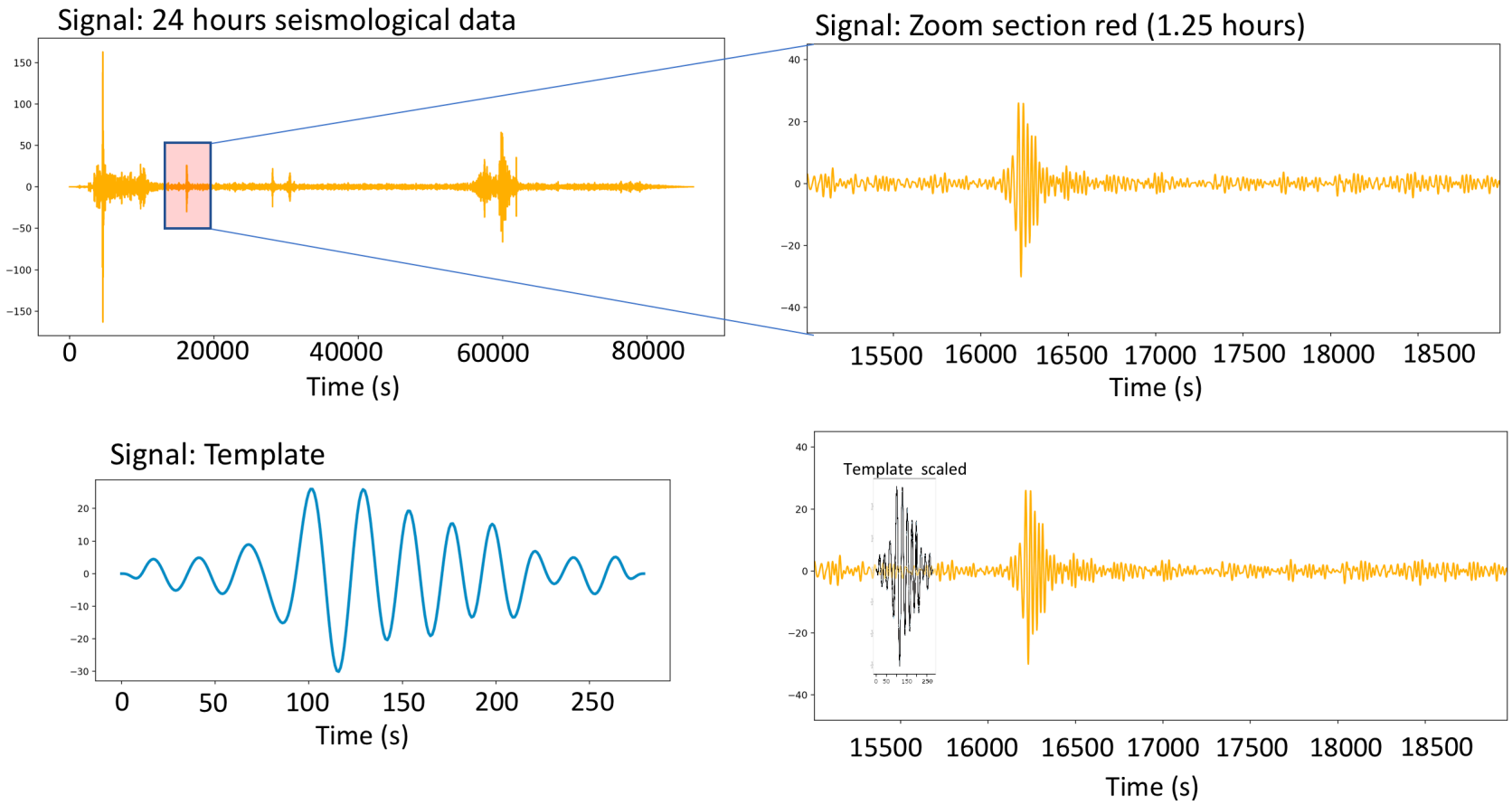

Figure 7: Matched-filter technique: Template signal (blue) run over the continuous data (orange) measuring similarity between the template and the continuous data throughout estimation of the cross-correlation coefficients by using cross correlation technique.

5.3 Seismological network of Colombia

The National Seismological Network of the Colombian Geological Survey (RSNC) is in charge of monitoring seismic activity and mitigating seismic disasters in Colombia, and contributes to scientific development of the country through analysis of seismic activity and the seismic hazard assessment.

After the explosive eruption of Nevado del Ruiz volcano in Colombia on 13 November 1985 causing death over 25,000 people and significant economic loss, Canadian International Development Agency in collaboration with seismologists from Canada and Colombia explored a possibility to establish a seismic system for monitoring the most dangerous volcanoes in the region, understanding about the nature of volcanic activity, estimating hypocentral locations of tectonic earthquakes in Colombia, and providing warning for impending danger related with geological hazards such as landslides (Buchbinder & Sarria, 1994).

In 1993, 13 seismic stations with similar characteristics were installed along the volcanic chain and surroundings. Each station equipped with one vertical sensor Geotech S-13 seismometer and satellite communication to continuously send data to the data center in Bogota. Since then, RSNC grew slowly until 2010 when RSNC obtained a funding to upgrade and increase seismic instrumentation to expand monitoring coverage and to improve seismicity detection capability and quality of reported information.

RSNC now has 58 permanent stations transmitting data continuously in real time. SGC also has three seismic and volcano observatories (OVS), in Manizales, Popayan and Pasto in charge of monitoring volcanic activity in Colombia.

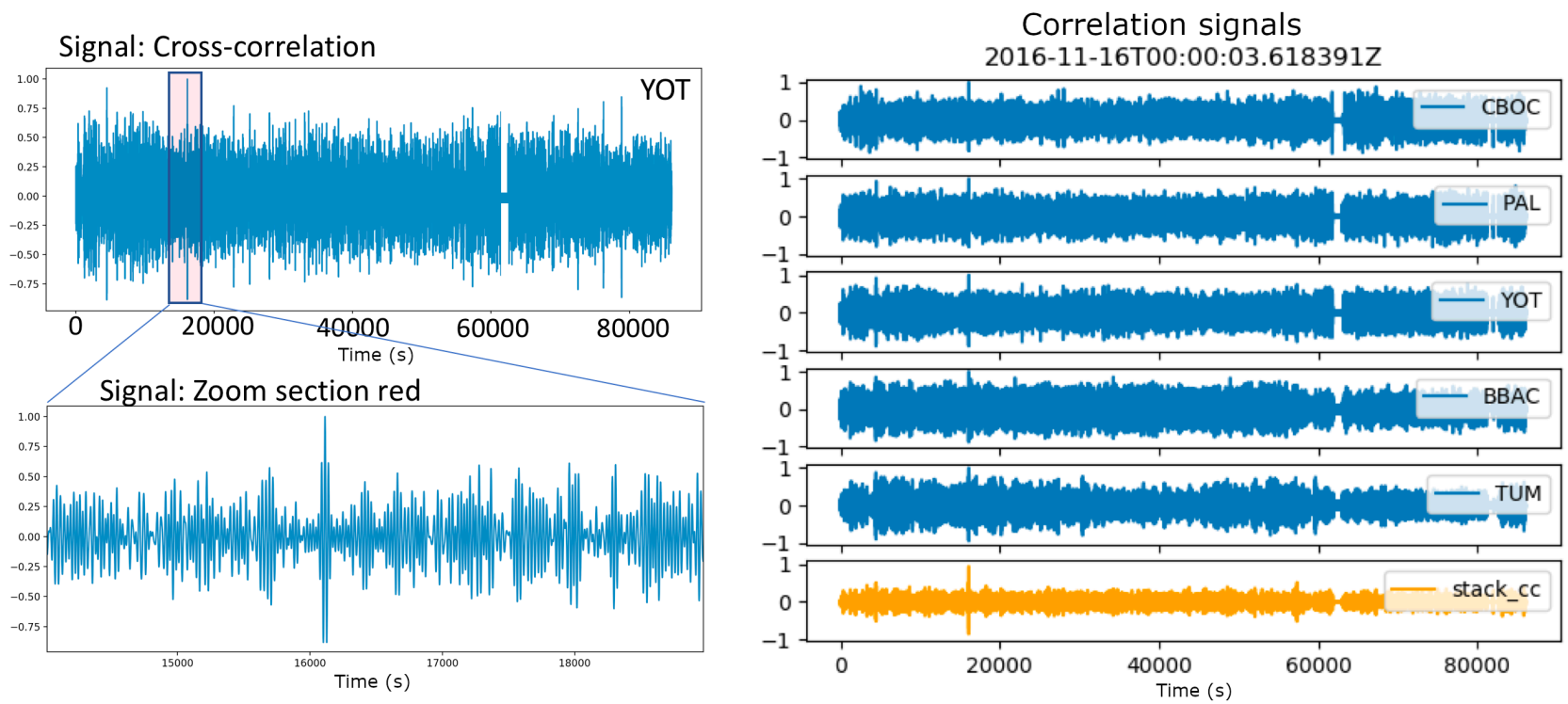

Figure 8: Matched filter after cross correlation signals. Blue signals are the cross-correlation signals after measuring similarity between a template and the continuous data at each station. Slightly earlier from 20000 s there is a signal detected by high cross correlation value. The stacked cross-correlation function enhances (orange) the detection of the signal.

5.4 VLF earthquake search

The VLF search was done by applying a low-frequency filter (0.02–0.05 Hz) to seismograms and to identify a long-period waveform with distinct amplitude. When the distinct amplitude is identified, a high-frequency filter (2.0–8.0 Hz) is applied to the raw signal. Then, the two filtered signals are examined to check if there is a corresponding high frequency distinct amplitude signal at the time of the low frequency signal. If the distinct amplitude signals are found in both low- and high-frequency filtered waveforms, then the observed event signal corresponds to a local ordinary earthquake since a VLF earthquake contains only low frequencies (Ito et al., 2007). Therefore, the detected signals were discarded. However, if the distinct amplitude is only observed in low-frequency filtered waveforms, the event could be a VLF earthquake. Subsequently, the possible VLF event is checked with earthquakes reported by SGC, Geophysics Institute of National Polytechnic School of Ecuador (IG-EPN), Incorporated Research Institutions for Seismology (IRIS) and United States Geological Survey (USGS) catalogues to confirm that the event is not a local ordinary earthquake.

5.4.1 Data

Several studies of slow earthquakes have reported VLF earthquakes along the plate boundaries in the updip or downdip portion in proximity of the seismogenic region. To perform the search for VLF earthquakes in the Colombia-Ecuador subduction zone, I selected eight broadband seismic stations (120 s period) managed by SGC located along the western margin of the Colombian coast and the southern part of the North Andean cordillera, seven broadband stations (120 s period) from IG-EPN, and two broadband stations (120 s period) located in Panama and Ecuador managed by IRIS. Continuous seismic waveform data recorded at each station were used in this study (Figure 9).

All of these waveform data were stored in the mini-seed format as continuous waveforms with 24-hour length in the individual three components (up-down, west-east and north-south) in the RSNC-SGC data base. The time period selected for my VLF earthquake search in the Colombia-Ecuador subduction zone was from January 2016 to September 2017.

5.4.2 Visual search

A template waveform of a VLF earthquake is needed to perform an automatic search using the matched-filter technique; therefore, a visual search is necessary to find at least one VLF earthquake to use its waveform as a template. In this study, continuous waveforms recorded by the stations in Figure 9 were used in searching for low-frequency signals corresponding to VLF earthquakes. The continuous waveforms stored in 24-hour waveforms were preprocessed to perform a visual search by splitting the 24-hour waveforms in 60 minutes with a 10 minutes overlap to avoid losing information at waveform edges.

The continuous seismograms were filtered in low and high-frequency bands of 0.02–0.05 and 2.0–8.0 Hz, respectively, to visually search for VLF earthquake waveforms in time windows of 60 min. I found several distinct low-frequency signals by applying the low-frequency bandpass filter; however, not all signals corresponded to VLF earthquakes. Some of the low-frequency signals showed corresponding distinct short-period signals coming from regular earthquakes.

5.4.3 Software

The software used to preprocess the raw seismic waveforms was Python through the module of ObsPy, which was developed by an open-source project dedicated to provide a Python framework for processing seismological data (Beyreuther et al., 2010; Megies et al., 2011; Krischer et al., 2015). The software used to visualize continuous waveforms to

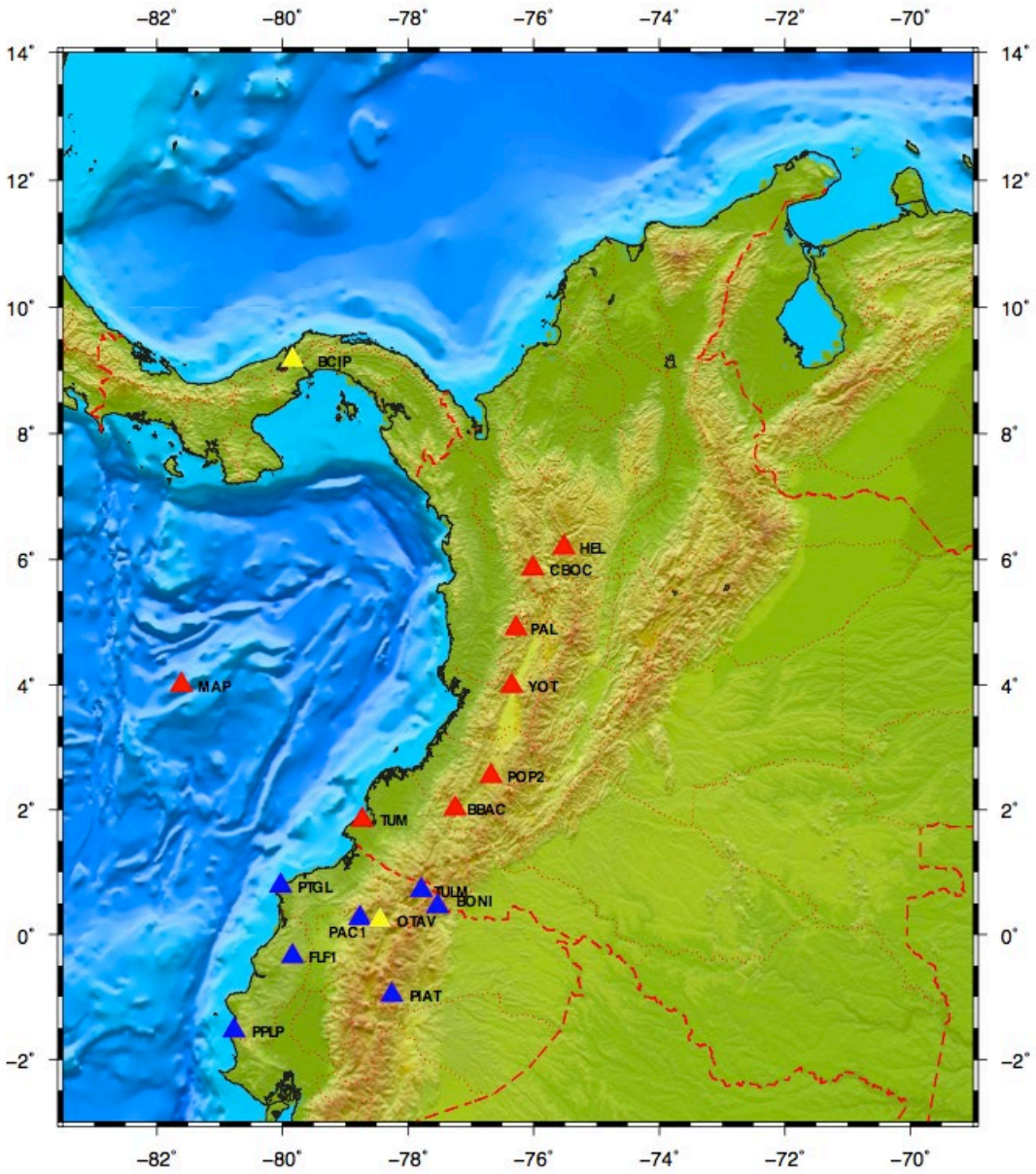

Figure 9: Broadband stations used in searching for VLF earthquakes. Colombia Geological Survey (red), Geophysics Institute, National Polytechnic School (blue), and Incorporated Research Institutions for Seismology (yellow).

perform the VLF visual search is SEISAN, an earthquake analysis software (Havskov & Ottemoller, 1999). Figure 10 shows an example of the visualized continuous waveforms by using SEISAN, showing seismograms registered at start time of 2016-01-01 19:29:59 to 60 minutes.

5.5 Repeating earthquake search

5.5.1 Nazca and South American plates boundary

5.5.1.1 Data

The seismic monitoring network managed by RSNC recorded seismicity located in the interplate region along the northern part of CESZ. I selected two types of seismographs: broadband-type (120 s period) and short period-type (1 s period). They are distributed along the southwestern part of Colombia over the Western, Central, and Easter Cordilleras along the eastern foothill margin of the Cordilleras, along the Colombian Pacific coast, and at Gorgona and Malpelo Islands (Figure 11a). As mentioned above, RSNC started with 13 stations, each site with one vertical short-period seismometer, and the network has been growing and today consist of with more than 50 stations equipped with broadband and/or short-period seismometers (Buchbinder & Sarria, 1994). Figure 11b shows how the number of stations in the study area has been changing.

Hypocenter determinations have been routinely performed by staff of RSNC and estimated source information has been reported in the SGC seismic catalog. This activity is done by picking the seismic phases manually and computed by the HYPOCENTER program (Lienert et al., 1986; Lienert & Havskov, 1995) through SEISAN software. (Havskov & Ottemoller, 1999). A 1-D crustal velocity model for Colombia and station

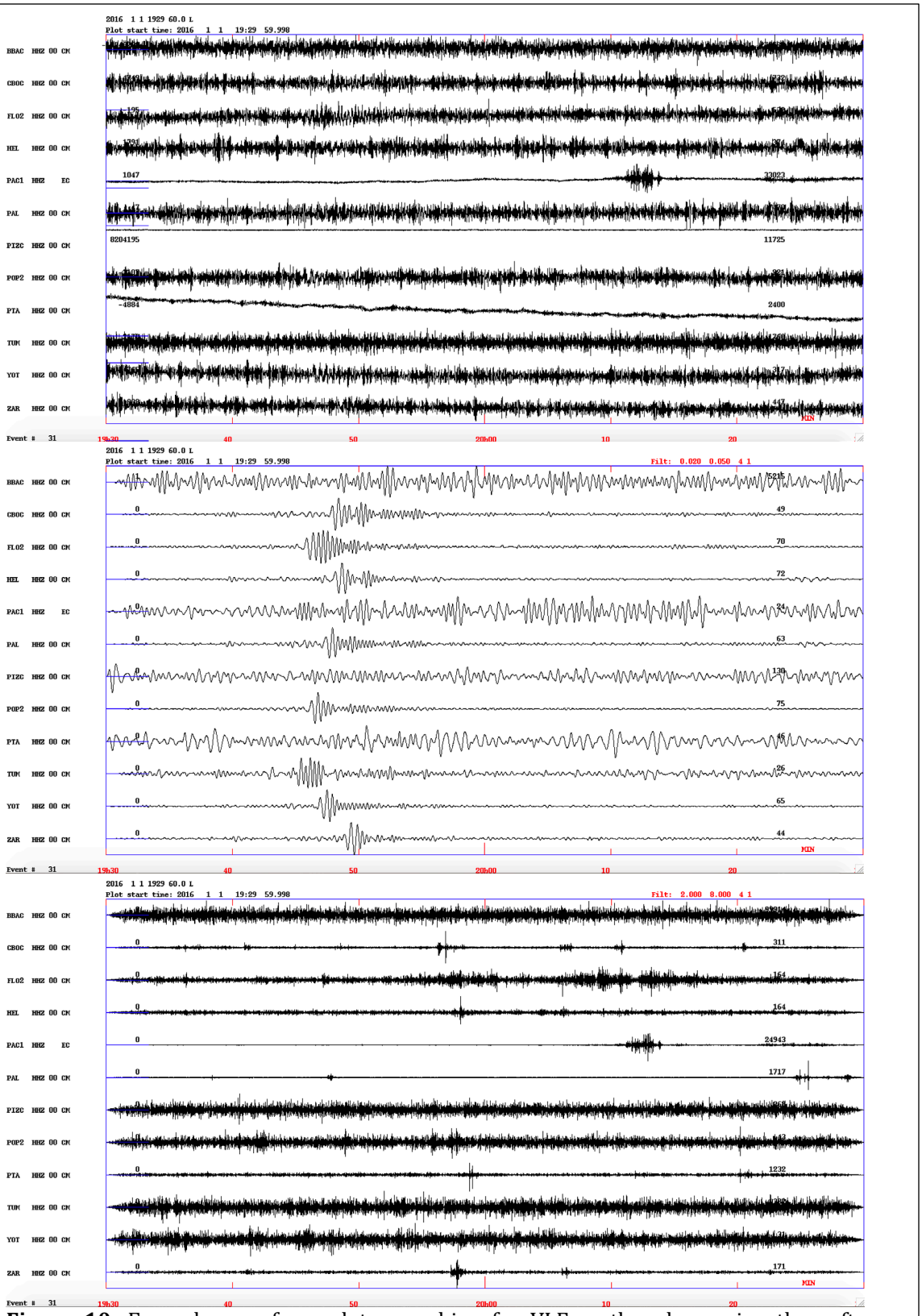

Figure 10: Example waveform plots searching for VLF earthquakes, using the software SEISAN. This figure shows three panels, the first, second and third panels display the raw data, the filtered signal with the bandpass filter between 0.02 and 0.05 Hz and the signal filtered by the bandpass filter between 2.0 and 8.0 Hz, respectively.

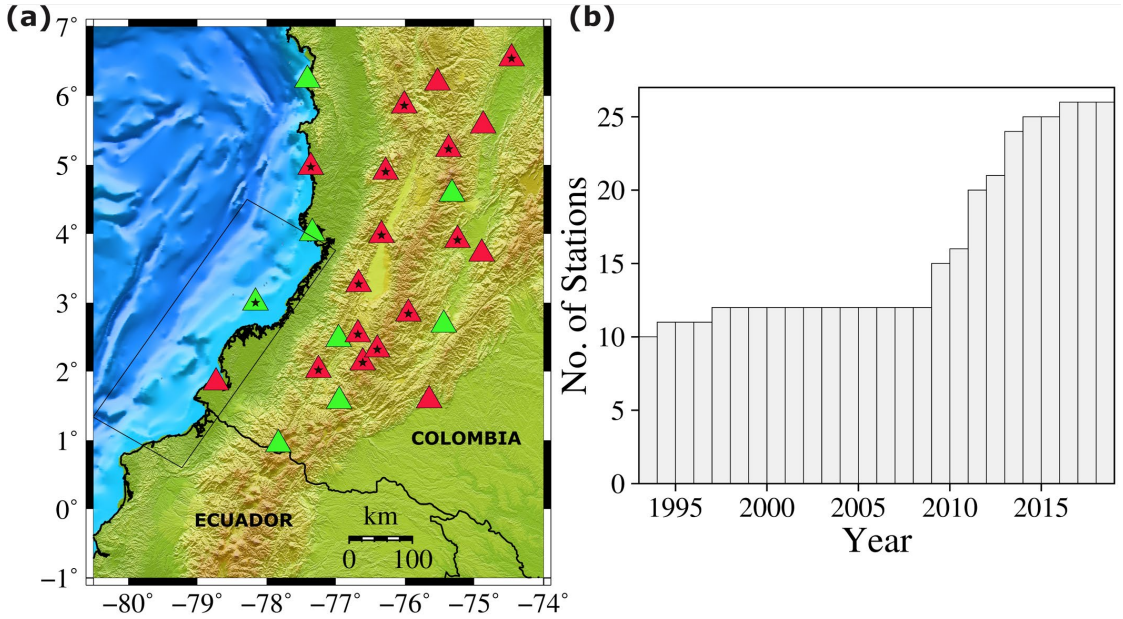

Figure 11: (a) Locations of broadband (red triangles) and short period (green triangles) seismic stations used in the present study. The stations with black stars represent those installed after 2009. (b) The number of stations operated per year from 2003 to 2018.

corrections were assumed to perform the hypocenter determinations using the algorithm mentioned above (Ojeda & Havskov, 2001).

In this study, I selected the earthquakes reported in the SGC catalog, located within the quadrilateral area shown in Figure 12 in the southern part of the Colombia subduction zone with a local magnitude (M_L) larger than 1.9. This magnitude was selected as a threshold because it represents the completeness magnitude for the SGC catalog in this area. This study selected 1442 earthquakes with magnitudes ranging between 1.9 and 6.2 and depths between 0 and 100 km. Most earthquakes were located by using less than eight stations, and their hypocenter determination uncertainty is less than 50 km in latitude, longitude, and depth for most of the earthquakes (Figures 12 and 13).

5.5.1.2 Searching of repeating earthquakes

In this study, I used spatial separation and waveform cross correlation as the initial and secondary constraints in searching for potential repeating earthquakes in the Colombia subduction zone. To satisfy the constraints, I proceeded as follows: for spatial separation, the hypocenter differences between pair of events were computed, these pairs were formed using all the events in the catalog, and the differences were compared to each other. I selected one event as a reference event (RE). All reminder events with hypocentral differences from the RE smaller than 50 km were called neighbor events (NE). I formed RE-NE pairs, and each RE-NE pair was considered as a potential pair to perform the cross-correlation analysis (Figure 14). I selected all events as REs. For each RE, I selected a group of NE which satisfied the distance constrain.

More than 170,000 potential pairs satisfied the initial spatial separation constraint. The seismic waveforms recorded by RSNC were preprocessed for each event, in which windows with a 300-s length after the origin time were selected to include *P*- and *S*-waves in the individual seismograms. The waveforms were filtered using a bandpass filter between 2 and 8 Hz. Subsequently, I performed the cross-correlation analysis and computed the cross-correlation coefficients (CC-values) for all RE-NE pairs. Each CC

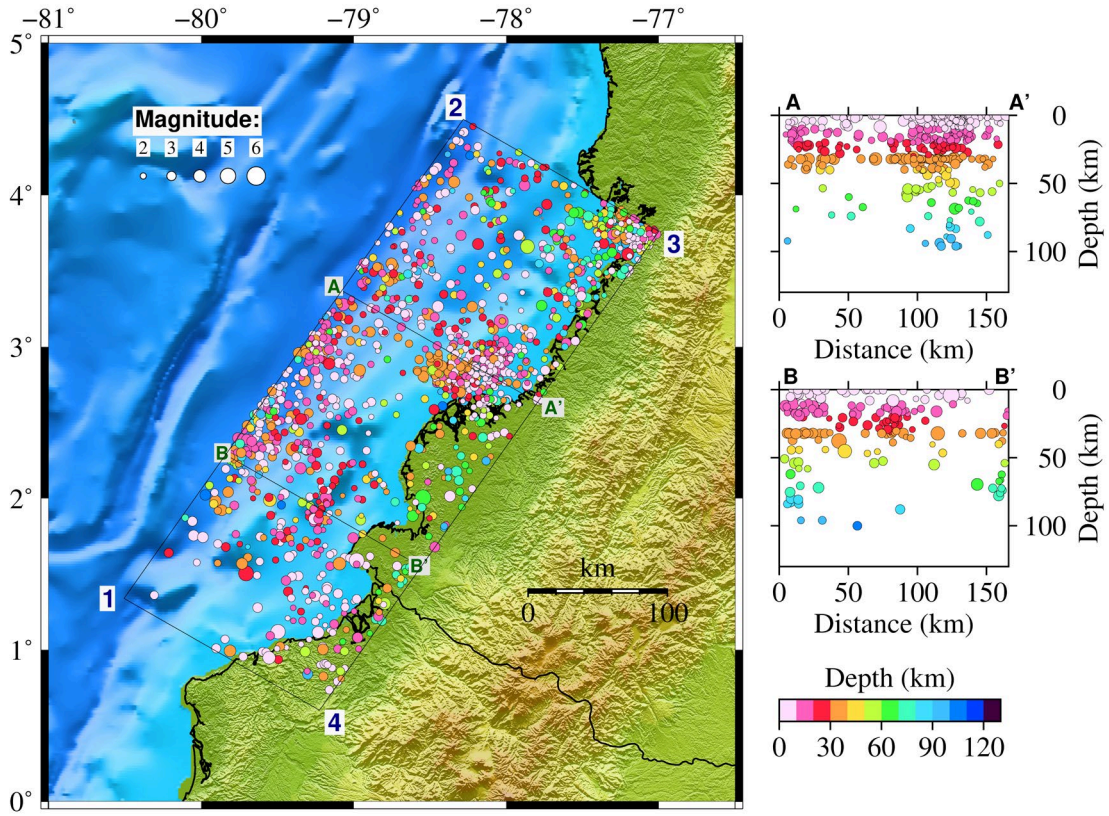

Figure 12: Source distributions of earthquakes used in this study. The hypocenter locations of earthquakes were obtained from the SGC catalog for the selected event within the area (1: 1.34°N, 80.51°W, 2: 4.5°N, 78.28°W, 3: 3.76°N, 70.00°W, 4: 0.60°N, 79.22°W). Right panels represent the cross sections along A–A′ and B–B′ (Bermúdez-Barrios & Kumagai, 2020).

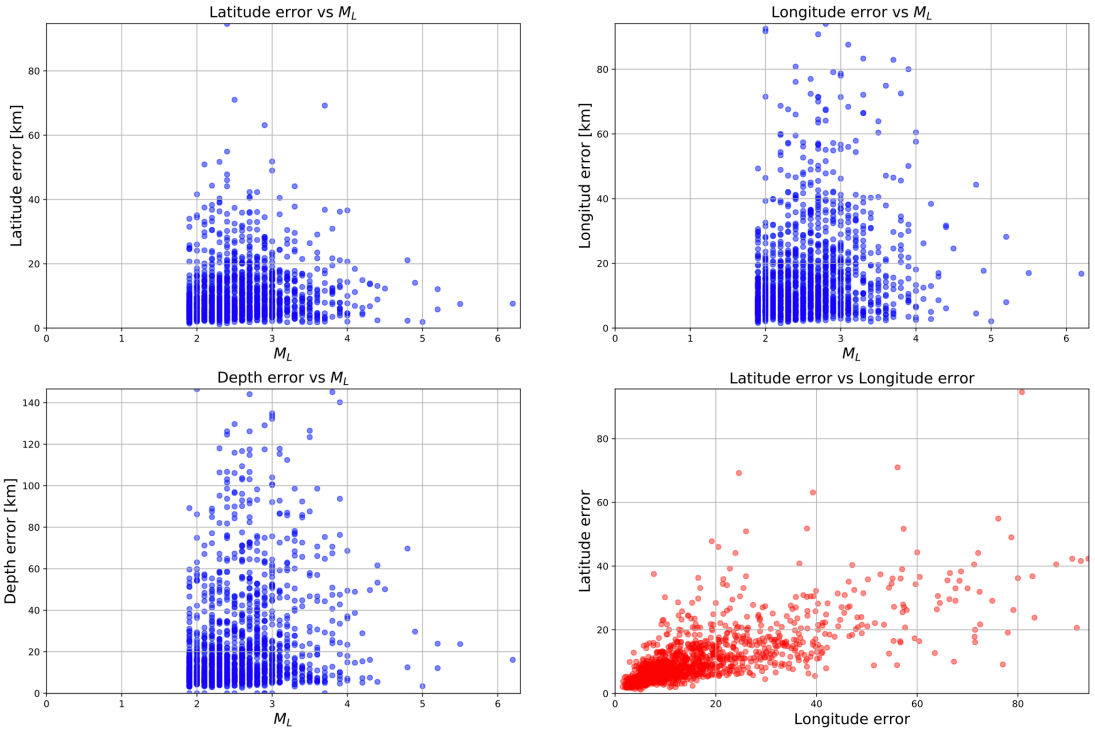

Figure 13: Uncertainty in hypocentral parameters estimated by routine hypocenter determinations by SGC for earthquakes located in the Colombia-Ecuador subduction zone between 1993 and 2018.

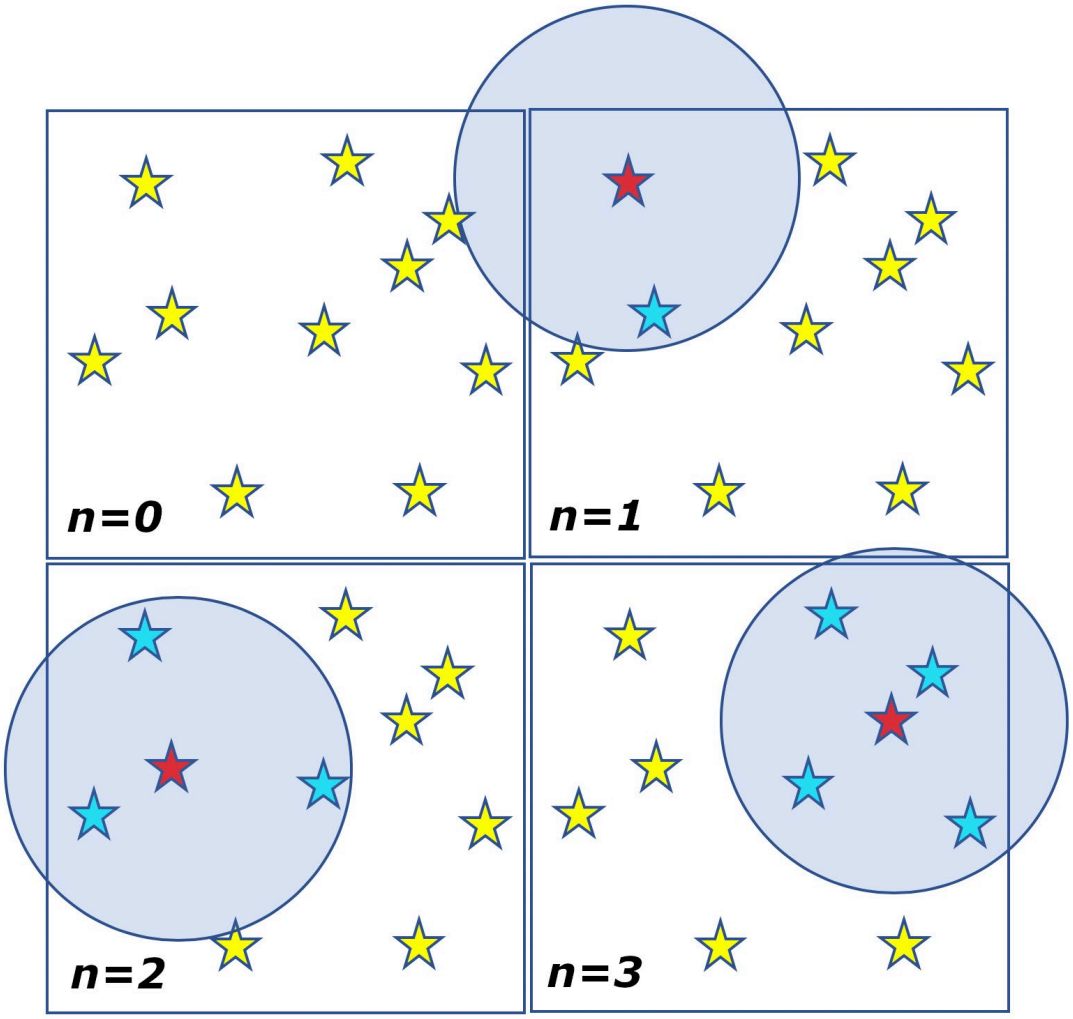

Figure 14: Sketch to explain the spatial separation between earthquakes and the selection of neighbor events. The first step, n = 0, represents all events without selecting any events. The next step, n = 1, one reference event (RE) (red star) is selected and all events far from RE less than 50 km is selected as neighbor event (NE) (blue star). The same procedure is done for steps n = 2 and n = 3 and so on until run all events in the catalog.

value was computed by using waveforms with the same stations in the two events. The CC-values computed for each pair depended on the number of same stations that were registered in each event of each RE-NE pair. If one station met the threshold condition, the earthquake pair was selected as a repeating earthquake candidate. The scripts to prepare data and to perform the cross-correlation analysis were developed by using ObsPy (Megies et al., 2011; Krischer et al., 2015).

5.5.2 Caribbean and South American plates boundary

5.5.2.1 Data

RSNC reported the seismicity located along the northern part of Colombia in the interplate boundary between the Caribbean and South American plates. Figure 15 shows the station distribution used in my search for repeating earthquakes in the southern Caribbean subduction zone. In this study, I selected the earthquakes located within the quadrilateral area shown in Figure 16 from the SGC catalog.

This study selected 5,805 earthquakes with M_L ranging between 2.0 and 6.0 and depths between 0 and 100 km. Most of the earthquakes were located with less than nine stations, and the hypocentral determination uncertainty is less than 50 km in latitude, longitude, and depth for most of the events. However, there are few earthquakes with larger uncertainty in all spatial directions. Another highlighted feature in this catalog is the large number of earthquakes that occurred at depths ranging between 0 and 5 km (Figure 17).

I searched for repeating earthquakes in the Caribbean region in the same way as in the Pacific region by considering the spatial separation and waveform cross correlation as constrains: Hypocentral differences between RE and NE smaller than 50 km and computing the cross-correlation coefficient between RE-NE pairs.

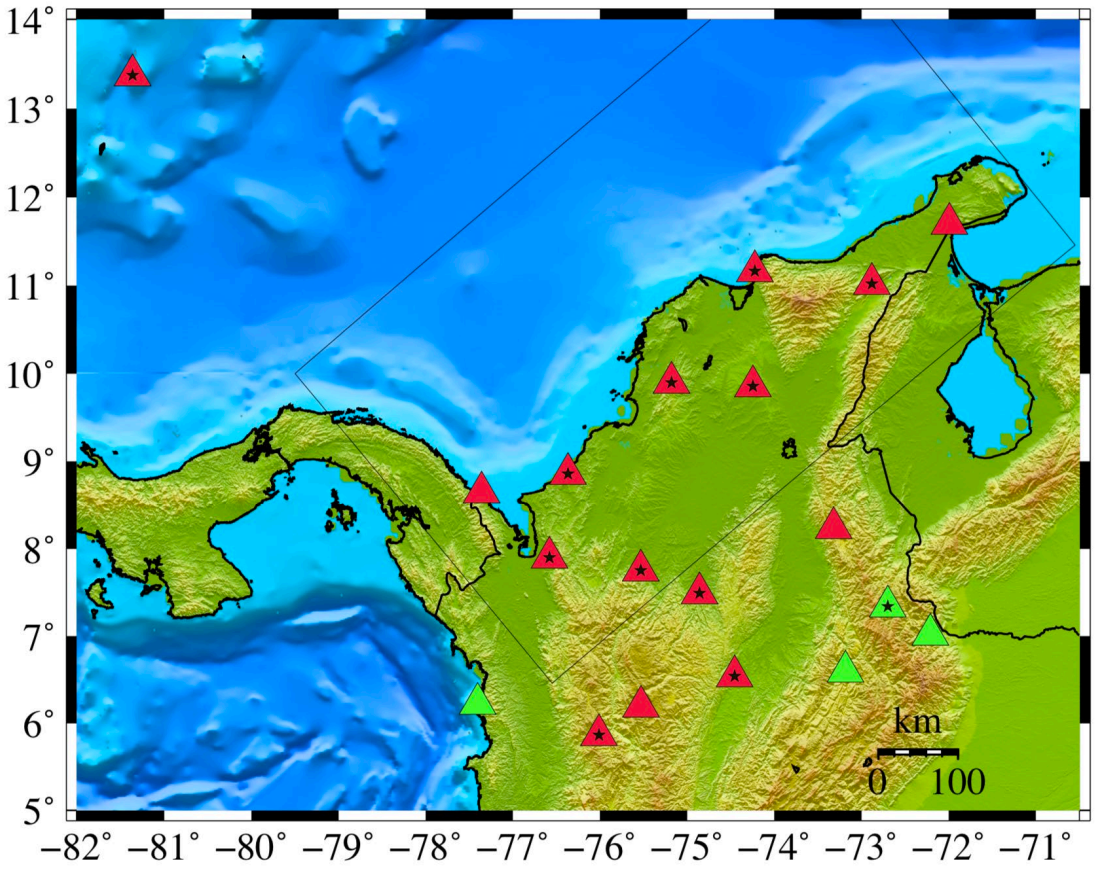

Figure 15: Locations of broadband (red triangles) and short period (green triangles) seismic stations used in the search for repeating earthquakes in the southern Caribbean subduction zone. The stations with black stars represent those installed after 2009.

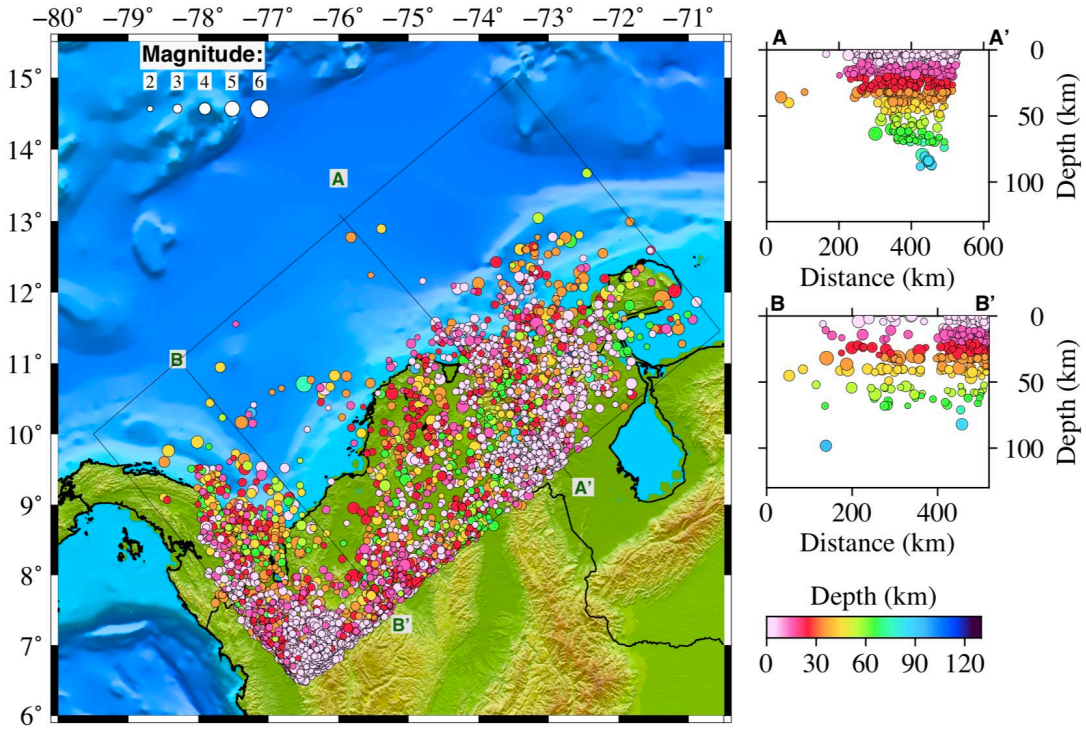

Figure 16: Source distribution of earthquakes used in this study. The hypocenter locations of earthquakes were obtained from the SGC catalog for the selected event within the area: (10.00°N, 79.51°W), (15.00°N, 73.50°W), (11.46°N, 70.54°W), (6.45°N, 76.54°W). Right panels represent the cross sections along A–A′ and B–B′.

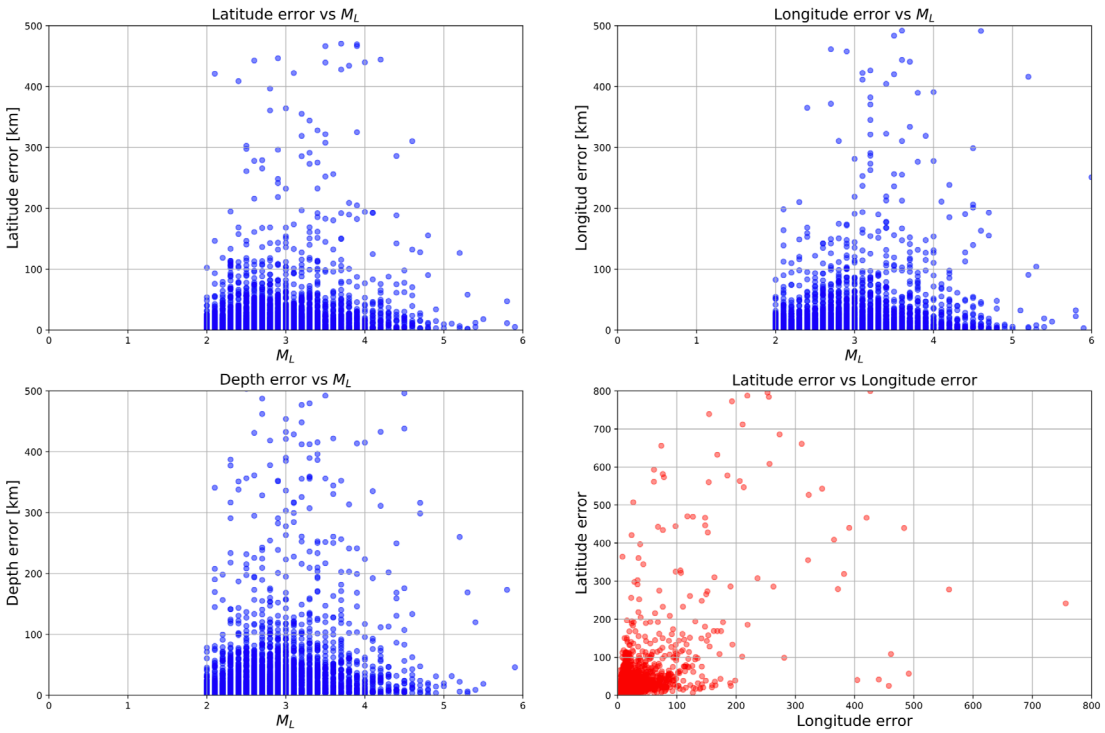

Figure 17: Uncertainty in hypocentral parameters estimated by routine hypocenter determinations by SGC for earthquakes located in the southern Caribbean subduction zone between 1993 and 2018.

CHAPTER 6

6. RESULTS

6.1 Very-low-frequency earthquakes

I performed a visual search for VLF earthquakes to find at least one of these events and then performing an automatic search by using the matched-filter technique. During this visual search for VLF earthquakes for one year and ten months of data, several low-frequency waveforms without corresponding high-frequency waveforms were identified; however, none of these was a VLF earthquake.

After my identification of the first event (2016-02-10 10:32) with similar features to those reported in the other studies (Obara & Ito, 2005; Ito et al., 2007), I consulted the local earthquake catalogs of SGC and IG-EPN, but they did not report any events. Therefore, I assumed this event as a VLF earthquake. I then used the matched-filter technique to automatically search for more VLF earthquakes using the event as a template.

I detected several events, and some of them were visible at a distant station located in Panama. Then, I consulted the international catalogs of USGS and IRIS, and found that the template and detected events occurred in the southern part of the Mexican west coast, indicating that what I found was signals of surface waves coming from distant earthquakes originated in the coast of Mexico (Figure 18).

A similar case occurred with events originated in the Tonga region and the Nazca-Cocos boundary plate. Figures 19 and 20 show examples of the waveforms corresponding to these detected events. Thus, the search for the VLF earthquakes at the Colombia-Ecuador subduction zone was not successful, and during the span time from January 2016 to September 2017, no VLF earthquakes were found.

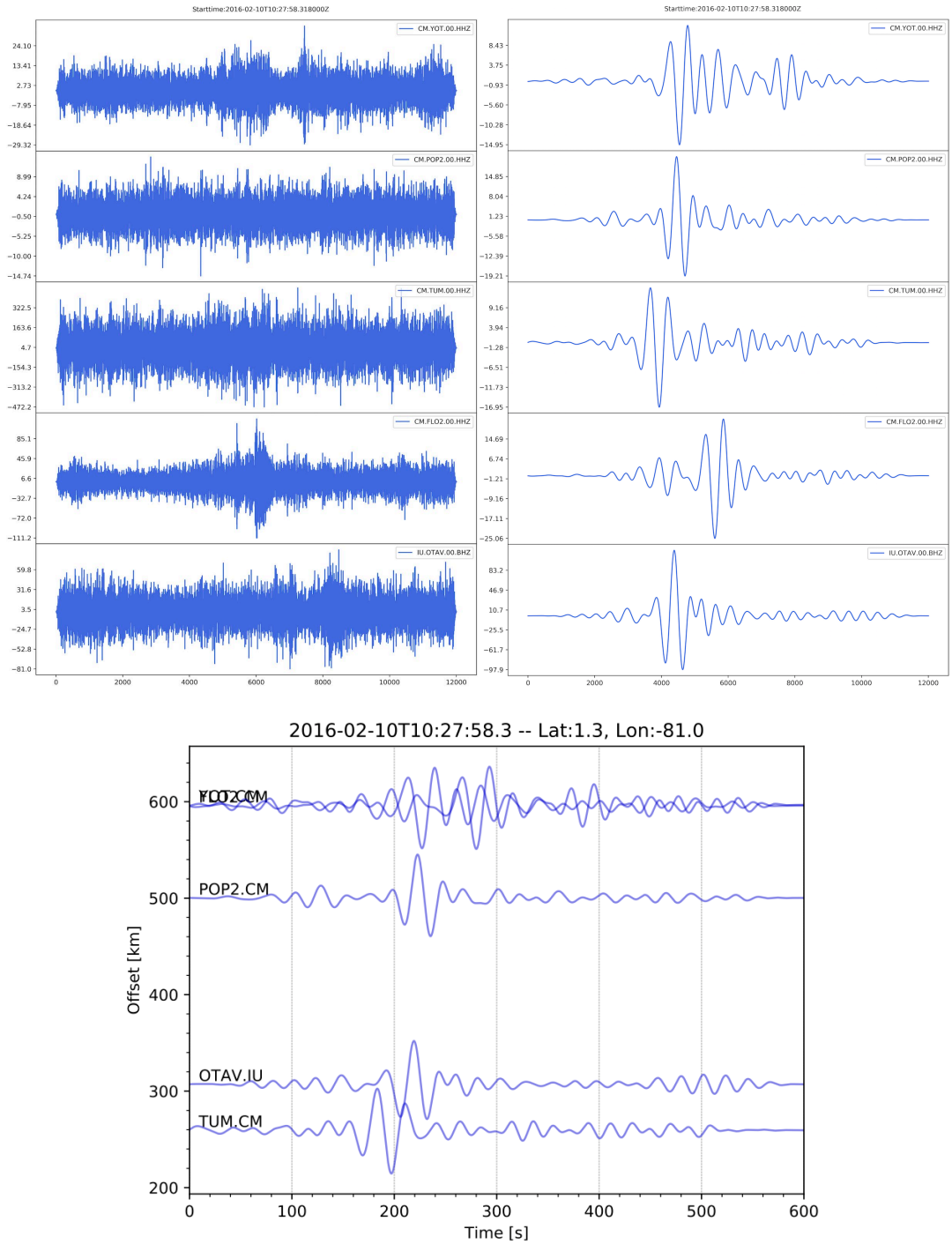

Figure 18: Example of an event originated in the west coast of Mexico, showing similar features to a VLF earthquake. Top left and right panels are the signals filtered in 2–8 Hz and 0.02–0.05 Hz, respectively. The bottom panel shows the low-pass filtered waveforms plotted again distance.

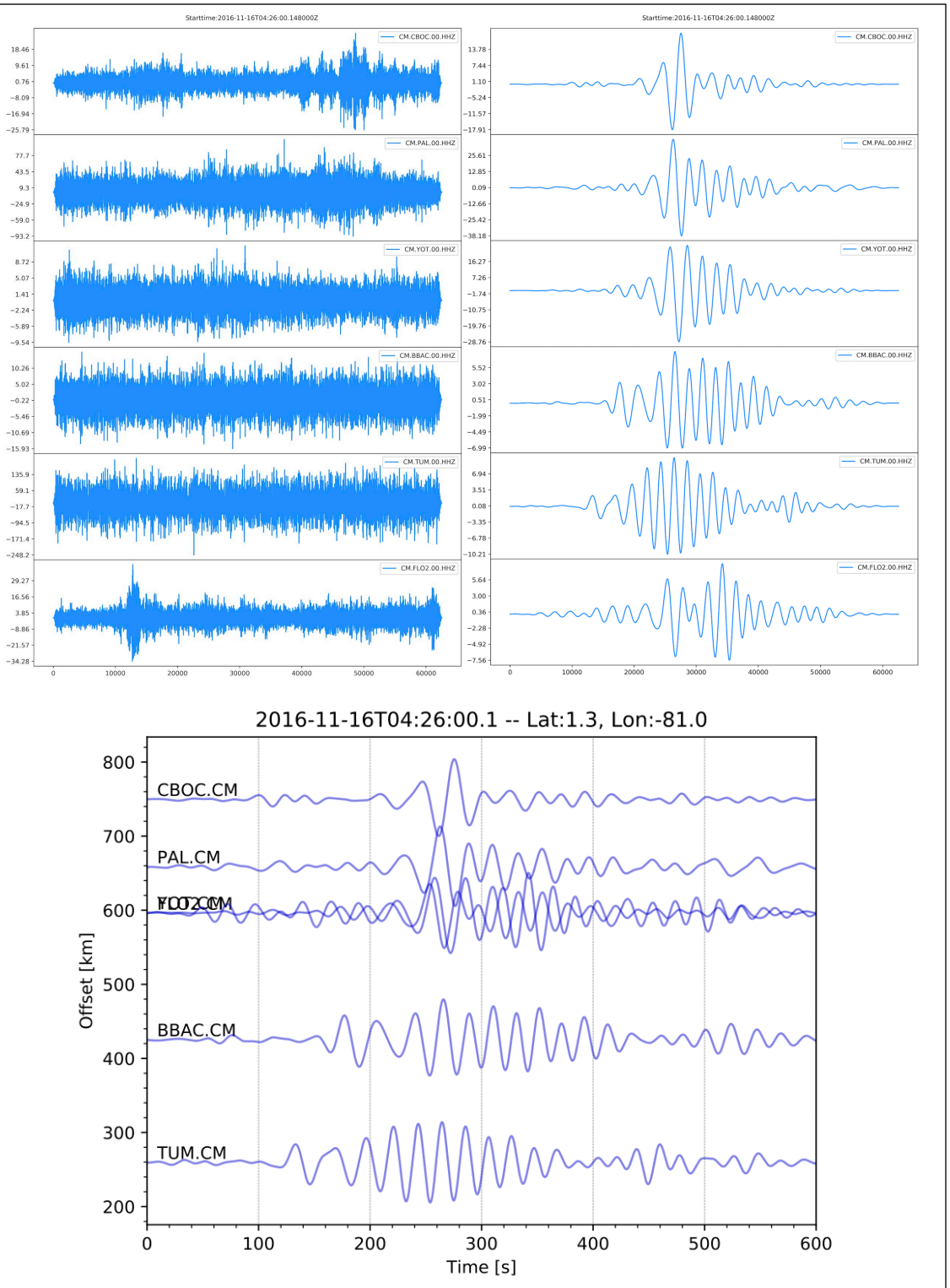

Figure 19: As in Figure 18, but an event occurred in the Tonga region.

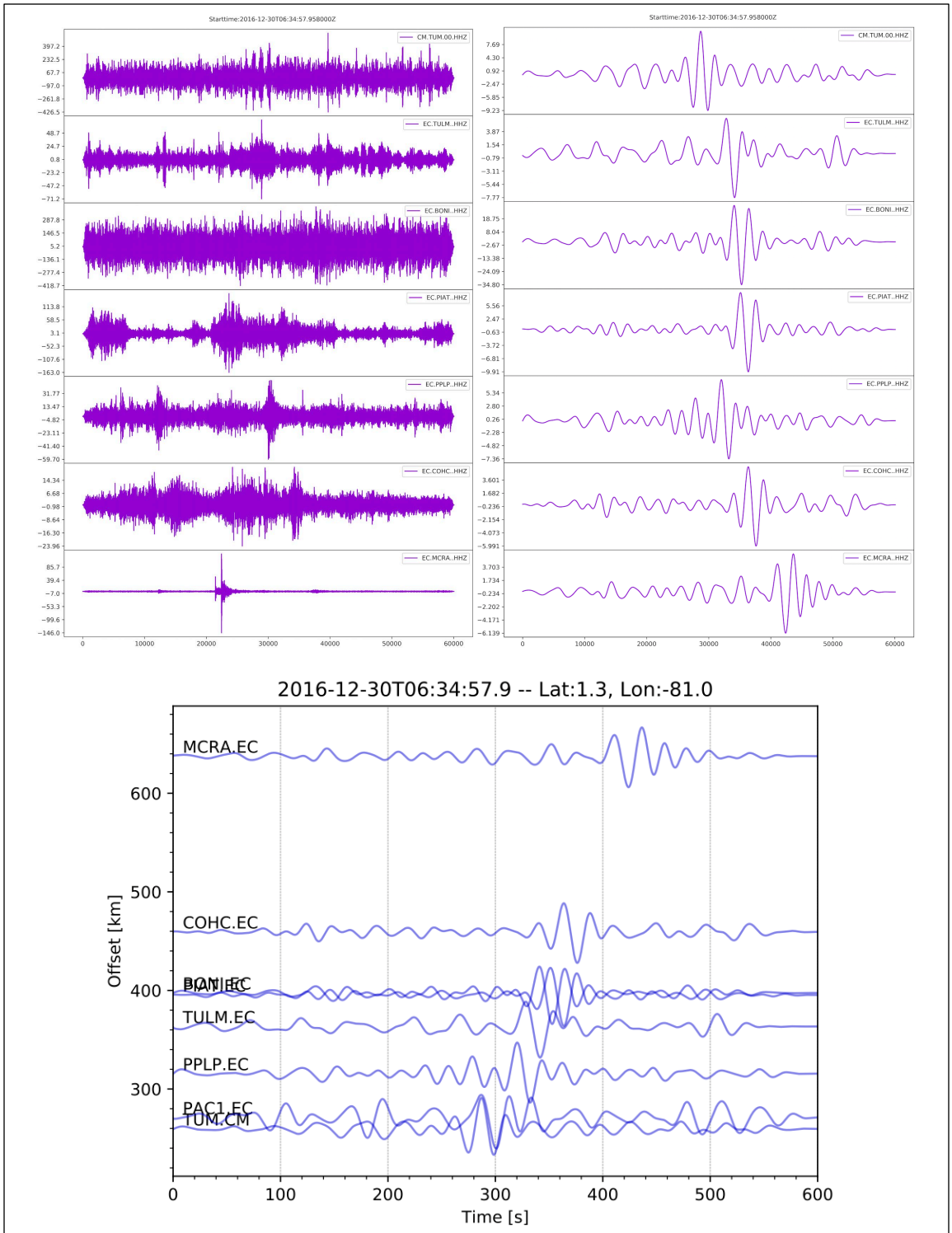

Figure 20: As in Figure 18, but an event occurred in the Nazca-Cocos plate boundary.

6.2 Repeating earthquakes in the Colombia-Ecuador subduction zone

I performed waveform similarity assessment by cross correlation to find repeating earthquakes, in which I applied the waveform cross correlation to all RE-NE pairs recorded in the same stations. For 174,830 earthquake pairs, I computed 1,215,486 correlations. Figure 21 shows the complete distribution of CC-values obtained in this study. I needed to define a threshold for the CC-values to establish a measure of high similarity between the waveforms. Igarashi et al. (2003) obtained the threshold from events with a distinct peak in the range of 0.9 to 1.0 in the CC-value distribution. However, in the events used here, the number of events decreased with increasing CC-value (Figure 21), and no indication of a suitable threshold was shown.

In order to choose the most suitable CC-value as a threshold, I used different CC-values as candidates to select the best value. I used CC-values of 0.80, 0.85, 0.90, and 0.95 as CC threshold candidates, and created sequences of possible repeating earthquakes using these CC threshold candidates. To create the possible repeating earthquake sequences, I searched for correlated event pairs satisfying the CC threshold candidate requirement. After obtaining these correlated pairs, the pairs with one event in common were grouped in the same sequence; therefore, each sequence can be formed by two, three, or more events. In this process I found 74 sequences with a CC-value of 0.80, 62 sequences with a CC-value of 0.85, 36 sequences with a CC-value of 0.90, and 15 sequences with a CC-value of 0.95. The number of sequences found in this analysis decreased with increasing threshold candidate, and I observed a similar trend in the number of events forming each sequence, and this number ranges between 2 and 10 events with a CC-value of 0.80, 2 and 8 events with a CC-value of 0.85, 2 and 6 events with a CC-value 0.90, and 2 and 5 events with a CC-value of 0.95 (Figure 22).

Up to this point, I searched for the repeating earthquakes by analyzing spatial variations throughout waveform similarity using cross correlation, and formed the sequences with the correlated events. However, to select repeating earthquakes, I need to analyze the time behavior for events comprising each sequence; therefore, I analyzed temporal

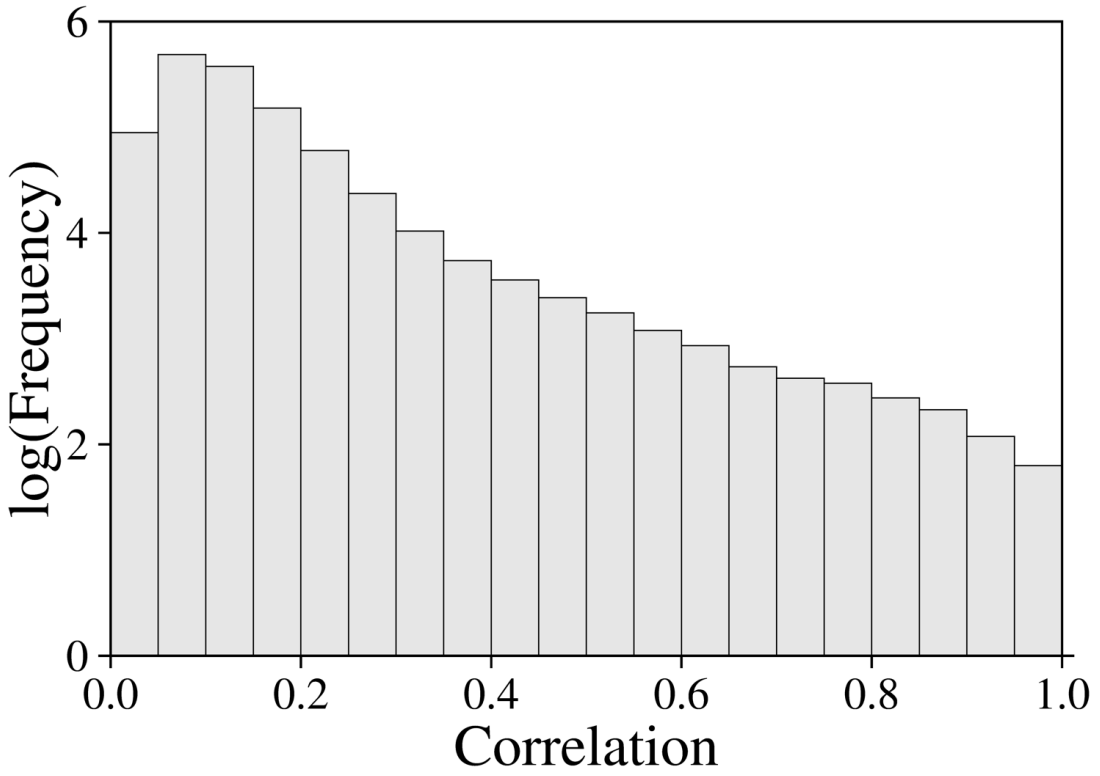

Figure 21: Frequency distribution of the cross-correlation coefficients between earthquake pairs with hypocenter differences of < 50 km, located within the Colombia-Ecuador subduction zone (Bermúdez-Barrios & Kumagai, 2020).

characteristics for all possible sequences of repeating earthquakes. I evaluated the time intervals of successive events in each sequence for all four CC-value threshold candidates. I found that events comprising the sequences occurred with short time intervals varying between minutes and days (short-term events), occurred with more extended time intervals varying from months to years (long-term events), and occurred including both types of short and long interval times.

Notably, the number of earthquakes per sequence decreased when I used a tighter CC-value to build the repeating earthquake sequences. New sequences appeared when I relaxed the CC-value criteria from 0.95 to 0.80, adding more potential repeating earthquakes to the sequences previously selected with tighter criteria. The addition of new earthquakes mostly occurred at short timescales.

Lengliné & Marsan (2009) showed that similar earthquakes occurred near each other and with long time intervals between them are tightly clustered at the barycenter of the asperity, and those with short time intervals occur randomly in any place of the source area of the repeating sequence. This result indicates that the short-term events, of which the spatial distributions are not concentrated spatially, may be triggered events, and this is why the short-term events are not co-located. Moreover, the long-term events show a tightly concentrated spatial distribution. Therefore, the time interval is a useful diagnostic feature for identifying triggered events among the sequences selected by waveform similarity and hypocenter location (Uchida, 2019).

Figure 23 shows the results of the frequency distribution of the recurrence time intervals of the repeating earthquake candidates using two different CC threshold values (0.80 and 0.90), in which each bin represents the recurrence time interval of successive earthquakes. Figure 23 also shows that when I used a low threshold of 0.80, the number of short-term events became large compared with the number of events using a higher threshold (0.90). The number of long-term events decreases while the recurrence time interval increases in the year (Figure 23a) and day scales (Figure 23b), suggesting that sequences formed by aftershocks, triggered events, or non-similar events dominate for

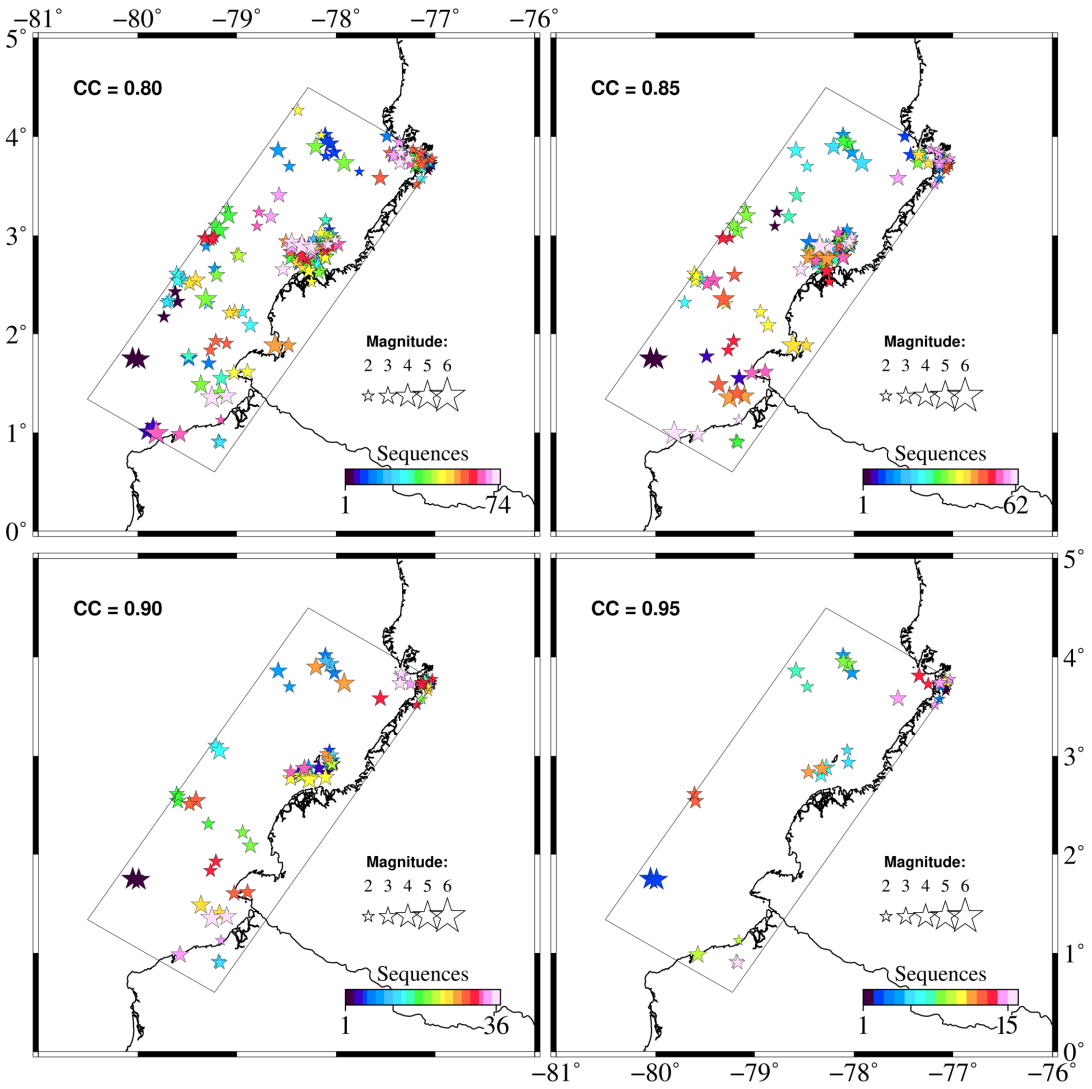

Figure 22: Plots of epicentral locations of earthquakes found by the cross-correlation (CC) waveform analysis with CC threshold values of 0.80. 0.85, 0.90, and 0.95; the color scale represents the individual sequences (Bermúdez-Barrios & Kumagai, 2020).

short intervals. In a comparison between sequences selected by using a loose 0.8 and a tight 0.9 threshold, the large difference in the number of earthquakes in the short-term interval portion shows that most of the short-term events have relatively low similarity (Figure 23). Thus, the short-term events can be interpreted as triggered events that are close but not co-located (Uchida 2019).

According to the plot representing the recurrence time interval distribution in Figure 23a with the year scale, the largest number of earthquakes was observed in the time interval of 0-4 months, and in Figure 23b with the day scale, the number of earthquakes rapidly decrease within five days. For each CC-value selected as a threshold, I studied the possible repeating earthquakes by forming sequences of successive earthquakes using the minimum recurrence time as mentioned earlier: 0 days, five days, and four months. I show the results of the sequences analyzed here from zero days to four months in Figure 24. The sequences created in this way show similar spatial distribution, however, sequences formed by large clusters with short intervals disappear when the recurrence time increases. Finally, I excluded the short-term earthquakes (0 days and five days) because they correspond to triggered events. Then, I selected four months for the minimum recurrence time to form the sequences of repeating earthquakes.

A CC-value of 0.8 selected as a threshold can be a loose criterion to establish similarity, and by contrast, a CC-value of 0.95 can be a strict criterion. According to the data set used in this study, which was obtained from a sparse network with limited coverage station and with large noise levels, I selected a threshold CC-value of 0.90 and a minimum time interval of 4 months to keep high waveform similarity and to exclude triggered events. I showed examples of high similarity waveforms in Figure 25.

Figure 26a shows the spatial distributions of repeating earthquakes with the threshold CC-value of 0.90 and the sequences selected after excluding the short-term sequences, and Figure 26b shows the sequences of repeating earthquakes representing the set of repeating earthquakes. I obtained the locations of the sequences as the averages of the repeating earthquake locations of the individual sequences.

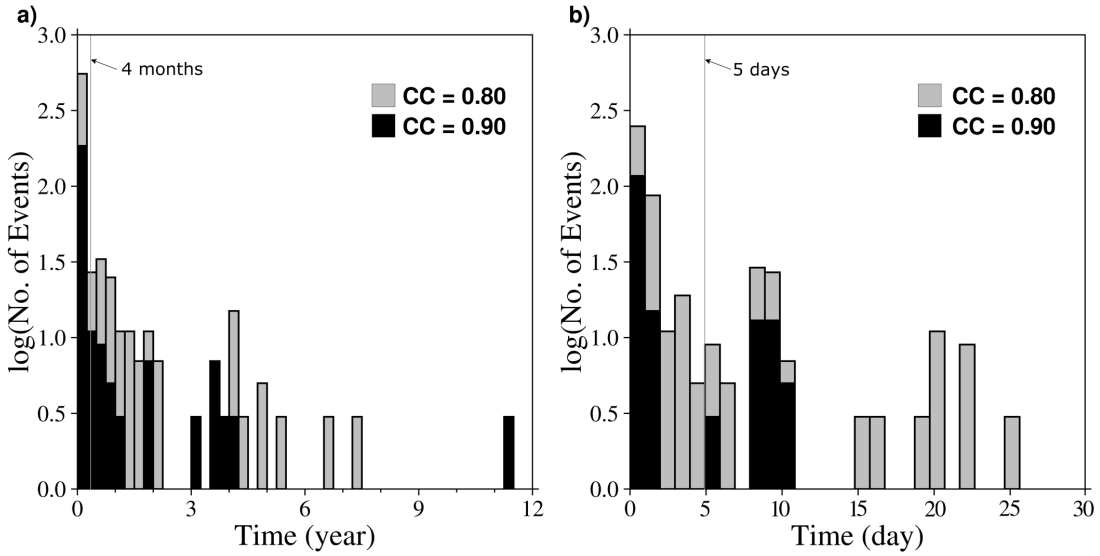

Figure 23: The number of earthquakes against the time intervals of successive earthquakes found by using cross correlation (CC) threshold values of 0.80 (gray) and 0.90 (black). (a) 0 to 12 years with 4-month interval bins. (b) 0 to 30 days with 1-day interval bins (Bermúdez-Barrios & Kumagai, 2020).

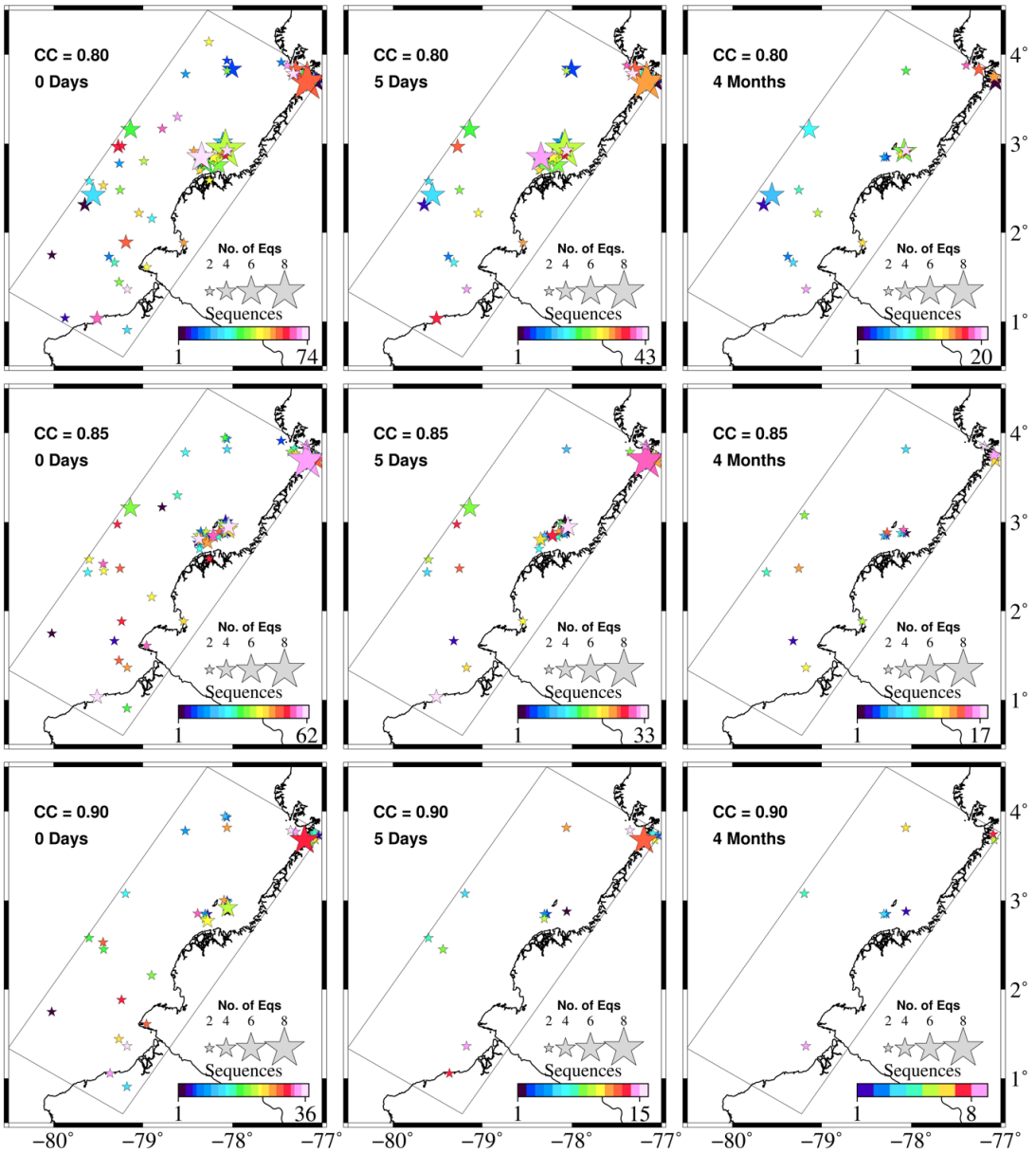

Figure 24: Spatial distributions of the groups of possible repeating earthquakes found by using cross correlation (CC) threshold values of 0.80, 0.85, and 0.90 and minimum time intervals of 0 days, 5 days, and 4 months. The color scale represents the individual sequences (Bermúdez-Barrios & Kumagai, 2020).

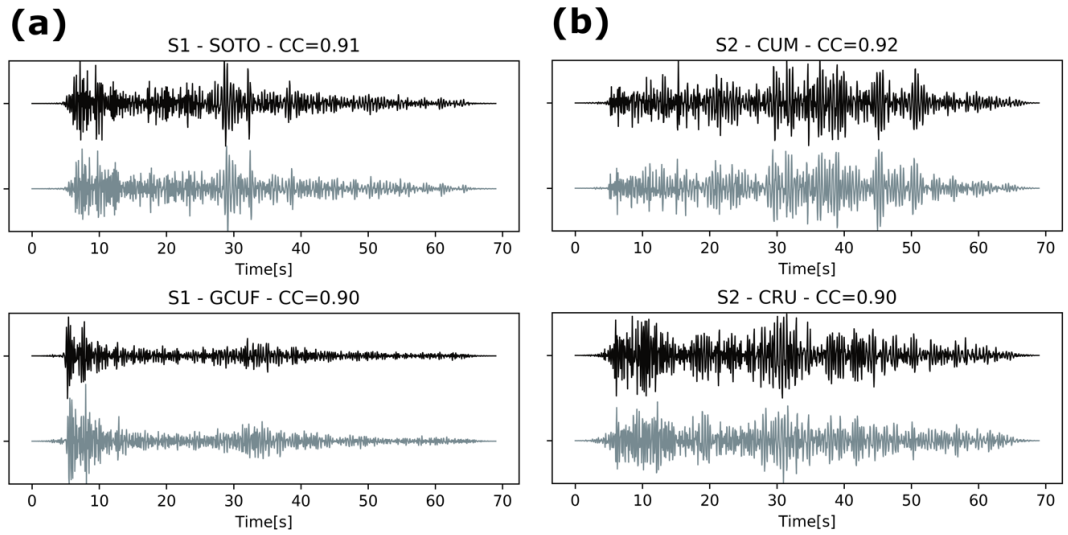

Figure 25: Examples of seismograms from repeating earthquake sequences recorded at different stations. (a) Record of the earthquakes that occurred at 18:56 on February 18, 2012 with M_L 2.3 (black) and at 15:07 on February 29, 2016 with M_L 2.3 (gray), recorded at SOTO and GCUF stations. (b) Record of the earthquakes that occurred at 06:06 on November 02, 2007 with M_L 2.7 (black) and at 23:39 on August 11, 2016 with M_L 2.9 (gray), recorded at CUM and CRU stations (Bermúdez-Barrios & Kumagai, 2020).

The study area was divided into four regions Z1, Z2, Z3, and Z4 (Figure 26). Magnitude-time plots of the repeating earthquakes in the individual sequences are shown in Figure 27.

In Z1, there are three sequences of repeating earthquakes, each one formed by two events (Figure 26 and Table 1). One of them is located in the offshore region and has a long-term recurrence time interval of approximately 11 years. The other sequence is located near the coast, with a recurrence time of approximately ten months (Figures 26 and 27).

In Z2, there is one repeating earthquakes sequence formed by two events located in the offshore region (Figure 26 and Table 1), and the recurrence interval time is about one year (Figure 27).

In Z3, there are three repeating earthquakes sequences, they are distributed near the coastal region. The individual sequences are formed by two repeaters in each sequence (Figure 26 and Table 1). There is a wide range of time intervals for these sequences: the recurrence interval time range from 2 to 5 years (Figure 27).

In Z4, there is only one sequence formed by two events (Figure 26 and Table 1) with a recurrence interval time as six months. The sequence in Z4 is located toward the coastal region, in the southern part of the study area (Figure 27).

According to the criteria to select repeating earthquakes: high waveform similarity, and relatively long recurrence time (Figures 25–27), I considered that the earthquakes that form the sequences found in this study (Figures 26 and 27 and Table 1) were likely caused by repeating slip in a small but strong asperity surrounded by a creeping zone on the plate boundary, therefore they are considered as repeating earthquakes.

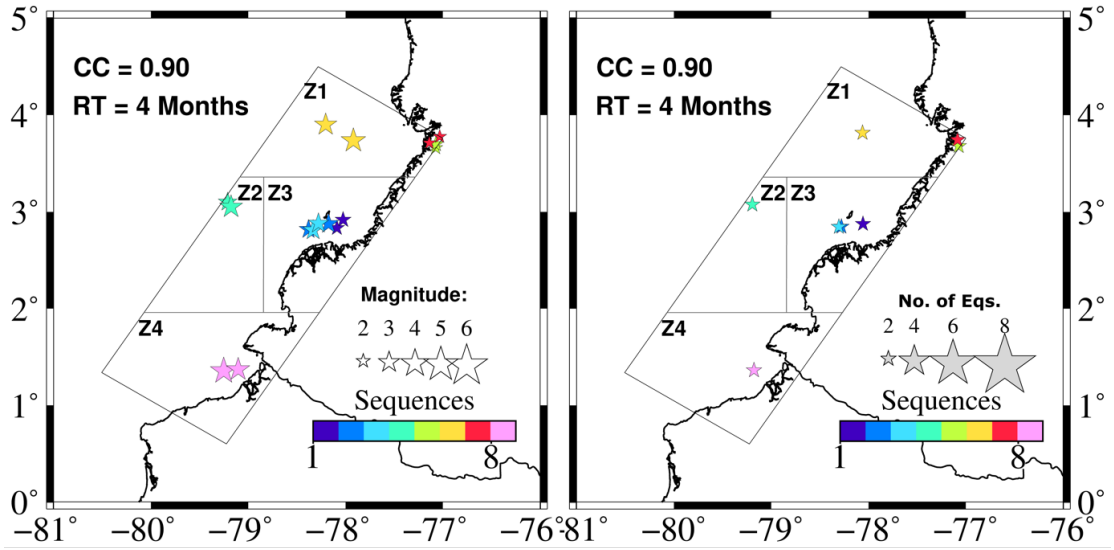

Figure 26: Distributions of the estimated repeating earthquakes using a cross-correlation (CC) threshold value of 0.90 and a minimum time interval of 4 months. (a) Epicenter locations of the repeating earthquakes, with the size of stars representing the magnitude of earthquake and the color scale representing the sequences. (b) Averaged epicenter locations of the repeating earthquakes in the individual sequences, with the size of the stars representing the number of earthquakes (No. of Eqs.) in each sequence. Regions Z1–Z4 are used to separate the sequences (Bermúdez-Barrios & Kumagai, 2020).

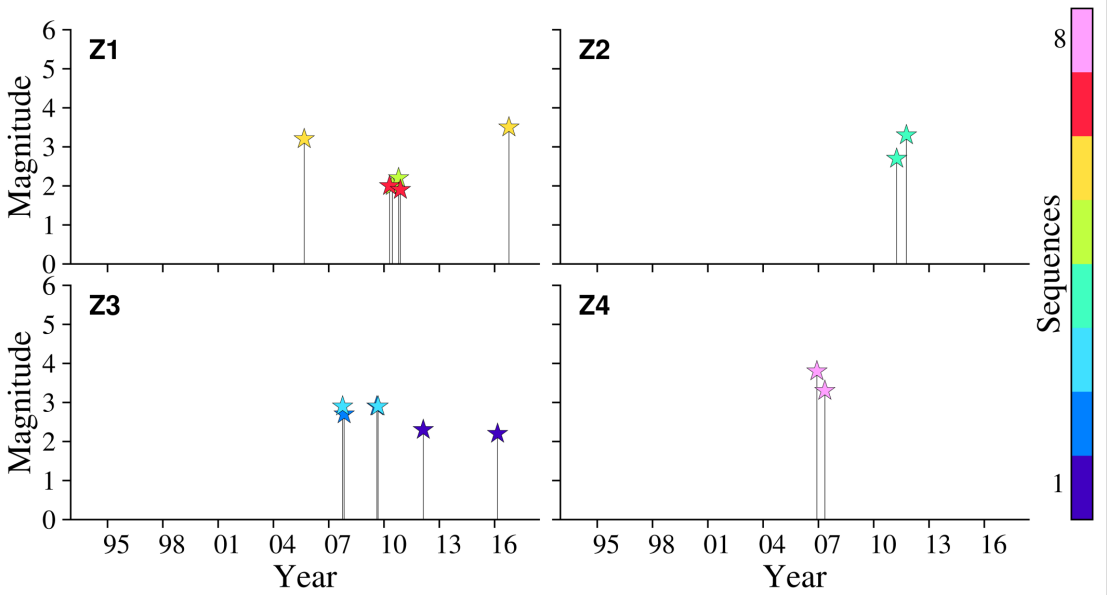

Figure 27: Magnitude-time plots of the repeating earthquakes in the individual sequences in regions Z1–Z4. The color scale represents the sequences and is the same as that used in Figure 26 (Bermúdez-Barrios & Kumagai, 2020).

Table 1: Sequences, the number of earthquakes in each sequence, and slip rates estimated by using time-predictable (TP) and size-predictable (SP) models (Bermúdez-Barrios & Kumagai, 2020).

Sequence	Zone	No. of Eqs.	Slip rate (cm/yr)	
			TP	SP
S1	Z3	2	2.81	2.63
S2	Z3	2	8.23	9.35
S3	Z3	2	8.64	8.64
S4	Z2	2	27.62	40.51
S5	Z1	2	27.50	31.24
S6	Z1	2	1.81	2.19
S7	Z1	2	15.93	14.95
S8	Z4	2	68.51	49.79

6.2.1 Slip rate estimation

Nadeau & Johnson (1998) suggested a relation between scalar moment M_0 (dyn·cm) and fault slip (cm) for repeating earthquakes that occurred in Parkfield, California, where the tectonic loading rate was assumed to be equal to the average slip rate on the plate boundary. The scaling relation is given as:

$$\log(d) = -2.36 + 0.17\log(M_0). \quad (1)$$

Here, Nadeau & Johnson (1998) used equation (1) to estimate the slip on the plate boundary for each repeating earthquake in the sequence and the slip rate for each sequence. The slip rate is the slope of the cumulated slip of each repeating earthquake sequence (Figure 28), in which a step increase in the slip represents the occurrence of an earthquake.

For 102 events among 1442 events analyzed in this study, their moment magnitudes (M_w) and local magnitudes (M_L) were estimated by using the SEISAN software (Ottemöller et al., 2014). Assuming a proportional relationship between M_L and M_w (Deichmann, 2018; Malagnini & Munafò, 2018), the following relationship was obtained (Figure 29):

$$M_L = 0.92M_w - 0.14. \quad (2)$$

I used the relationship (2) to estimate M_w from M_L for the repeating earthquakes found in this study. M_0 was estimated from M_w using the relationship proposed by Hanks & Kanamori (1979). I calculated the slip of each repeating earthquake by using (1) and estimated slip rates of each sequence by using the time- and size- predictable models of Shimazaki & Nakata (1980) (Figure 29 and Table 1).

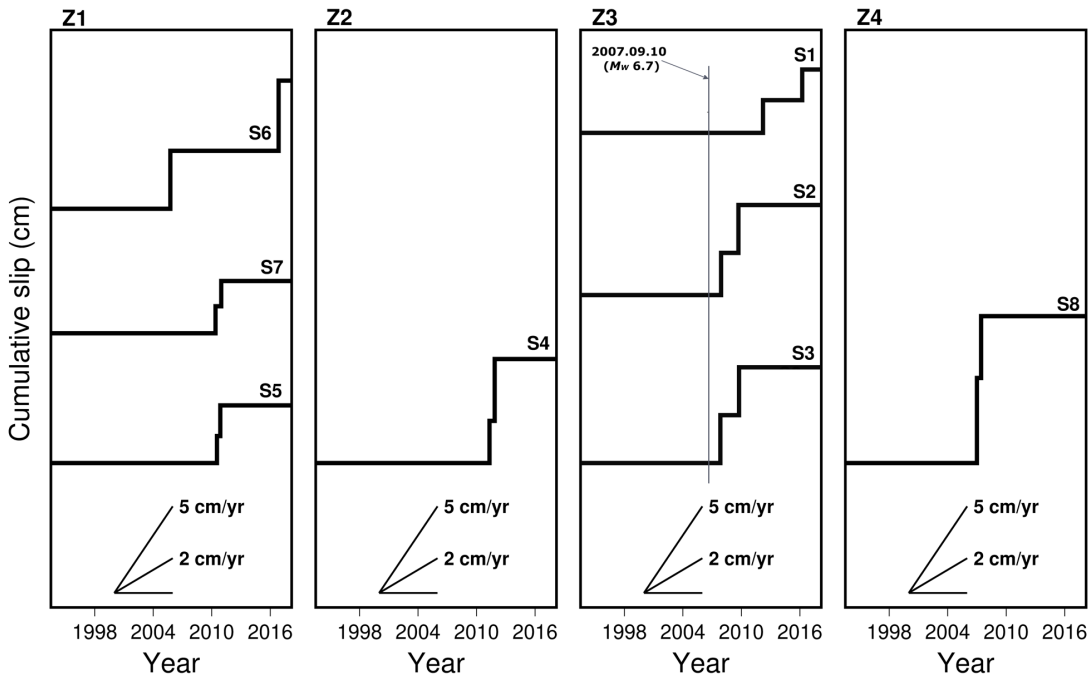

Figure 28: Plots of cumulative slip of the repeating earthquakes in the individual sequences in regions Z1–Z4 during 1993–2018. Slip rates are shown at the bottom of each panel as references (Bermúdez-Barrios & Kumagai, 2020).

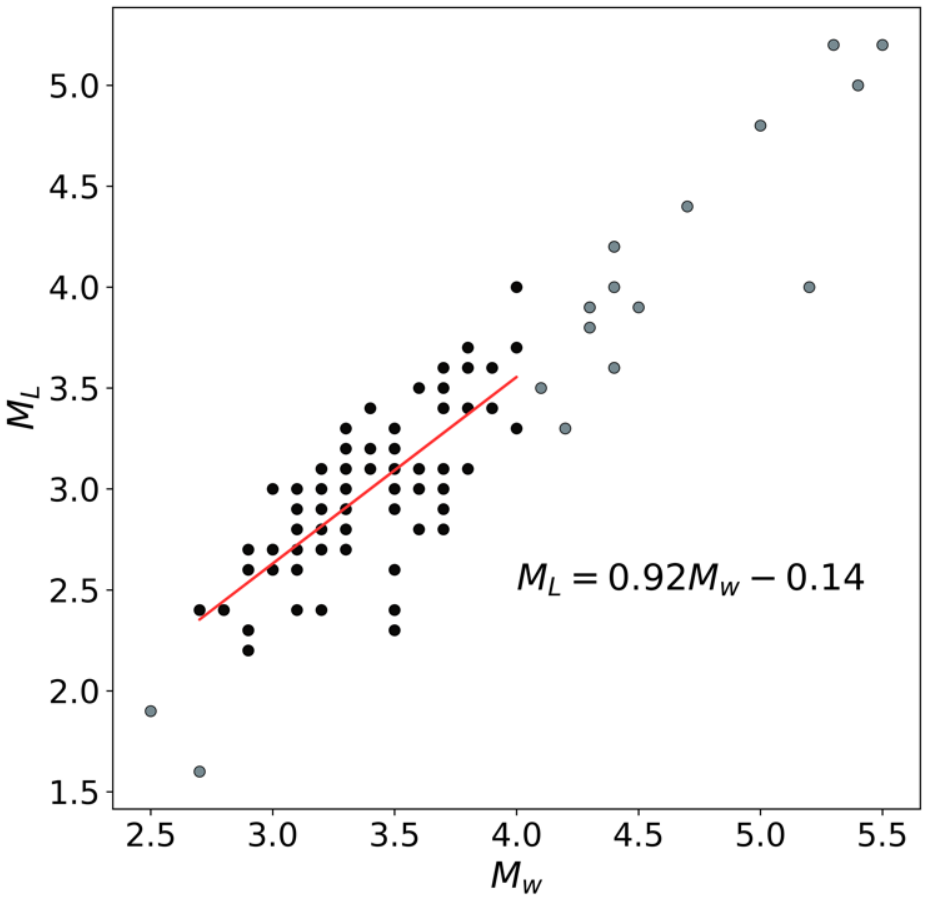

Figure 29: Plot of M_L against M_w for 102 events, for which both M_L and M_w were measured among 1,442 events analyzed in this study. Gray circles represent whole 102 events, and overlapped with black circles events with $2.0 < M_w < 4.0$, selected for fitting to a first-degree polynomial. The slope for the fit was 0.92, and the intersection point with vertical axes was –0.14. The fitting is represented by the red line. The equation represents the relationship between M_L and M_w (Bermúdez-Barrios & Kumagai, 2020).

According to the specified regions in Figure 26, I estimated the slip values for each repeating earthquake and the rate slip values for each sequence for the events located within the regions Z1, Z2, Z3, and Z4 (Table 1).

6.3 Repeating earthquakes along Caribbean and South America plate boundary

Using similar spatial separation and waveform cross-correlation constrains in my search for potential repeating earthquakes in the Colombia subduction zone, I also considered those constrains to search for repeating earthquakes along the Caribbean plate boundary in the southern Caribbean subduction zone. The SGC catalog used in this study contained 5,805 events. In the procedure for estimating the spatial separation between the earthquakes, I formed 2,685,557 RE-NE pairs, and computed 23,173,820 correlations. The distribution of all the CC-values is shown in Figure 30.

Based on the trend of the CC-value distribution, which is similar to the distribution in the Colombia subduction study, I selected a CC threshold value of 0.9 as in the Colombia subduction study. I then formed the sequences selecting the correlated pair of earthquakes and adding the pairs of earthquakes when both pairs shared a common event. Figure 31 displays the spatial distributions of the sequences with similar earthquakes correlated with a CC-value of 0.9 or larger.

After analyzing the spatial distributions, I performed the temporal analysis to select the suitable minimum recurrence interval between earthquakes from the same sequence, to select the repeating earthquakes and to discard the events corresponding to aftershocks or triggered events. I followed the procedure explained in section 6.2 and showed the distributions of the recurrence time intervals in Figure 32.

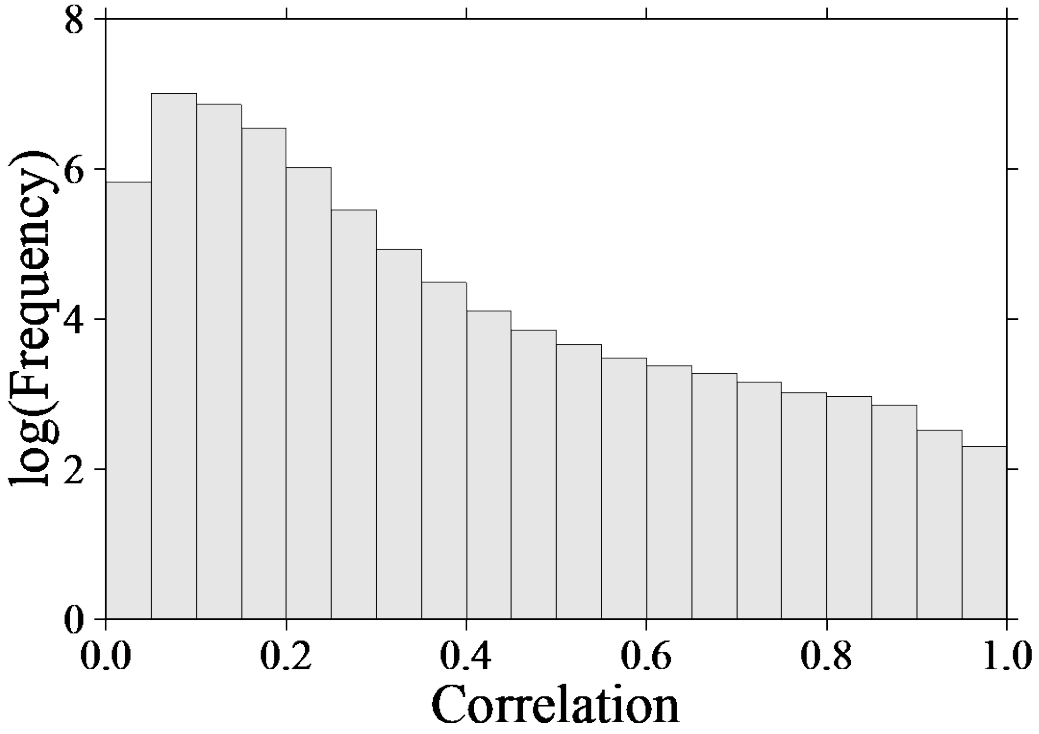

Figure 30: Frequency distribution of the cross-correlation coefficients between earthquakes pairs with hypocenter differences of < 50 km located in the Southern Caribbean subduction zone.

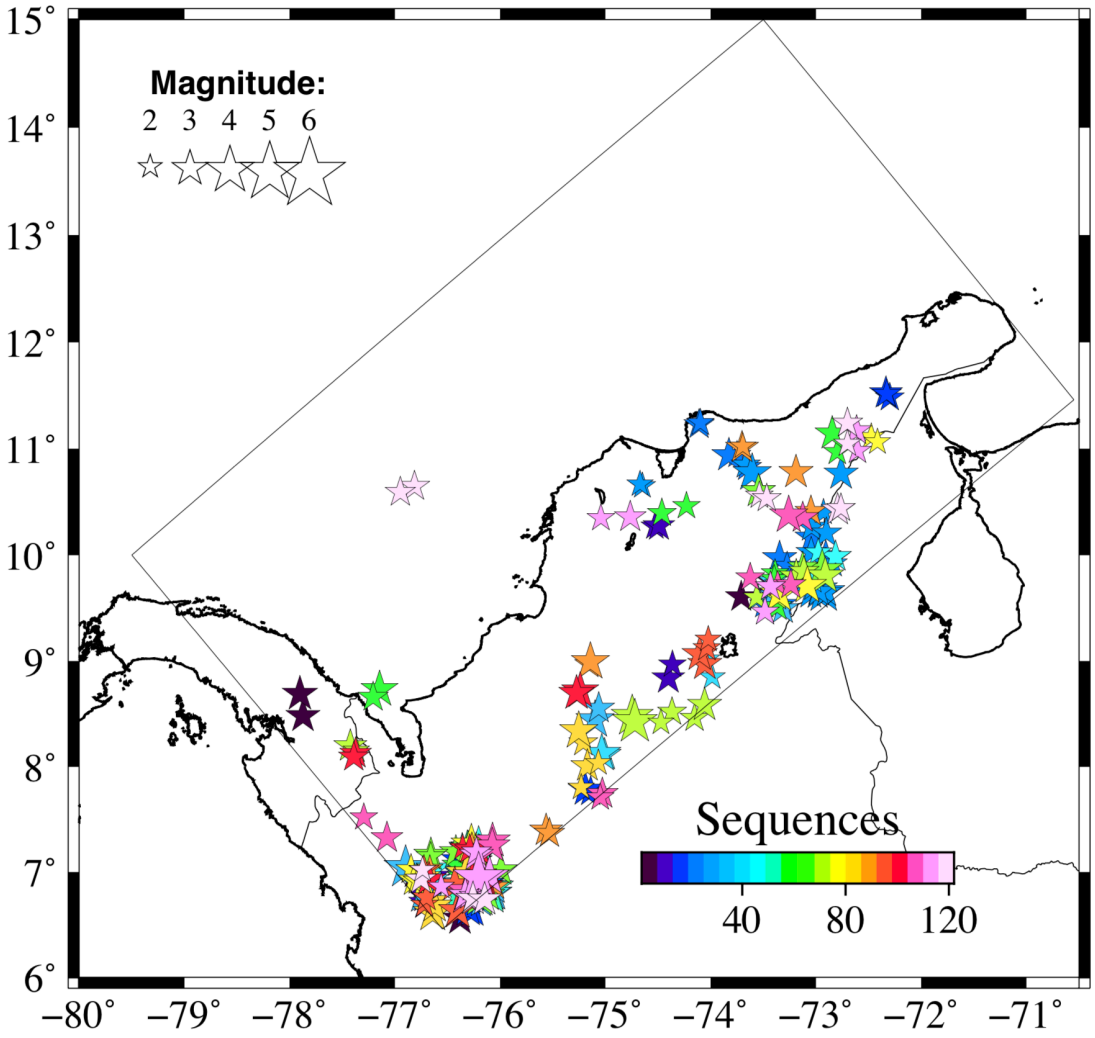

Figure 31: Distribution of earthquakes with CC < 0.9, in which the size of stars represents the magnitude and the color scale indicates the individual sequences. No restrictions by recurrence time intervals between successive earthquakes were applied.

As a trend similar to that in Colombia subduction region, the number of short-term events is much larger when I selected for earthquakes with loose threshold CC-value (0.8) than when I selected for earthquakes using a tight threshold CC-value (0.9). This may indicate that earthquakes occurred close to each other in time are more frequent and less similar than earthquakes with longer recurrence times, which are more correlated. According to the recurrence interval time distributions shown in Figure 32, the largest number of interval time was observed to be the time interval of 0–11 months. Therefore, I formed the repeating earthquake having recurrence intervals longer that 11 months in the southern Caribbean subduction zone.

I identified six well-defined groups of repeating earthquakes in the southern Caribbean subduction zone. Figure 33a shows the distributions of repeating earthquakes with a threshold CC-value of 0.90 and the sequences selected after excluding the short-term sequences. Figure 33b shows the sequences of repeating earthquakes and represents the set of selected repeating earthquakes. In Figure 33b, I obtained the locations of the individual sequences as the averaged locations of the repeating earthquakes. The magnitude-time plots of the repeating earthquakes are shown in Figure 34.

6.3.1 Slip rate estimation

Equation (1) was used to estimate slip on the plate boundary to each repeating earthquake in the sequences and the slip rate for each sequence. Moment magnitudes (M_w) and local magnitudes (M_L) were estimated using the SEISAN software (Ottemöller et al., 2014) for 363 events from the 5805 events analyzed. I assumed here a proportional relationship between M_L and M_w (Diechman 2018; Malagnini & Munafò, 2018). I obtained the following relationship for the southern Caribbean subduction zone (Figure 35):

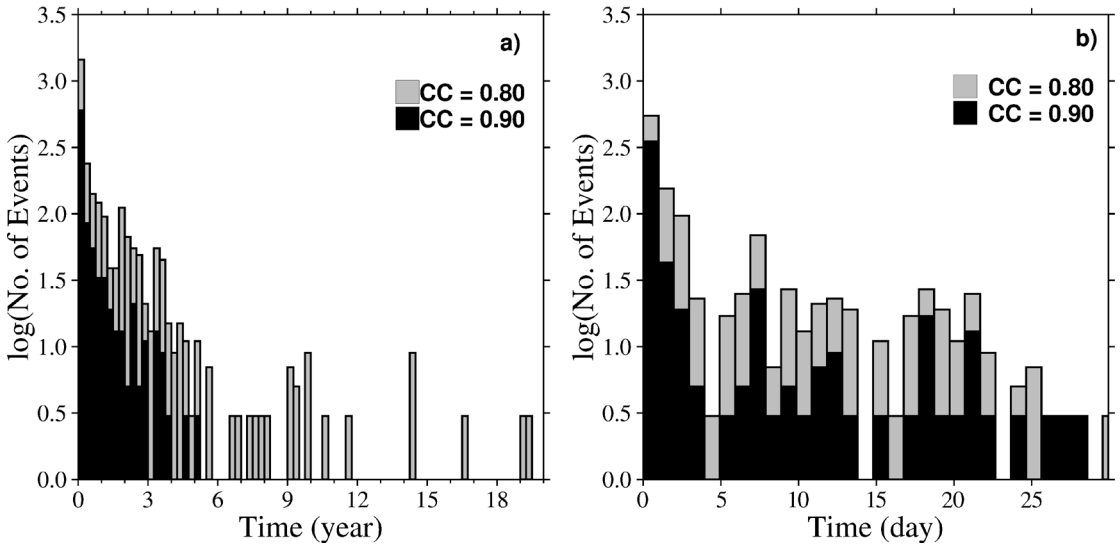

Figure 32: Frequency distributions of time intervals of successive earthquakes found by using cross correlation (CC) threshold values of 0.80 (gray) and 0.90 (black). (a) 0 to 18 years with 4-month interval bins. (b) 0 to 30 days with 1-day interval bins.

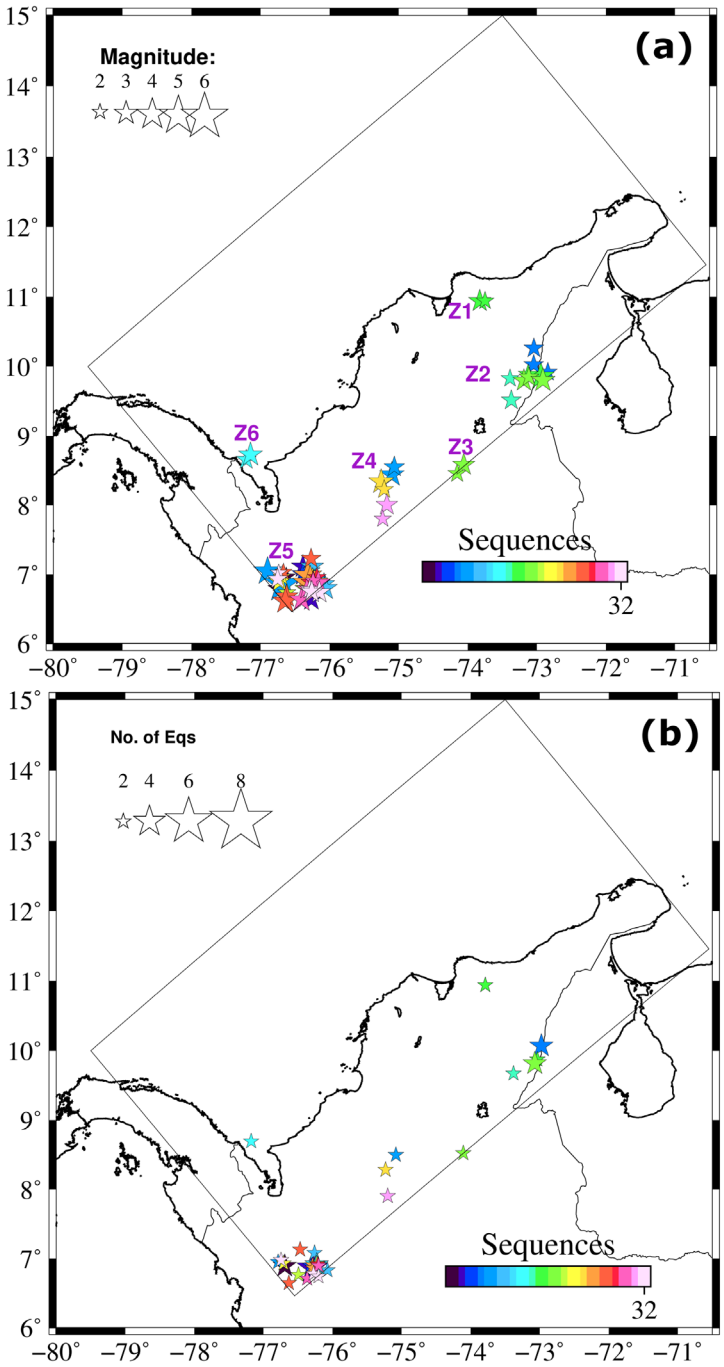

Figure 33: Distributions of the estimated repeating earthquakes using a cross-correlation (CC) threshold value of 0.90 and a minimum time interval of 11 months. (a) Epicenter locations of the repeating earthquakes, with the size of stars representing the magnitude of earthquake and the color scale representing the sequences. Regions Z1–Z6 are used to separate the sequences. (b) Averaged epicenter locations of the repeating earthquakes in the individual sequences, with the size of the starts representing the number of earthquakes (No. of Eqs.) in each sequence.

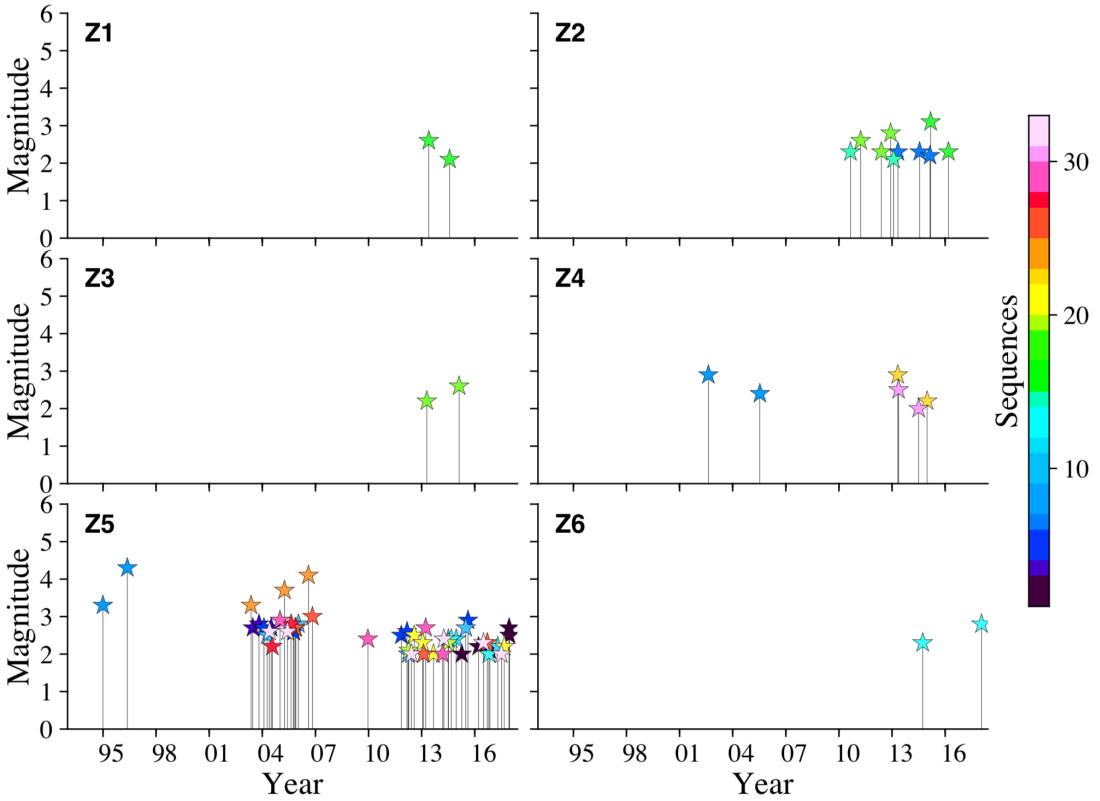

Figure 34: Magnitude-time plots of the selected repeating earthquakes in the individual sequences in regions Z1–Z6. These regions are shown in the Figure 33a.

$$M_L = 0.96M_w - 0.24 \quad (3)$$

I used this relationship (Eq. 3) to estimate M_w from M_L for the repeating earthquakes found in this study. After M_w estimation, I estimated M_0 using the relationship proposed by Hanks & Kanamori (1979). I calculated the slip rates of each sequence by using the time- and size-predictable models of Shimazaki & Nakata (1980) (Figure 36 and Table 2). In Z2 and Z5 regions, the slip rates were not estimated because the repeating earthquakes occurred there may not be generated by the slip accumulation in the interplate region.

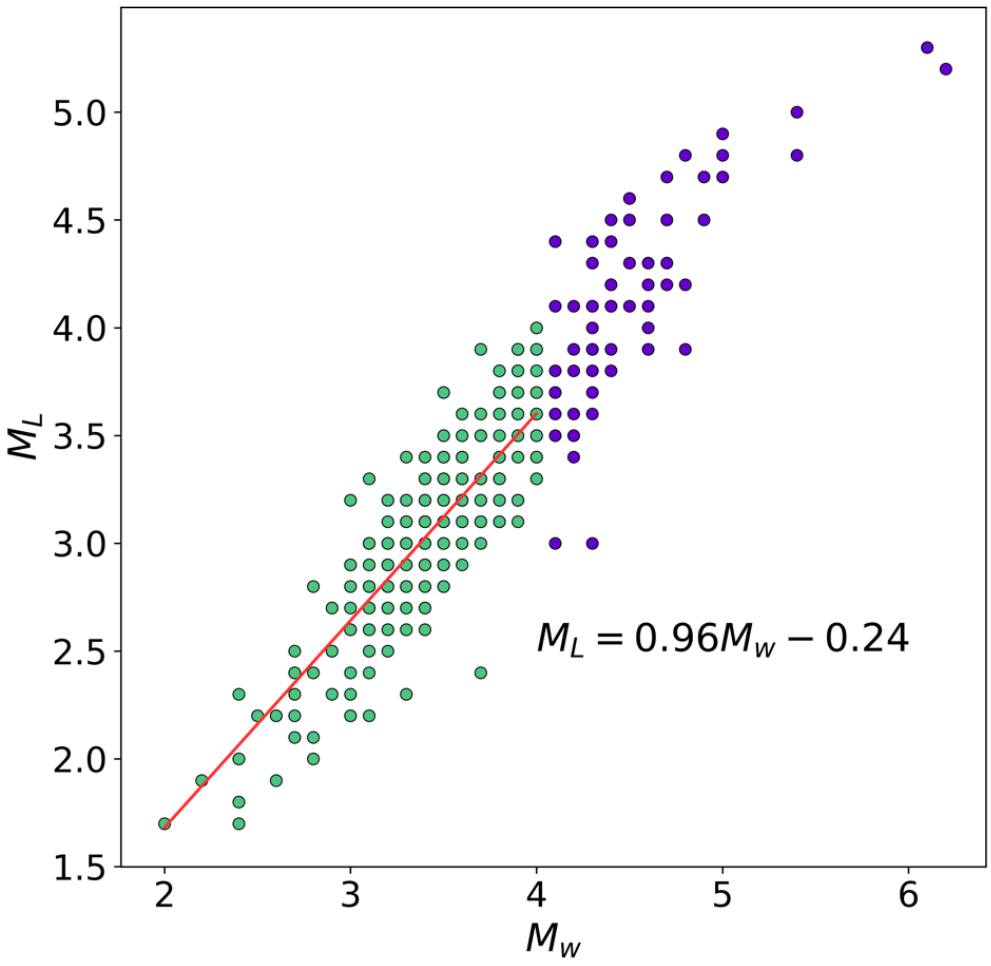

Figure 35: Plots of M_L against M_w for 363 events, for which both M_L and M_w were measured among 5,805 events analyzed in this study. Purple circles represent whole the 363 events, and overlapped with green circles events with $2.0 < M_w < 4.0$, selected for fitting to a first-degree polynomial. The slope for the fit was 0.96, and the intersection point with vertical axes was –0.24. The fitting is represented by the red line. The equation represents the relationship between M_L and M_w.

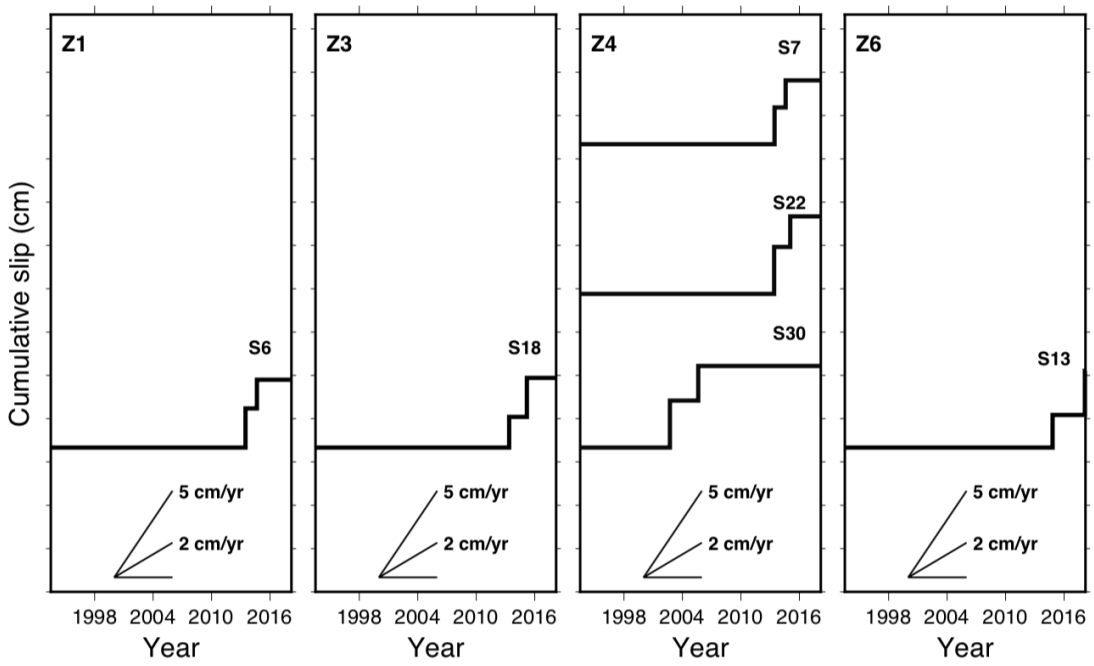

Figure 36: Plots of cumulative slip of the repeating earthquakes in the individual sequences in regions Z1, Z3, Z4 and Z6, in the southern Caribbean subduction zone, during 1993–2018. Slip rates are shown at the bottom of each panel as references.

Table 2: Sequences, the number of earthquakes in each sequence, and slip rates estimated by using time-predictable (TP) and size-predictable (SP) models.

Sequence	Zone	No. of Eqs.	Slip rate (cm/yr)	
			TP	SP
S6	Z1	2	11.98	11.67
S18	Z3	2	5.81	7.42
S7	Z4	2	5.59	4.12
S22	Z4	2	9.80	6.39
S30	Z4	2	11.20	8.25
S13	Z6	2	3.39	4.61

CHAPTER 7

7. DISCUSSION

7.1 Very-low-frequency earthquakes

After exploring the data set of continuous waveform data registered by broadband stations located near the Colombia subduction zone, which resulted in negative results in the search for VLF earthquakes, I would need to answer the following question: Why VLF earthquakes were not found in the Colombia subduction zone? I have three possible explanations to address this question as follows.

1. Several studies have reported VLF earthquakes in different places around the world. In the Nankai region, Japan (Ito & Obara, 2006a; Ito et al., 2007) and in Japan Trench off the Pacific coast of Tohoku (Matsuzawa et al., 2015), VLF earthquakes were identified through F-net and Hi-net from NIED. In Cascadia, under northern Washington (Ghosh et al., 2015), five VLFs were identified using seven three-component broadband stations deployed in a region of 2 degrees per 2 degrees. In Mexico, Frank et al. (2013) identified VLF earthquakes at Guerrero Coast using dense temporal seismic networks deployed by the Meso-American Subduction Experiment and Guerrero Gap Experiment (G-GAP) arrays. In Costa Rica, 54 VLF earthquakes were identified through a network 12 broadband stations, deployed in an area of 1 latitude degree per 1 longitude degree (Walter et al., 2013). Therefore, VLF earthquakes have been identified in regions where dense networks exist. Even though RSNC has an outstanding network in the region of south and central America, the capacity of earthquake detectability in the coastal region is low, although the station coverage in the coastal region has been improving in the recent years.

Figure 9 shows the stations used in searching for VLF earthquakes. The stations are sparse, and some of them work intermittently due to sudden damages. The stations near the coast or near islands are affected by large oceanic noise, and other stations near or over the Cordilleras are relatively far from the area of study to obtain good signal-to-noise ratios. Therefore, the current station configuration might not be enough to detect slow earthquakes in the Colombia-Ecuador subduction zone.

2. However, there might exist reasons based on tectonic features affecting the occurrence

of VLF earthquakes. Ito & Obara (2006) proposed that high pressure of fluid can weaken fault in accretionary prism by reducing normal stress on the fault plane and the resulting behavior of stick-slip movement can generate earthquakes with low drop stresses in low-velocity regions. Therefore, the generation of VLF earthquakes can be related to the fluid presence within fault zones and the low seismic velocity of the accretionary prism. Thus, the absence of VLF earthquakes can be explained with a possible mechanism involving materials with low or slow dehydration process such that the amount of fluid is not enough to keep high pore pressure and the pressure of fluid cannot weaken the fault; therefore, earthquakes with low drop stress may not be generated.

3. In northwestern Japan, in the off-Fukushima region, a notable increase of VLF earthquake activity was reported after the Fukushima-Oki earthquake in 2008 (M_w 6.9). Similarly, in the off-Iwate region, the number of VLF earthquakes increased in two different periods in the middle of 2012 and at the beginning of 2015, and both periods of increased activity were preceded by two aftershocks of the Tohoku-oki earthquake with M_w 6.2 and M_w 6.7, respectively. Therefore, Baba et al. (2018) suggested that VLF earthquakes may sometimes be activated by after-slip of interplate earthquakes with M_w ranging between 6 and 7. In the northern part of the Colombia-Ecuador subduction zone, only four earthquakes with magnitude 6 or larger occurred there during the period studied here. Three of them with normal focal mechanisms indicting that they are not interplate earthquakes, and one earthquake in 1996-04-27 08:40:41 with a thrust focal mechanism; however, the coverage station to register this earthquake was low, since broadband stations were not deployed at that epoch.

I mentioned three reasons why I consider that the visual search for VLF earthquakes was unsuccessful in the northern part of the Colombia-Ecuador subduction zone. However, as future works, according to Baba et al. (2018), synthetic waveforms can be generated using a three-dimensional velocity structure model and use the synthetic waveforms as a template to perform an automatic search by using a matched-filter technique. This method significantly increased the detection of VLF earthquakes in the Tohoku region, which were first found by Matsuzawa et al. (2015) by visual searching. Therefore, the method could be also used in searching for VLF earthquakes in Colombia.

7.2 Repeating earthquakes in Colombia subduction zone

The small number of repeating earthquakes in the sequences found in the current study contrasts with the large number of repeating earthquakes found in Japan (Igarashi et al., 2003), California (Nadeau & Johnson, 1998), and Mexico (Dominguez et al., 2016), where the sequences with more repeating earthquakes improve the temporal resolution for the monitoring of the quasi-static slip and allow to identify a clear recurrence interval for each sequence. According to Figure 11b, the amount of stations deployed in the area of this study increased after 2009. Before 1 January 2009, SGC reported 606 earthquakes which represent 42 % of the catalog used in this study. Moreover, after 1 January 2009, SGC reported 836 earthquakes corresponding to 58 % of the catalog events. These reports are consistent with the number of repeating earthquakes found in this study, because 13 earthquakes (36 %) occurred before 1 January 2009 and 23 earthquakes (64 %) after 1 January 2009. The events selected in this study have local magnitude (M_L) greater than 1.9. This magnitude represents the completeness magnitude (M_c) for the most recent events. Due to the increase in the number of stations over time (Figure 11b), M_c has changed with time. Figure 37 shows the temporal variation in M_c. The catalog of earthquakes may be incomplete because of difficulties with hypocenter determinations before 2009, and this may have resulted in a small number of repeating earthquakes in this study. Note that some repeating earthquakes may have been under-sampling before 2009 because the waveform database may have been incomplete.

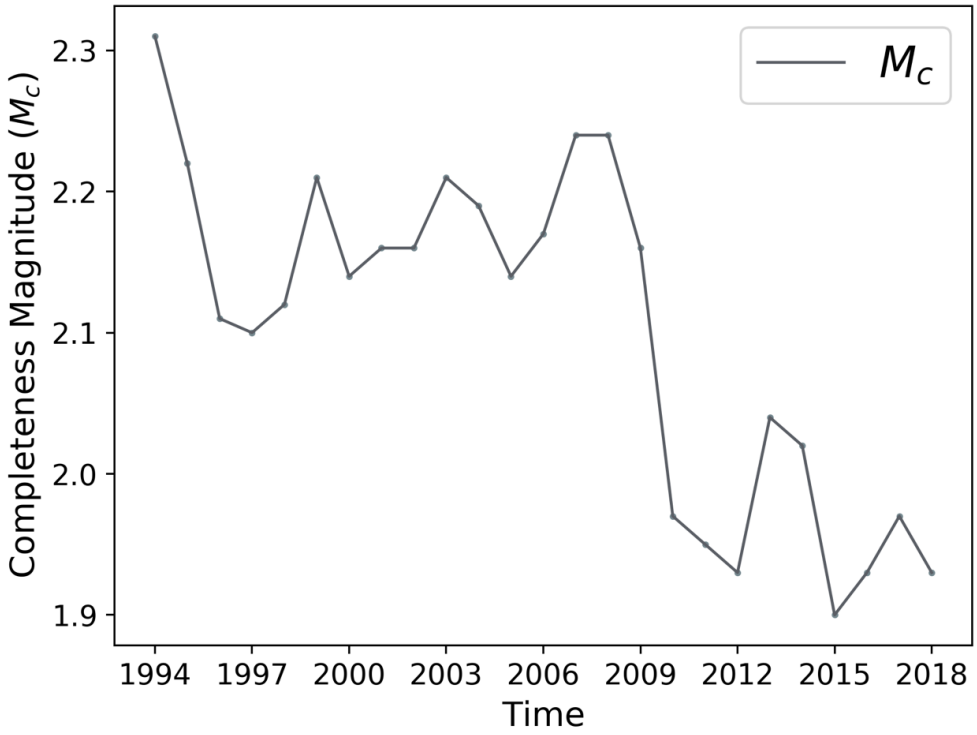

Figure 37: Plots of completeness magnitude (M_c) as a function of time, for the catalog of earthquakes located in the Colombia subduction zone.

My results showed large variations in the estimates of the slip rates (Figure 28 and Table 1). Those sequences with slip rates of several cm/yr (S1–S3 and S6) are consistent with the convergence rate in this region, which is 5.4 cm/yr (Mora-Páez et al., 2019). The sequences with a large slip rate (S4, S5, S7, and S8) are formed by repeating earthquakes with short inter-event times.

The events in the Z3 region (S1–S3) occurred after the large M_w 6.7 earthquake with a normal focal mechanism on 10 September 2007 (Figure 38). The focal mechanism reported by the Global CMT catalog indicates the M_w 6.7 earthquake is not an interplate earthquake. However, according to the occurrence time and distribution of the repeating earthquakes in Z3 (Figures 26–28), the repeating earthquakes occurred after the large earthquake and near each other; therefore, this intraplate earthquake may have accelerated the slip rates of S2 and S3, since the sequences are comprised by earthquakes with short recurrence times and large slip rates.

In Z4, the S8 sequence shows an anomalously large slip rate value, and I did not find any space and time correspondence of these repeating earthquakes with nearby large earthquakes, and a mechanism that explains such large slip rates is unknown (Figures 26–28).

Because of the non-periodic behavior of the repeating earthquakes found in the other regions such as Tonga and Japan (Yu, 2013; Uchida & Matsuzawa, 2013), I consider that the S5 and S7 sequences in Z1 and the S4 sequence in Z2 (Figure 28) with short-term recurrence intervals and large slip rates may represent portions of non-periodic sequences with longer recurrence intervals. However, I cannot estimate recurrence intervals for these sequences because the study period is short.

I could not estimate the focal mechanisms associated with our repeating earthquakes because of their small magnitudes, which resulted in limited phase readings with polarities.

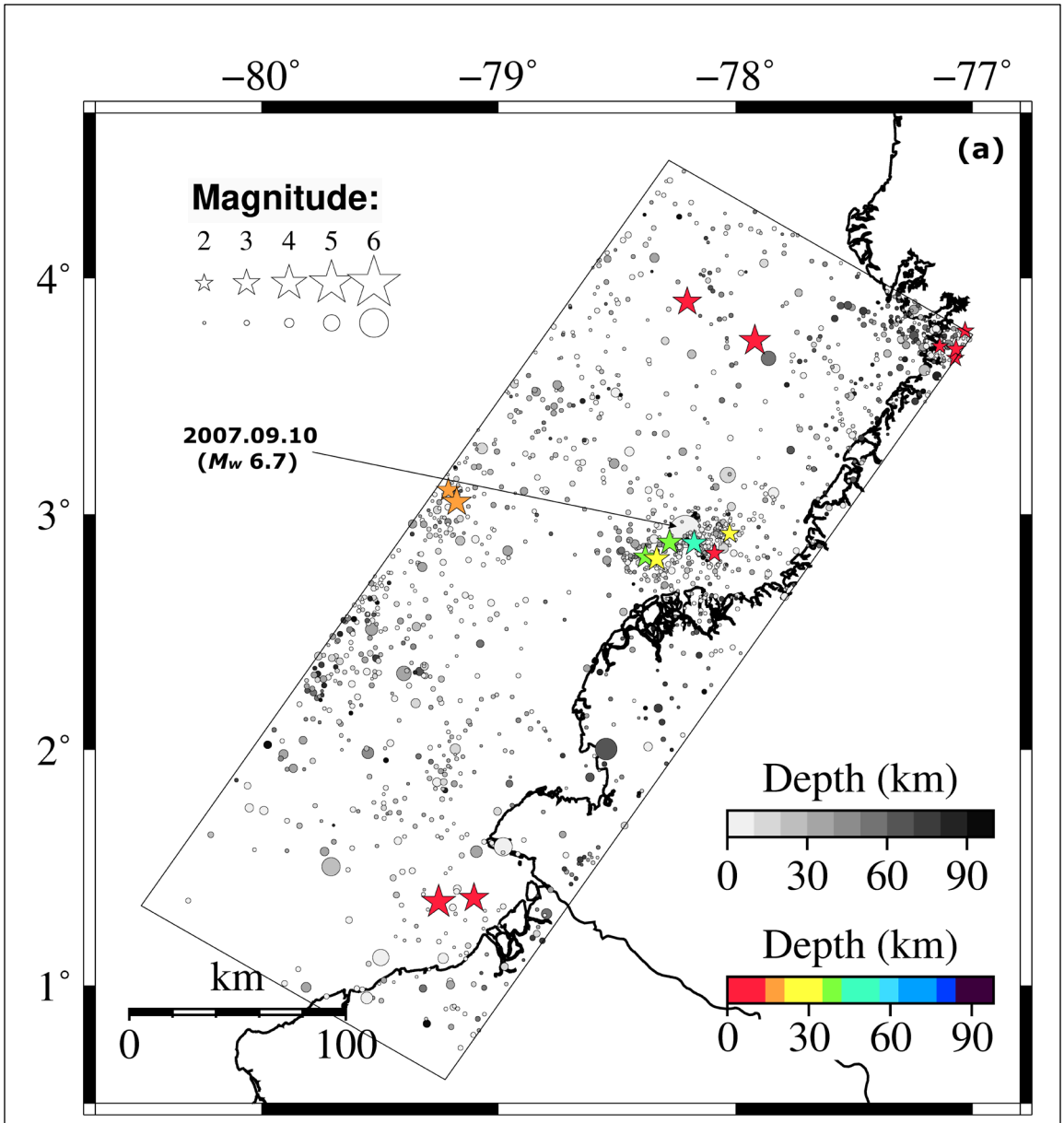

Figure 38: Locations of the repeating earthquakes (colored stars) with the background seismicity (gray circles) in our study area. The color scale representing depth in this figure. The arrow indicates the location of the earthquake with magnitude M_w 6.7, with normal focal mechanism, occurred in 10 September 2007 (Bermúdez-Barrios & Kumagai, 2020).

In this study, I present the first evidence for the existence of repeating earthquakes along the Colombia subduction zone. According to Igarashi et al. (2003), repeating earthquakes are not observed within large asperities or strongly coupled regions but they have been observed in low coupling regions, rupturing small asperities in surrounding regions of large asperities. My results indicate the existence of repeating earthquakes near the trench and the coast, and these regions correspond to low coupling estimates by Sagiya & Mora-Páez (2019) (Figure 39), which is strong evindence for low coupling values and not artifacts in the estimation. I did not find repeating earthquakes in strongly coupled regions (Figure 39), where a large slip of the 1979 Tumaco earthquake was estimated by Yoshimoto et al. (2017b).

Most of the repeating earthquakes I found in this study have slip rates larger than the plate convergence rate, except for S1 in Z3 and S6 in Z1, and this is consistent with the distribution of the repeating earthquakes reported here, since S1 and S6 are located in the outer part of the strong coupled region. This strong coupled region is considered as a slip deficit region; therefore, slip rates are low for S1 and S6. The remainder repeating earthquakes are located over a weak coupled region corresponding with a slip excess region where the rate slip is larger than the plate convergence rate (Figure 39).

The finding of the repeating earthquakes near the trench in the northern part of Colombia-Ecuador subduction zone suggests that this region is weakly coupled; therefore, repeating earthquakes are expected in this region. Sagiya & Mora-Páez (2019) assumed that the interplate coupling along the trench was zero in their GPS data inversion because they could not resolve coupling near the trench by using land GPS data. Therefore, they could not confirm whether the coupling near the trench is weak or not based on their coupling estimates. The finding of repeating earthquakes near the trench may provide evidence for weak coupling in this region, which implies that a large earthquake near the trench along the Colombia subduction zone would be unlikely. However, repeating earthquakes found near the trench are few, and further investigations are required to strengthen that conclusion.

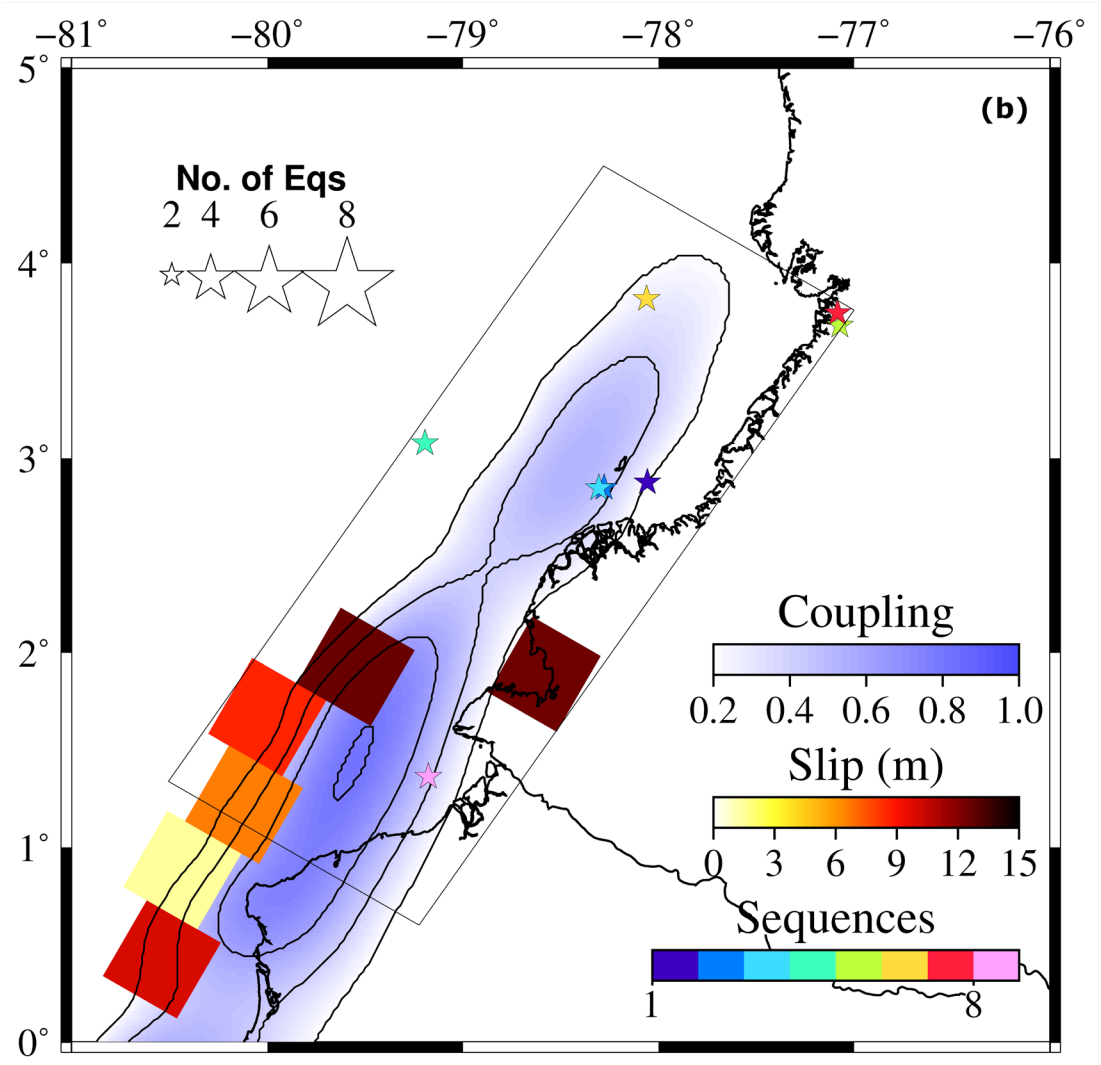

Figure 39: Spatial distributions of the sequences of the repeating earthquakes (colored stars), the interplate coupling (purple area) estimated by Sagiya & Mora-Páez, (2019) and slip distributions (colored squares) estimated by Yoshimoto et al. (2017a) for the 1906 Colombia-Ecuador earthquake (Bermúdez-Barrios & Kumagai, 2020).

Yoshimoto et al. (2017a) showed that during the 1906 Colombia-Ecuador earthquake (M_w 8.4), large slip occurred near the trench in the southern part of the Colombia-Ecuador subduction zone. This result indicates that this region may be strongly coupled so that such a large earthquake occurred. Therefore, the results in the current study show that weak coupling exists in the northern CESZ, and thus different coupling characteristics may exist between the northern and southern parts of CESZ near the trench, suggesting that the northern and southern parts of CEZS along the trench may have different ruptures modes. To further clarify the coupling characteristics, it is important to search for repeating earthquakes in the southern part of CEZS, which should be investigated in future studies.

7.3 Repeating earthquakes in southern Caribbean subduction zone

Figure 40 shows the distribution of the repeating earthquakes in the southern Caribbean region found in this study. I defined six clear clusters of Z1 to Z6. A clear feature in this distribution is that many sequences of repeating earthquakes comprise clusters Z2 and Z5, which may be explained as follows. A large number of crustal earthquakes are mainly distributed in and around clusters Z2 and Z5. The location of Z2 is Cesar, Colombia, a region known by host mining activities; about 90 % of the whole carbon production in Colombia is mined from Cesar along with La Guajira region (Figure 33a). The location of cluster Z5 coincides with the Murindo seismic zone, which has generated large earthquakes on 17 and 18 October 1992 with M_w 6.6 and 7.1, respectively. This intense seismic activity is considered to be a consequence of the collision between the Panama microplate, the Andean block, and the Nazca plate subduction under Colombia (Dionicio & Sánchez, 2012; Farbiarz et al., 2000) (Figure 33a). Therefore, I discarded the sequences located in Z2 and Z5 because the mechanisms generating these earthquakes do not correspond with the mechanism for the repeating earthquakes in the subduction zone interplate region. Figures 34 and 36 show that there is a large number of sequences with successive events closer in time in Z2 and Z5 than those in Z1, Z3, Z4, and Z6, which is consistent with the proposed mechanism causing earthquakes in Z2 and Z5. In Z2, the repeating earthquakes are probably triggered by the mining activity in the region. In Z5, the repeating earthquakes are probably triggered by the intense seismic activity in the Murindo seismic zone.

In Figure 40, I show the final distribution of the repeating earthquakes detected in this study after excluding those in Z2 and Z5. The repeating earthquake distribution is consistent with the coupling model of Lizarazo, (2020), since the repeating earthquakes are located in the low

coupling region. Based on the coupling model and the repeating earthquake distribution, the existence of a large asperity in northern Colombia is likely and implies that a large earthquake may occur in the region.

Most of the repeating earthquakes found in southern Caribbean subduction zone have a large slip value and sequences in Z1, Z4 and Z6 are located in the outer part weakly coupled region, indicating a region of slip excess, where the rate slip is larger than the interplate convergence rate (Igarashi et al., 2003). The strongly coupled region is considered to be a slip deficit region; therefore, absence of repeating earthquakes is reasonable. The remainder repeating earthquakes are located in a region where the coupling is not determined (Figures 40 and 41).

The convergence rate can be estimated from the repeating earthquakes, and is needed to estimate the recurrence interval. Although earthquake prediction is not possible, the maximum expected size of future events may be estimated by monitoring those zones; however, previous large events have not been reported within northwestern Colombia or Southern Caribbean, therefore, difficulties in estimating the recurrence time and expected size of an impending earthquake makes the assessment of seismic hazard complicated in this region. That is why the convergence rate estimated in this study is an important parameter which would help to improve the seismic assessment in the region.

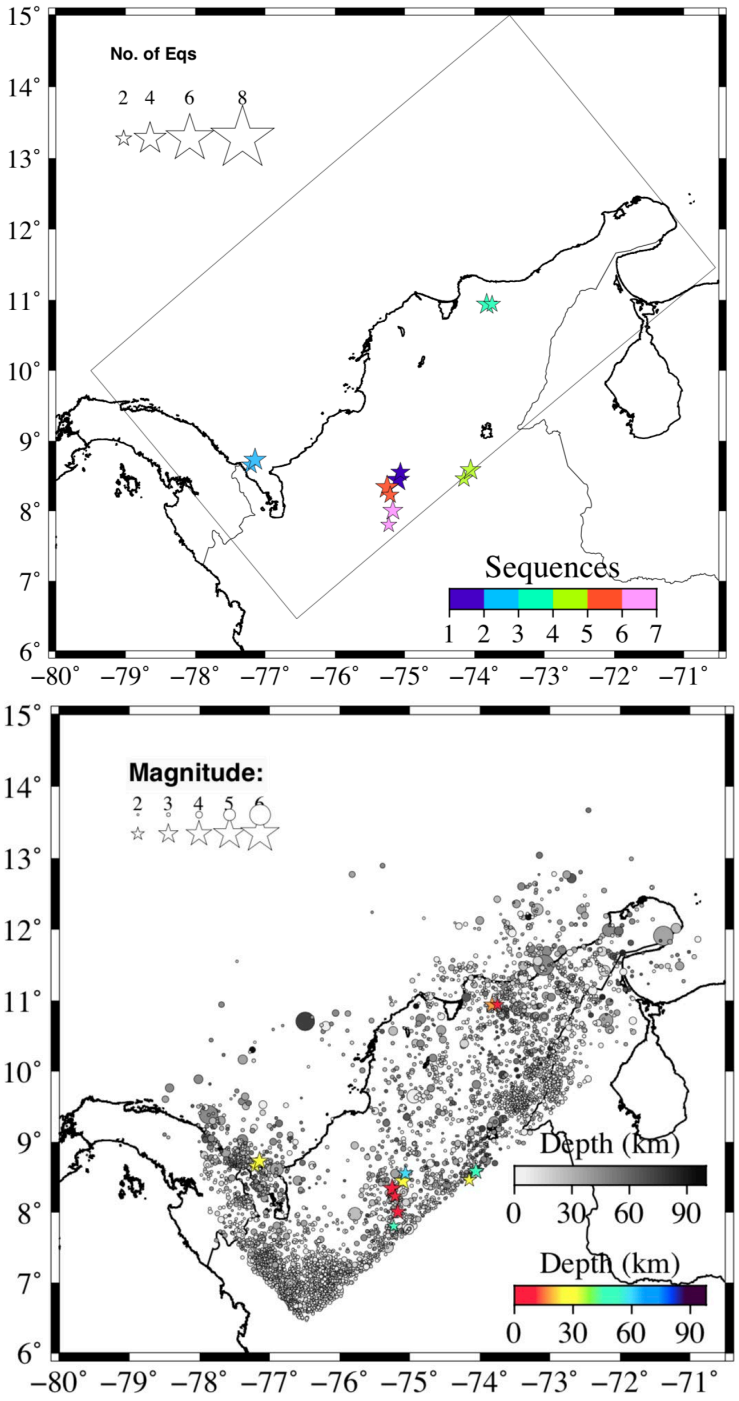

Figure 40: (Top) Spatial distributions of the sequences of the repeating earthquakes (colored stars). (Bottom) Spatial distributions of the sequences of the repeating earthquakes (colored stars), over the background seismicity. The whole seismicity reported in the catalog used for the current study.

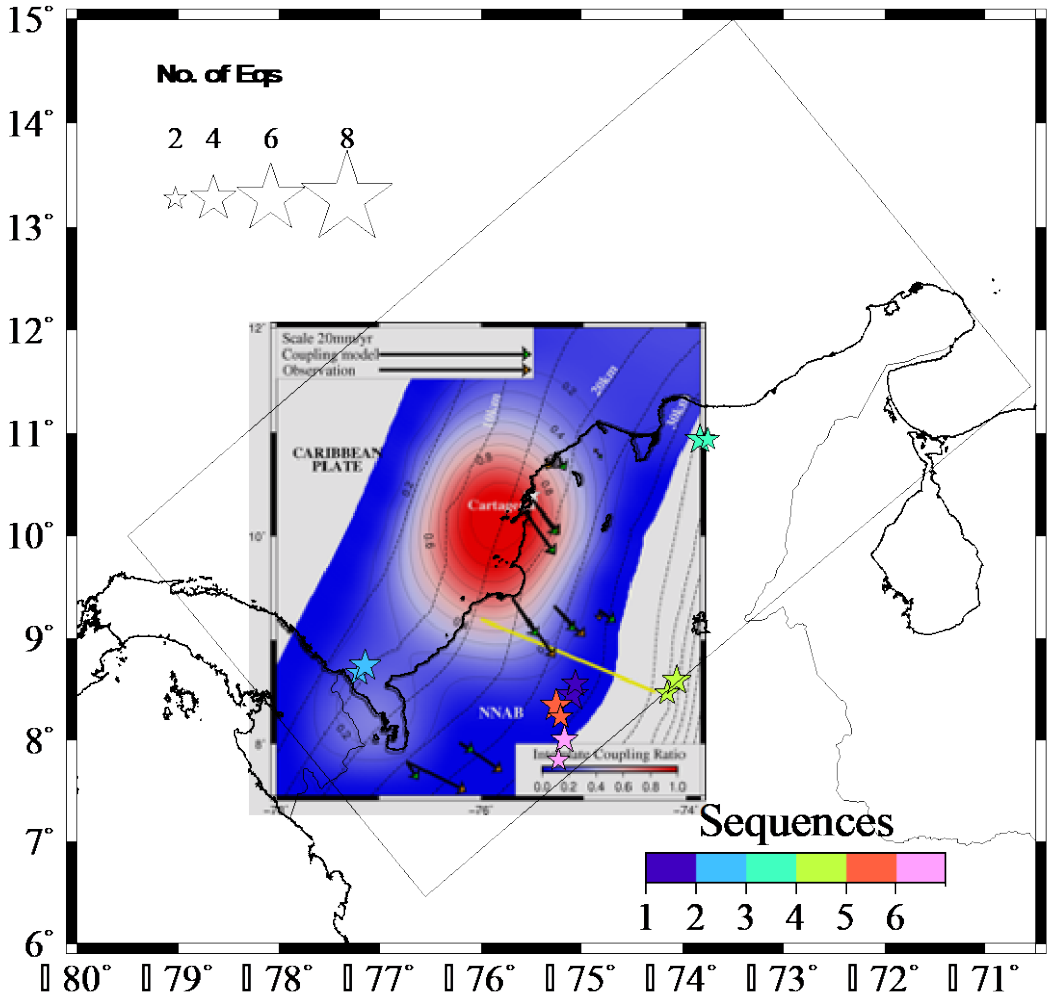

Figure 41: Spatial distributions of the sequences of the repeating earthquakes (colored stars), the interplate coupling (inset figure) estimated by Lizarazo (2020), red color indicating strong coupling and blue color indicanding weak coupling.

CHAPTER 8

8. CONCLUSIONS

In this study I searched for very low frequency earthquakes by a visual search of the continuous waveforms registered by the broadband stations of SGC deployed in and near the Colombia subduction zone. Two years and seven months of continuous data were examined by applying bandpass filters in low (0.01–0.02 Hz) and high (2–8 Hz) frequencies. By this search none of the VLF events were found and three reasons were proposed: 1) the low detectability capability of the network used for the search, 2) the existence of materials featured by low or slow dehydration and therefore low amount of fluid unable to keep high pore pressure, thus the pressure of fluid cannot weaken the fault, then earthquakes with low drop stress as VLF earthquakes could not be generated. And, 3) the absent of earthquakes with magnitude larger than 6, which have been seen in different studies as they increase the VLF activity after they occur.

I used the SGC earthquake catalog and seismic waveforms from the Colombia seismic network to find repeating earthquakes along the Colombia subduction zone. I grouped the earthquakes based on hypocentral differences and performed waveform similarity analysis throughout cross correlation technique. I found several groups of events related by CC-value larger than 0.8. Using a threshold of 0.90 and a minimum time interval of 4 months, 8 sequences of repeating earthquakes were identified. They were distributed near the trench and beneath the coastal region along the Colombia subduction zone. The earthquake distribution indicates that the repeating earthquakes did not occur within the large slip area of the 1979 Tumaco earthquake, where a relatively strong interplate coupling was estimated from a previous GPS data analysis by Sagiya & Mora-Páez (2019). My estimated repeating earthquakes located offshore near the trench suggest that the interplate coupling in this region is weak. It has been shown that large slip of the 1906 Colombia-Ecuador earthquake occurred along the trench in the southern part of the Colombia-Ecuador subduction zone, and my finding suggests the northern and southern parts of the Colombia-Ecuador subduction zone along the trench may have different rupture modes.

Similarly, by using the same methodology, repeating earthquakes in the southern Caribbean subduction zone were also found. They are located in the intraplate region and near the coast. They are distributed within the low coupling region of the interplate coupling model of Lizarazo (2020) around a fully locked region that represents a large asperity indicating strong coupling. This agrees with the repeating earthquake description given by Igarashi et al. (2003) that most of repeating earthquakes did not occur in strongly coupled areas inferred from GPS data

analyses. Therefore, the distribution of the repeating earthquakes found in this study is consistent with the coupling model. Two other groups of repeating earthquakes were found but mechanisms generating these earthquakes did not correspond to plate subduction: One group occurred near the Murindo seismic zone, and this region is featured by the existence of a strike slip fault system. The other group was located in a region where mining activities are carried out, therefore, the repeating earthquakes found here may be triggered by these mining activities.

I found repeating earthquakes in the Colombia subduction zone and the southern Caribbean subduction zone, and they are the first repeating earthquakes reported in these subduction zones. These repeating earthquakes were located in regions surrounding the possible large asperity estimated by the coupling model of Sagiya & Mora-Paez (2019) or the rupture model presented by Yoshimoto et al. (2017b) in the Colombia subduction zone and that estimated by the coupling model of Lizarazo (2020) in the southern Caribbean subduction zone. The distributions of the repeating earthquakes found in this study contribute to constrain the geometry of the estimated large asperities, which is important for seismic hazard estimation to determine the magnitudes of possible forthcoming large earthquakes in the Colombia subduction zone and the southern Caribbean subduction zone.

BIBLIOGRAPHY

Ando, M., Tu, Y., Kumagai, H., Yamanaka, Y., & Lin, C.-H. (2012). Very low frequency earthquakes along the Ryukyu subduction zone. *Geophysical Research Letters, 39*(4).

Anstey, N. A., & Lerwill, W. E. (1966). Correlation in real time. *Proceedings of the Royal Society A*, 430-447.

Asano, Y., Obara, K., & Ito, Y. (2008). Spatiotemporal distribution of very-low frequency earthquakes in Tokachi-oki near the junction of the Kuril and Japan trenches revealed by using array signal processing. *Earth, Planets and Space, 60*, 871–875.

Baba, S., Takeo, A., Obara, K., Kato, A., Maeda, T., & Matsuzawa, T. (2018). Temporal Activity Modulation of Deep Very Low Frequency Earthquakes in Shikoku, Southwest Japan. *Geophiysical Research Letters, 45*(2), 733-738.

Benioff, H., & Press, F. (1958). Progress Report on Long Period Seismographs. *Geophysical Journal of the Royal Astronomical Society, 1*(3), 208-215.

Bermúdez-Barrios, J. C., & Kumagai, H. (2020). Repeating earthquakes along the Colombian subduction zone. *Journal of Disaster Research, 15*(5).

Beroza, G. C., & Ide, S. (2009). Deep tremors and slow quakes. *Science, 324*(5390), 1025-1026.

Beroza, G. C., & Ide, S. (2011). Slow earthquakes and nonvolcanic tremor. *Annual review of earth and planetary sciences, 39*, 271-296.

Beyreuther, M., Barsch, R., Krischer, L., Megies, T., Behr, Y., & Wassermann, J. (2010). ObsPy: A Python Toolbox for Seismology. *Electronic Seismologist*.

Bohnhoff, M., Wollin, C., Domigall, D., & Küperkoch, L. (2017). Repeating Marmara Sea earthquakes: Indication for fault creep. *Geophysical Journal International, 210*(1), 332-339.

Brodsky, E., & Mori, J. (2007). Creep events slip less than ordinary earthquakes. *Geophysical Research Letters, 34*(16).

Brown, J. R., Beroza, G. C., Ide, S., Ohta, K., Shelly, D. R., Schwartz, S. Y., . . . Kao, H. (2009). Deep low-frequency earthquakes in tremor localize to the plate interface in multiple subduction zones. *Geophysical Research Letters, 36*(19).

Buchbinder, G. G., & Sarria, A. (1994). A satellite-based seismic and volcanic monitoring system for Colombia. *Bulletin of the Seismological Society of America, 84*(5), 1670–1674.

Chiarabba, C., Gori, P. D., Faccenna, C., Speranza, F., & al, e. (2015). Subduction system and flat slab beneath the Eastern Cordillera of Colombia. *Geochemistry, Geophysics, Geosystems, 17*(1), 16-27.

Chlieh, M., Mothes, P., Nocquet, J.-M., & al, e. (2014). Distribution of discrete seismic asperities and aseismic slip along the Ecuadorian megathrust. *Earth and Planetary Science Letters, 400*, 292-301.

Deichmann, N. (2018). The relation between ME, ML and Mw in theory and numerical simulations for small to moderate earthquakes. *Journal of Seismology, 22*, 1645–1668.

Dionicio, V., & Sánchez, J. J. (2012). Mapping of b-values, earthquake relocation, and Coulomb stress changes during 1992–2007 in the Murindó seismic zone, Colombia. *Journal of Seismology, 16*, 375–387.

Dominguez, L. A., Taira, T., & Santoyo, M. A. (2016). Spatiotemporal variations of characteristic repeating earthquake sequences along the Middle America Trench in Mexico. *Journal of Geophysical Research Solid Earth, 121*(12), 8855-8870.

Farbiarz, J., Jaramillo, J., & Villarraga, M. (2000). Microzonation of the city of Medellín. *World Conference on Earthquake Engineering 2000*.

Frank, W. B., Shapiro, N. M., Kostoglodov, V., Husker, A. L., Michel Campillo, J. S., & Prieto, G. A. (2013). Low-frequency earthquakes in the Mexican Sweet Spot. *Geophysical Research Letters, 40*(11), 2661-2666.

Ghosh, A., Huesca-Pérez, E., Brodsky, E., & Ito, Y. (2015). Very low frequency earthquakes in Cascadia migrate with tremor. *Geophysical Research Letters, 42*(9), 3228-3232.

Gibbons, S. J., & Ringdal, F. (2006). The detection of low magnitude seismic events using array-based waveform correlation. *Geophysical Journal International, 165*(1), 149–166.

Hanks, T. C., & Kanamori, H. (1979). A moment magnitude scale. *Journal of Geophisical Research Solid Earth, 84*(B5), 2348-2350.

Havskov, J., & Ottemoller, L. (1999). SeisAn Earthquake Analysis Software. *Seismological Research Letters, 70*(5), 532–534.

Hayward, T. W., & Bostock, M. G. (2107). Slip Behavior of the Queen Charlotte Plate Boundary Before and After the 2012, MW 7.8 Haida Gwaii Earthquake: Evidence From Repeating Earthquakes. *Journal of Geophysical Research Solid Earth, 122*(11), 8990-9011.

Hillebrandt-Andrade, C. v. (2013). Minimizing Caribbean Tsunami Risk. *Science*.

Hilst, R. V., & Mann, P. (1994). Tectonic implications of tomographic images of subducted lithosphere beneath northwestern South America. *Geology, 22*(5), 451-454.

Ide, S., Beroza, G. C., Shelly, D. R., & Uchide, T. (2007). A scaling law for slow earthquakes. *Nature, 447*, 76-79.

Igarashi, T., Matsuzawa, T., & Hasegawa, A. (2003). Repeating earthquakes and interplate aseismic slip in the northeastern Japan subduction zone. *Journal of Geophysical Research Solid Earth, 108*(B5).

Ito, Y., & Obara, K. (2006). Dynamic deformation of the accretionary prism excites very low frequency earthquakes. *Geophysical Research Letters, 33*(2).

Ito, Y., & Obara, K. (2006a). Very low frequency earthquakes within accretionary prisms are very low stress-drop earthquakes. *Geophysical Research Letters, 33*(9).

Ito, Y., Obara, K., Sekine, S., & Hirose, H. (2007). Slow earthquakes coincident with episodic tremors and slow slip events. *Science, 315*(5811), 503-506.

Kanamori, H., & McNally, K. C. (1982). Variable rupture mode of the subduction zone along the Colombia-Ecuador coast. *Bulletin of Seismology Society of America, 72*(4), 577-593.

Katsumata, A., & Kamaya, N. (2003). Low-frequency continuous tremor around the Moho discontinuity away from volcanoes in the southwest Japan. *Geophysical Research Letters, 30*(1), 20-1-20-4.

Kimura, H., Kasahara, K., Igarashi, T., & Hirata, N. (2006). Repeating earthquake activities associated with the Philippine Sea plate subduction in the Kanto district, central Japan: A new plate configuration revealed by interplate aseismic slips. *Tectonophysics*, 101-118.

Krischer, L., Megies, T., Barsch, R., Beyreuther, M., Lecocq, T., Caudron, C., & Wassermann, J. (2015). ObsPy: a bridge for seismology into the scientific Python ecosystem. *Computational Science & Discovery, 8*(1).

Lengliné, O., & Marsan, D. (2009). Inferring the coseismic and postseismic stress changes caused by the 2004 Mw = 6 Parkfield earthquake from variations of recurrence times of microearthquakes. *Journal of Geophysical Research Solid Earth, 114*(B10).

Li, L., Chen, Q.-f., Niu, F., & Su, J. (2011). Deep slip rates along the Longmen Shan fault zone estimated from repeating microearthquakes. *Journal of Geophysical Research Solid Earth, 116*(B9).

Lienert, B. R., & Havskov, J. (1995). A Computer Program for Locating Earthquakes Both Locally and Globally. *Seismological Research Letters, 66*(5), 26–36.

Lienert, B. R., Berg, E., & Frazer, L. N. (1986). HYPOCENTER: An earthquake location method using centered, scaled, and adaptively damped least squares. *Bulletin of the Seismological Society of America, 76*(3), 771–783.

Lizarazo, S. C. (2020). *Active deformation and seismic potential in Colombia revealed by GeoRED GPS data.*

Malagnini, L., & Munafò, I. (2018). On the Relationship between ML M L and Mw M w in a Broad Range: An Example from the Apennines, Italy. *Bulletin of the Seismological Society of America, 108*(2), 1018–1024.

Matsuzawa, T., Asano, Y., & Obara, K. (2015). Very low frequency earthquakes off the Pacific coast of Tohoku, Japan. *Geophysical Research Letters, 42*(11), 4318-4325.

Matsuzawa, T., Uchida, N., Igarashi, T., Okada, T., & Hasegawa, A. (2004). Repeating earthquakes and quasi-static slip on the plate boundary east off northern Honshu, Japan. *Earth, Planets and Space, 56*, 803–811.

Maury, J., Ide, S., Cruz-Atienza, V. M., Kostoglodov, V., González-Molina, G., & Pérez-Campos, X. (2016). Comparative study of tectonic tremor locations: Characterization of slow earthquakes in Guerrero, Mexico. *Journal Geophysical Research Solid Earth, 121*(7), 5136-5151.

Megies, T., Beyreuther, M., Barsch, R., Krischer, L., & Wassermann, J. (2011). ObsPy – What can it do for data centers and observatories? *INGV Annals of Geophysics, 54*(1).

Mendoza, C., & Dewey, J. (1984). Seismicity asociated with the great Colombia-Ecuador earthquakes of 1942, 1958, and 1979: Implication for barrier models of earthquake rupture. *Bulletin of Seismological Society of America, 74*(2), 577-593.

Mora-Páez, H., N.Kellogg, J., Freymueller, J. T., Mencin, D., M.S.Fernandese, R., Diederix, H., . . . Peláez-Gaviria, J.-R. (2019). Crustal deformation in the northern Andes – A new GPS velocity field. *Journal of South American Earth Sciences, 89*, 76-91.

Nadeau, R. M., & Johnson, L. R. (1998). Seismological studies at Parkfield VI: Moment release rates and estimates of source parameters for small repeating earthquakes. *Bulletin of the Seismological Society of America, 88*(3), 790-814.

Nakano, M., Hori, T., Araki, E., Kodaira, S., & Ide, S. (2018). Shallow very-low-frequency earthquakes accompany slow slip events in the Nankai subduction zone. *Nature Communications, 9*.

Nocquet, J.-M., Jarrin, P., Vallée, M., Mothes, P. A., Grandin, R., Rolandone, F., . . . Char. (2017). Supercycle at the Ecuadorian subduction zone revealed after the 2016 Pedernales earthquake. *Nature Geoscience, 10*, 145-149.

Obara, K. (2002). Nonvolcanic deep tremor associated with subduction in southwest Japan. *Science, 296*(5573), 1679-1681.

Obara, K., & Ito, Y. (2005). Very low frequency earthquakes excited by the 2004 off the Kii peninsulaearthquakes: A dynamic deformation process in the large accretionary prism. *Earth Planets Space, 57*, 321–326.

Obara, K., & Kato, A. (2016). Connecting slow earthquakes to huge earthquakes. *Science, 353*(6296), 253-257.

Ojeda, A., & Havskov, J. (2001). Crustal structure and local seismicity in Colombia. *Journal of Seismology, 5*, 575-593.

Ottemöller, L., Voss, P., & Havskov, J. (2014). *Seisan earthquakes analysis software Windows, Solaris, Linux and Macosx.*

Peng, Z., & Gomberg, J. (2010). an integrated perspective of the continuum between earthquakes and slow-slip phenomena. *Nature Geoscience, 3*, 599–607.

Penington, W. D. (1981). Subduction of the eastern Panama Basin and seismotectonics of northwestern South America. *Journal of Geophysical Research Solid Earth, 86*(B11), 10753-10770.

Ramos, V. (1999). Plate tectonic settings of Andean Cordillera. *Episodes, 22*, 183-190.

Royer, A., & Bostock, M. (2014). A comparative study of low frequency earthquake templates in northern Cascadia. *Earth and Planetary Science Letters, 402*, 247-256.

Rubinstein, J., Shelly, D., & Ellsworth, W. (2010). Non-volcanic tremor: A window into the roots of fault zones. In *New frontiers in integraded solid earth sciences.* Springer.

Sagiya, T., & Mora-Páez, H. (2019). Interplate coupling along the Nazca subduction zone on the Pacific coast of Colombia deducted from GeoRED GPS observation data. *The Geology of Colombia, 4*, 615-661.

Sallarès, V., Charvis, P., Flueh, E., & al, e. (2003). Seismic structure of Cocos and Malpelo Volcanic Ridges and implications for hot spot-ridge interaction. *Journal of Geophysical Research: Solid Earth, 108*(B12).

Schwartz, S., & Rokosky, J. (2007). Slow slip events and seismic tremor at circum-Pacific subduction zones. *Reviews of Geophysics, 45*(3).

Shelly, D., Beroza, G. C., & Ide, S. (2007). Non-volcanic tremors and low-frequency earthquakes swarms. *Nature, 446*, 305–307.

Shelly, D., Beroza, G. C., Ide, S., & Nakamula, S. (2006). Low-frequency earthquakes in Shikoku, Japan, and their relationship to episodic tremor and slip. *Nature, 442*, 188–191.

Shimazaki, K., & Nakata, T. (1980). Time-predictable recurrence model for large earthquakes. *Geophysical Research Letters, 7*(4), 279-282.

Swenson, J. L., & Beck, S. L. (1996). Historical 1942 Ecuador and 1942 Peru subduction earthquakes, and earthquake cycles along Colombia-Ecuador and Peru subduction segments. *Pure and Applied Geophysics*.

Syracuse, E. M., Maceira, M., Prieto, G., & al, e. (2016). Multiple plates subducting beneath Colombia, as illuminated by seismicity and velocity from the joint inversion of seismic and gravity data. *Earth and Planetary Science Letters, 444*, 139-149.

Taboada, A., Rivera, L., Fuenzalida, A., Cisternas, A., & al, e. (2000). Geodynamics of the northern Andes: Subductions and intracontinental deformation (Colombia). *Tectonics, 19*(5), 787-813.

Trenkamp, R., N.Kellogg, J., Freymueller, J. T., & Mora, H. P. (2002). Wide plate margin deformation, southern Central America and northwestern South America, CASA GPS observations. *Journal of South American Earth Sciences, 15*(2), 157-171.

Uchida, N. (2019). Detection of repeating earthquakes and their application in characterizing slow fault slip. *Progress in Earth and Planetary Science, 6*.

Uchida, N., & Bürgmann, R. (2019). Repeating Earthquakes. *Annual Review of Earth and Planetary Sciences, 47*, 305-332.

Uchida, N., & Bürgmann, R. (2019). Repeating Earthquakes. *Annual Review of Earth and Planetary Sciences, 47*, 305-332.

Uchida, N., & Matsuzawa, T. (2013). Pre- and postseismic slow slip surrounding the 2011 Tohoku-oki earthquake rupture. *Earth and Planetary Science Letters, 374*, 81-91.

Uchida, N., Matsuzawa, T., Hasegawa, A., & Igarashi, T. (2003). Interplate quasi-static slip off Sanriku, NE Japan, estimated from repeating earthquakes. *Geophysical Research Letters, 30*(15).

Vargas, C. (2020). Subduction geometries in northwestern South America. *The Geology of Colombia, 4*.

Vargas, C., & Mann, P. (2013). Tearing and breaking off of subducted slabs as the result of collision of the Panama Arc-Indenter with northwestern South America. *Bulletin of the Seismological Society of America, 103*(3), 2025-2046.

Wagner, L. S., Jaramillo, J. S., Ramírez-Hoyos, L. F., & al, e. (2017). Transient slab flattening beneath Colombia. *Geophysical Research Letters, 44*(13), 6616- 6623.

Waldhauser, F., & Ellsworth, W. L. (2000). A double-difference earthquake location algorithm: Method and application to the northern Hayward fault, California. *Bulletin of the Seismological Society of America, 90*(6), 1353–1368.

Walter, J. I., Schwartz, S. Y., Protti, M., & Gonzalez, V. (2013). The synchronous occurrence of shallow tremor and very low frequency earthquakes offshore of the Nicoya Peninsula, Costa Rica. *Geophysical Research Letters, 40*(8), 1517-1522.

Yamashita, T. (1980). Quasistatic crack extentions in an inhomogeneous voscoelastic medium- A posible mechanism for the occurrence of aseismic faulting. *Journal of Physics of the Earth, 28*, 309-306.

Yao, D., Walter, J. I., Meng, X., Hobbs, T. E., Peng, Z., Newman, A. V., . . . Protti, M. (2017). Detailed spatiotemporal evolution of microseismicity and repeating earthquakes following the 2012 Mw 7.6 Nicoya earthquake. *Journal of Geophysical Research Solid Earth, 122*(1), 524-542.

Ye, L., HirooKanamori, Avouac, J.-P., Li, L., heung, K. F., & Lay, T. (2016). The 16 April 2016, MW 7.8 (MS 7.5) Ecuador earthquake: A quasi-repeat of the 1942 MS 7.5 earthquake and partial re-rupture of the 1906 MS 8.6 Colombia–Ecuador earthquake. *Earth and Planetary Science Letters, 454*, 248-258.

Yoshimoto, M., Kumagai, H., Acero, W., & al, e. (2017a). Depth-dependent rupture mode along the Ecuador-Colombia subduction zone. *Geophysical Research Letters, 44*(5), 2203-2210.

Yoshimoto, M., Kumagai, H., Sagiya, T., Mora, H., & Pulido, N. (2017b). New view on the rupture mode along the Colombia-Ecuador subduction zone. *AGU Fall Meeting 2017.*

Yu, W.-c. (2013). Shallow-focus repeating earthquakes in the Tonga–Kermadec–Vanuatu subduction zones. *Bulletin of the Seismological Society of America, 103*(1), 463–486.